



SENSORLESS FIELD ORIENTED CONTROL OF THREE-PHASE INDUCTION
MOTOR USING FUZZY PI CONTROLLER



KARCHUNG -

A Thesis Submitted to the Graduate School of Naresuan University
in Partial Fulfillment of the Requirements
for the Master of Engineering in (Electrical Engineering)

2019

Copyright by Naresuan University

SENSORLESS FIELD ORIENTED CONTROL OF THREE-PHASE INDUCTION
MOTOR USING FUZZY PI CONTROLLER



A Thesis Submitted to the Graduate School of Naresuan University
in Partial Fulfillment of the Requirements
for the Master of Engineering in (Electrical Engineering)
2019
Copyright by Naresuan University

Thesis entitled "Sensorless Field Oriented Control of Three-Phase Induction Motor
using Fuzzy PI Controller"

By KARCHUNG -

has been approved by the Graduate School as partial fulfillment of the requirements
for the Master of Engineering in Electrical Engineering of Naresuan University

Oral Defense Committee

..... Chair

(Associate Professor Somporn Ruangsinchaiwanin, PhD)

..... Advisor

(Associate Professor Somporn Ruangsinchaiwanin, PhD)

..... Internal Examiner

(Assistant Professor Sakda Somkun, PhD)

..... Internal Examiner

(Assistant Professor Akaraphunt Vongkunghae, PhD)

Approved

.....
(Professor Dr. Paisarn Muneesawang)

for Dean of the Graduate School

| | |
|-----------------------|---|
| Title | SENSORLESS FIELD ORIENTED CONTROL OF THREE-PHASE INDUCTION MOTOR USING FUZZY PI CONTROLLER |
| Author | KARCHUNG - |
| Advisor | Associate Professor Somporn Ruangsinchaiwanin, PhD |
| Academic Paper | Thesis M.Eng. in Electrical Engineering, Naresuan University, 2019 |
| Keywords | Clarke and park transformation, compressor motor / induction motor, fuzzy logic controller, sensorless/open-loop vector control, PI controller, Rotor-Flux MRAS, Space Vector Modulation (SVM), Total Harmonic Distortion (THD) |

ABSTRACT

Due to enormous application of induction motor, it is must that the control mechanisms are investigated through proper research. This thesis mains to investigate sensorless vector control of induction motor using Fuzzy Logic Controller. The purpose of using FLC is to guarantee fast response and improved dynamic performance of the drive system. The whole control is reinforced by a Rotor-Flux Model Reference Adaptive System (RF-MRAS) for rotor flux and speed estimation. Also, space vector modulation algorithm is proposed to provide fixed switching frequency, better DC bus utilization and reduce the total harmonic distortion in the inverter. The proposed method is simulated in MATLAB software. The robustness of the overall system is tested under load torque injection while running the simulation. The simulation result showed that the indirect FOC with proposed observer provides good performance dynamic characteristics for different operating modes.

The universal voltage source inverter is developed in the laboratory with TMS320F28069M Texas Instrument's launchpad. With the developed inveter, two different experimental setup are proposed for this project. Firstly, the closed-loop

speed control algorithm is investigated for 3 hp, 4 pole cage induction motor in the laboratory coupled to induction generator connected to resistive load. The speed and current controller parameters are derived from simulation work. The experimental result showed equivalent behavior as the simulation work. The second experiment is proposed on controlling the 7 kW compressor motor for the commercial air conditioning system based in Electrical Engineering Laboratory; Naresuan University. In this method, the motor parameters were not available. For this reason, the open-loop control algorithm was implemented. This was implemented with two important aims. These are reducing energy consumption and to ensure thermal comfort to the occupant in the building. A variable speed compressor using voltage source inverter along with then fuzzy logic controller (FLC) is proposed. FLC was developed to imitate the performance of human expert operators by encoding their knowledge in the form of linguistic rules. The Fluke Data Logger is used to monitor electrical component of the system. The room temperature, outside atmospheric temperature and coolant pressure are also monitored throughout the measurement period. In the analysis; coefficient of performance (COP), energy consumption, THD, power factor and energy saving are calculated. from this measurement, the result showed a energy saving of 1.42 kWh for 6 hours measurement period. It also showed a reduced THD, improved power factor in inverter-fed operation compared to the normal operation. This can have tremendous cost saving to the medium and large energy user by reducing the demand charge. Moreover, reduced THD and improved power factor have advantages to the power grid operator and also to the interconnected system.

ACKNOWLEDGEMENTS

Firstly, I would like to thank His Majesty's Secretariat, Bhutan and Naresuan University for the bestowing me with this prestigious scholarship.

Secondly, I would sincerely like to acknowledge and thank my thesis and academic Advisor; Associate Professor Dr. Somporn Ruangsinchaiwanich for his timely guidance and support throughout the study period. I am indebted for financing the research and conference fees. The success of this thesis is entirely because of his guidance and support.

I also would like to convey my sincerest appreciation to my Co-advisor; Assistant Professor Dr. Sakda Somkun. He has been kind enough to provide his laboratory apart from providing his sole input while developing hardware and program.

Furthermore, I would like to thank my tutors, thesis committee, the Director and Foreign Student Officers of Division of International and Language Division (DIALD); Head of Department and Academic Officers of Department of Electrical and Computer Engineering and Faculty of Engineering; Deans and Academic Officers in Graduate School and the technicians in Electrical Engineering Departments; for their valuable support wherever possible in completing my master's study on time.

lastly, I would like to thank my wife, family, friends and all the people who are involved directly or indirectly in the successful completion of my Masters thesis.

Thank You all.

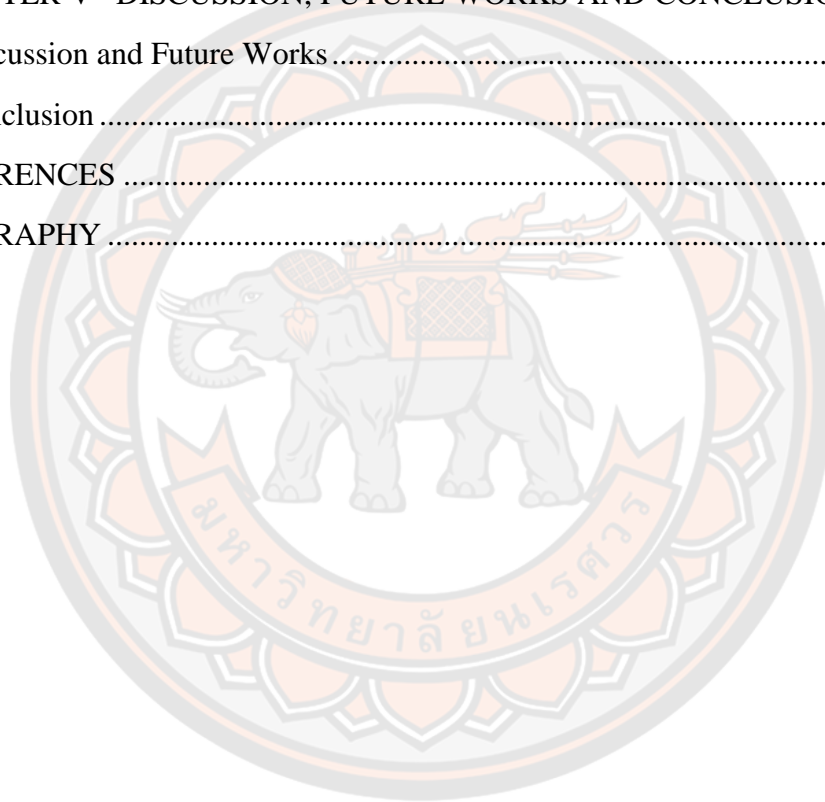
KARCHUNG -

TABLE OF CONTENTS

| | Page |
|--|-------------|
| ABSTRACT..... | C |
| ACKNOWLEDGEMENTS..... | E |
| TABLE OF CONTENTS..... | F |
| List of tables..... | I |
| List of figures..... | J |
| ABBREVIATIONS | M |
| CHAPTER I INTRODUCTION..... | 1 |
| Preface | 1 |
| Literature Survey | 2 |
| Aim of Research | 12 |
| Scope of Thesis..... | 13 |
| CHAPTER II DYNAMIC MODELING OF INDUCTION MOTOR | 14 |
| Introduction..... | 14 |
| Reference Frame Transformation | 14 |
| Arbitrary Reference Frame | 16 |
| Induction Motor Model..... | 19 |
| System Equations..... | 19 |
| Stator Voltage Equations | 20 |
| Rotor Voltage Equations..... | 20 |
| Flux Linkage Equations | 20 |
| Stator Inductance | 21 |
| Rotor Inductance..... | 22 |
| Mutual Inductances..... | 22 |
| Per Unit System | 23 |
| Base Quantities | 24 |

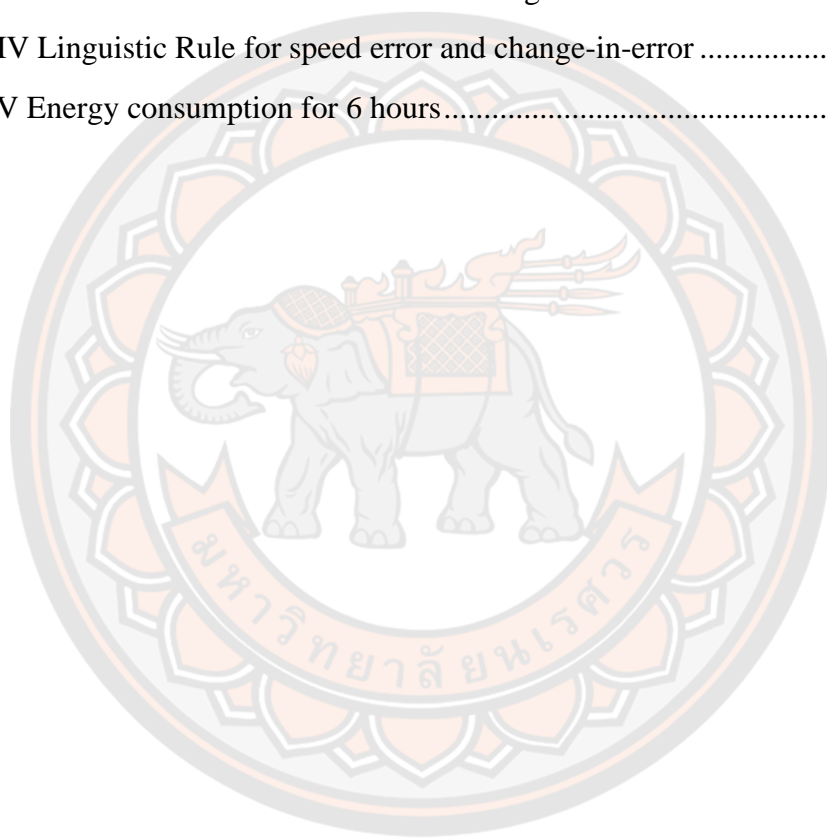
| | |
|--|-----------|
| Induction Motor in Stationary Frame | 26 |
| CHAPTER III PROPOSED SENSORLESS VECTOR CONTROL ARCHITECTURE | 32 |
| Introduction..... | 32 |
| Field Oriented Control | 32 |
| Voltage Source Inverter | 36 |
| Space Vector Modulation (SVM)..... | 40 |
| Sensorless Vector Control Model..... | 46 |
| Model reference Adaptive System (MRAS)..... | 48 |
| Reference Model..... | 49 |
| Adaptive Model | 50 |
| Adaptation Mechanism | 54 |
| Fuzzy Logic Controller..... | 54 |
| Membership functions | 55 |
| Fuzzy Inference Engine | 57 |
| Normalizing Factor..... | 62 |
| Controllers | 63 |
| Open-loop Control of Compressor Motor | 65 |
| CHAPTER IV HARDWARE DEVELOPMENT, EXPERIMENTAL WORKS AND RESULTS | 69 |
| Introduction..... | 69 |
| Practical Implementation of Proposed Method | 69 |
| Rectifier | 70 |
| DC-Link Capacitor | 71 |
| Voltage Source Inverter | 72 |
| IGBT | 73 |
| TMS320F28069M TI's Launchpad and CCS Programming..... | 76 |
| Fixed-Point Programming and Q-format Representation..... | 77 |
| DSP Programming | 79 |
| Generation of PWM | 81 |

| | |
|---|-----|
| ADC Configuration | 84 |
| Hardware Interrupt Service Routine (ISR) | 87 |
| EQEP | 88 |
| RESULTS | 90 |
| Software Simulation Results..... | 90 |
| 3-hp, 4-pole Motor Results | 94 |
| Results for Compressor Motor..... | 97 |
| CHAPTER V DISCUSSION, FUTURE WORKS AND CONCLUSION | 101 |
| Discussion and Future Works..... | 101 |
| Conclusion | 102 |
| REFERENCES | 103 |
| BIOGRAPHY | 113 |



List of tables

| | Page |
|---|-------------|
| Table I Various applications of FLC for different purposes by different companies | 10 |
| Table II Arbitrary Reference Equations in terms of $\psi s'$ and X's | 25 |
| Table III Two-Level Three Phase VSI Switching Table | 42 |
| Table IV Linguistic Rule for speed error and change-in-error | 59 |
| Table V Energy consumption for 6 hours..... | 100 |



List of figures

| | Page |
|--|-------------|
| Figure 1 3-phase to 2-phase transformation..... | 15 |
| Figure 2 Clarke Transformation in arbitrary reference frame | 16 |
| Figure 3 Park Transformation in arbitrary reference frame..... | 17 |
| Figure 4 Reference Frame Transformation matrices | 18 |
| Figure 5 Cross-sectional representation of Induction Motor | 20 |
| Figure 6 Dynamic Equivalent Circuit of Induction Motor | 27 |
| Figure 7 Simulink Model of Induction Motor | 29 |
| Figure 8 Q-axis Model..... | 29 |
| Figure 9 Clark Transformation of voltages..... | 30 |
| Figure 10 D-axis model | 30 |
| Figure 11 zero sequence model..... | 30 |
| Figure 12 Rotor Model..... | 31 |
| Figure 13 Inverse Clarke Transformation for motor currents..... | 31 |
| Figure 14 Types of Variable Frequency Drives (VFD) | 32 |
| Figure 15 Current and Flux vector in Synchronous Reference Frame | 33 |
| Figure 16 Block diagram of sensorless vector control method for IM..... | 36 |
| Figure 17 Two-Level Voltage Source Inverter Circuit..... | 39 |
| Figure 18 Switching algorithm for VSI. (a) switching states of inverter switches, (b) Hexagonal sectors for space vector..... | 41 |
| Figure 19 SVM with symmetrical switching sequence for sector 1. (a) Timing graph, (b) voltage synthesis to obtain reference voltage..... | 45 |
| Figure 20 Technique to select the sector number. | 46 |
| Figure 21 Vector Control Model of Induction Motor control with Fuzzy Logic Controller | 47 |
| Figure 22 Rotor-Flux MRAS system..... | 48 |
| Figure 23 Fuzzy-PI controller model..... | 55 |

| | |
|---|----|
| Figure 24 Membership function definition. (a) Triangular membership function, (b) Trapezoidal membership function | 56 |
| Figure 25 Membership Functions | 57 |
| Figure 26 Schematic of Fuzzy Logic Controller..... | 58 |
| Figure 27 Fuzzy Inference System | 61 |
| Figure 28 Scaling factors for fuzzy controller | 62 |
| Figure 29 Control Algorithm and setup with Proposed method..... | 66 |
| Figure 30 Setup for the proposed algorithm | 67 |
| Figure 31 Temperature Measurement Unit..... | 67 |
| Figure 32 Membership Functions for temperature controller..... | 68 |
| Figure 33 Laboratory Hardware Arrangement | 69 |
| Figure 34 Power supply and protection layout | 70 |
| Figure 35 Three-phase rectifier. (a) 3-phase rectifier module, (b) circuit configuration of the module | 71 |
| Figure 36 Inverter circuit showing DC-link Capacitor | 72 |
| Figure 37 Inverter circuit | 73 |
| Figure 38 IGBT Module. Semikron SKM100GB12T4, SEMITRANS2, N-Channel Dual Half Bridge IGBT Module, 160 A max, 1200 V, Panel Mount..... | 74 |
| Figure 39 Voltage Source Inverter circuit. (a) Inverter accessories and (b) sensor and rectifier..... | 75 |
| Figure 40 DSP Layout | 76 |
| Figure 41 Flowchart for the program execution in CCS..... | 80 |
| Figure 42 Action qualifier Module configuration and resultant PWM waveform | 82 |
| Figure 43 PWM outputs. (a) complementary waveform of PWM1A and PWM1B, (b) SVM wave obtained from low-pass RC-filter. | 83 |
| Figure 44 Flow chart for ADC conversion | 84 |
| Figure 45 Action Qualifier Module and resultant PWM waveform..... | 85 |
| Figure 46 ADC logic Layout Diagram | 86 |
| Figure 47 Rotary encoder disk. (a) rotary encoder disk, and (b) alternating pulse generated by encoder | 89 |

| | |
|---|-----|
| Figure 48 Simulation results for closed loop system. (a) Speed, (b) Stator Currents, (c) Q-axis currents (torque component)..... | 90 |
| Figure 49 Torque and flux components. (a) Load and Shaft torque, and (b) d-axis current | 91 |
| Figure 50 Comparative results for PI and Fuzzy PI controller. (a) Speed, (b) current, and (c) torque | 92 |
| Figure 51 sensorless behavior using Fuzzy Logic Controller. (a) Motor speed, (b) Torque producing current (I_q), (c) stator currents | 93 |
| Figure 52 currents and angle for the sensorless control. (a) d-axis current, (b) rotor position and sine and cosine of rotor position, and (c) Stationary reference frame currents..... | 94 |
| Figure 53 Forward-reversing phenomenon for induction motor | 95 |
| Figure 54 Step reference tracking behavior for motor | 96 |
| Figure 55 Hardware results for closed loop system. (a) Speed, (b) Stator current (I_a), (c) Q-axis current | 97 |
| Figure 56 Active Power requirement for each method | 98 |
| Figure 57 Power and power factor measurement. (a) Normal operation, (b) inverter-fed operation | 99 |
| Figure 58 Total Harmonic Distortion (THD) for voltage and current. (a) Normal operation, (b) inverter-fed operation..... | 99 |
| Figure 59 Coolant pressure and room temperature. (a) room temperature, (b) coolant pressure | 100 |

ABBREVIATIONS

| | | |
|--------------------|---|---|
| AC | = | Alternating current |
| DC | = | Direct current |
| A.C | = | Air conditioner |
| VFD | = | Variable frequency drive |
| C.T | = | Current transformer |
| FLC | = | Fuzzy logic controller |
| SVM | = | Space vector modulation |
| SPWM | = | Sine pulse width modulation |
| MRAS | = | Model reference adaptive system |
| RTD | = | Resistance temperature detector |
| CCS | = | Code composer studio |
| ADC | = | Analog to digital converter |
| ePWM | = | Enhanced pulse width modulation |
| eQEP | = | Enhanced quadrature encoder pulse |
| FOC | = | Field oriented control |
| VC | = | Vector control |
| PID | = | Proportional, integral and derivative |
| hp | = | Horse power |
| HVAC | = | Heating, ventilation and air conditioning |
| r_s | = | stator winding resistance, Ω |
| r_{pr} | = | rotor winding resistance, Ω |
| L_{ls} | = | stator winding leakage inductance, H |
| L_{lr} | = | rotor winding leakage inductance, H |
| L_s | = | stator self-inductance, H |
| L_r | = | rotor self-inductance, H |
| L_m | = | magnetizing inductance, H |
| P | = | number of poles, no |
| v | = | rms voltage, V |
| i | = | rms current, A |
| B | = | motor damping coefficient |
| J | = | moment of inertia |
| T_{em} | = | electromechanical torque (externally applied), Nm |
| T_{mech} | = | electromechanical torque, Nm |
| T_{damp} | = | damping torque, Nm |
| ω_e | = | synchronous speed, rad/sec |
| ω_r | = | rotor speed, rad/sec |
| ω_s | = | synchronous speed, rad/sec |
| f_{abc} | = | three-phase stator voltage, current or flux linkages |
| f_{abr} | = | three-phase rotor voltages, currents or flux linkages |
| $T_{dq0}(\theta)$ | = | Transformation matrix |
| f_{dq0s}^ω | = | stator voltages, currents or flux linkages in $d, q, 0$ – arbitrary frame |
| f_{dq0r}^ω | = | rotor voltages, currents or flux linkages in $d, q, 0$ – arbitrary frame |
| $f_{dq0r}'^\omega$ | = | Rotor voltage, current or flux linkage referred to stator in |

| | | |
|----------------|---|--|
| | = | arbitrary reference frame |
| f_{dq0s}^e | = | Stator voltage, current or flux linkage in synchronous reference frame |
| f_{dq0r}^e | = | Rotor voltage, current or flux linkage in synchronous reference frame |
| S_{bc} | = | Base power, VA |
| T_{bc} | = | base torque, Nm |
| I_{bc} | = | base current, A |
| V_{bc} | = | base voltage, V |
| λ_{bc} | = | base flux, Wb. turn |
| Z_{bc} | = | base impedance. Ω |
| θ_r | = | rotor position, rad |
| ϕ | = | phase angle between voltage and current, rad |
| l | = | Axial length of air-gap, m |
| r | = | radius to mean of air-gap, m |
| g | = | air-gap length, m |
| μ_0 | = | permeability of air or free space, H/m |
| N_s | = | Number of winding in stator, no |
| N_r | = | Number of windings on rotor, no |
| e_ω | = | Speed error, rad/sec |
| K_p | = | Proportional gain |
| K_i | = | Integral gain |
| K_1 | = | normalizing factor for error |
| K_2 | = | normalizing factor for derivative of error |
| K_3 | = | denormalizing factor for output |

CHAPTER I

INTRODUCTION

Preface

In the recent years, demand for electrical energy is increasing and thus the gap is becoming wider between the demand and supply of it. Of the total demand, almost 85-90% of it accounts for heating and cooling purpose in the households.

Air conditioners (ACs) has become indispensable commodity in modern life and thus, it is also one of the major contributors to energy consumption in a household. About 90% of the energy consumption is by the compressor motor and is also the backbone of air conditioning system which control the inside temperature. However, the conventional air conditioning system has simplest ON/OFF type of controller. If the inside temperature is greater than the set temperature, the compressor motor is turned On and OFF otherwise. This type of system creates discomfort the ear to the inhabitants and also neighbors in a way by the loud noise produced during frequent ON/OFF behavior. Also, frequent ON/OFF creates sudden fluctuation in room temperature creating health issues such as headache. Therefore, the air conditioning system which can have automatic control of room temperature is proposed in this project. The proposed system will have provision for compressor motor to have operation at reduced speed when the actual temperature reaches or is less than the set temperature so as to compensate the loss and maintain constant temperature throughout would have better energy saving while improving the human comfort. This can be achieved by employing the intelligent controller technique with variable frequency drive system. The latter is becoming famous for the speed control of induction motor which has capability to control due to its capability to provide variation in frequency in addition to the magnitude to the voltage signal by synthesizing the fixed DC voltage.

This work basically aims at obtaining speed control of induction motor to have better energy utilization while still serving as the most robust, simple and cheap motor in the market. This includes exploring for the variable frequency drive technology with intelligent controller techniques like noble fuzzy logic controller. Further, to reduce the cost of the combined VFD technique, the sensorless technology is investigated. This technique would improve reliability also. Furthermore, in order to reduce the harmonic distortion due to inverter, the space vector modulation algorithm is adopted. The combined sensorless algorithm is investigated in the compressor motor.

Literature Survey

The induction motor besieges the market and in the industries because of its innate advantages compared to any other motor not to forget the fan and compressor used in air conditioner uses induction motor. The main problem faced in past with the induction motor was its inability to have variable speed capability which many applications requires variable speed. Moreover, the demand for variable speed drives are increasing day by day in the industries especially in the field of Mechatronics and Robotics. It wouldn't be advisable and efficient to continue using DC motors like in the past. The IM possesses numerous superiority which motivated people to shift attention from DC motors to IM for variable speed applications which are summarized as (Hule, Bindu R., & Vincent, 2014):

- They have simple and rugged structure. An external resistance can be connected arbitrarily if starting torque is to be increased with reduced inrush currents for wound-rotor. It doesn't require field winding or additional supply to excite the windings. Moreover, it doesn't have commutators or brushes.
- No professional personnel are required to do maintenance. The electrical fault can be detected mostly using multimeter.
- Since no additional supply or equipment is required, it offers better economy of operation, and
- Compared with brushed motors, this motor can be designed to give substantially higher output ratings with lower weights and lower inertias for equivalent motor ratings, and

There are various traditional control techniques employed in induction motor (2017). There are basically six types of speed control techniques broadly classified out of which three are achieved at stator side and another three at rotor side. The control from stator side includes changing supply frequency, changing number of stator poles and changing the supply voltage. Similarly control from rotor side is achieved either by inserting resistance in the rotor circuit (in wound motor), injecting EMF in rotor circuit and, cascade connection methods. However, not even one of the classical speed control methods are feasible due to its own shortcomings in industrial applications.

Thanks to modern variable frequency drive technology, there are number of most recent and efficient speed control techniques employing the variable frequency drive technology for induction motor (Das, 2016). This was possible with the development of fast power electronic switches which ultimately gave birth to new industrial revolution (Rashid, 2001). The market for variable speed drive system is increasing in both size and number displacing the traditional fixed supply because the new system has improved efficiency in terms of energy conversion and functionality (Zipan Nie, Preindl, & Schofield, 2016). Owing to the fact that the increasing demand for bigger motors in the industries, multilevel inverters are also been designed and have been

receiving increased attention (Jih-Sheng Lai & Fang Zheng Peng, 1996). Using the same power switches, they have higher voltage ratings than their two-level equivalents. Also, their output voltage waveforms are distinctly superior to these in two-level inverters, especially in the square-wave mode. Innovation of variable-speed drives are a continuous process. Their development is characterized by ultra-fast, robust, economic and reliable drives for the use in factories and industries. The rapid advancements made in the field of microprocessors and DSPs has contributed significantly to the development of various high-performance ac drives, since it has become possible to introduce relatively complicated control systems in these drives. The Texas Instruments is one of the main developers for motion control DSP. For example, TMS320F28069M InstaSpin launchpad is developed particularly for the motor control purposes.

The two broad control techniques which can be achieved with the use of variable frequency drive are scalar control and vector control techniques. First, the scalar methods for VFD control work by optimizing the motor flux and keeping the strength of the magnetic field constant, which ensures constant torque production. Often referred to as V/Hz or V/f control, scalar methods vary both the voltage (V) and frequency (f) of power to the motor in order to maintain a fixed, constant ratio between the two, so the strength of the magnetic field is constant, regardless of motor speed (Alizadeh, Masoumi, & Ebrahim, n.d.). The appropriate V/Hz ratio is equal to the motor's rated voltage divided by its rated frequency. V/Hz control is typically implemented without feedback (i.e. open-loop), although closed-loop V/Hz control — incorporating motor feedback — is possible. V/Hz control is simple and low-cost, although it should be noted that the closed-loop implementation increases cost and complexity. Control tuning is not required but can improve system performance. Speed regulation with scalar control is only in the range of 2 to 3 percent of rated motor frequency, so these methods aren't suitable for applications where precise speed control is required. Open-loop V/Hz control is unique in its ability to allow one VFD to control multiple motors and is arguably the most-commonly implemented VFD control method.

Vector control, also referred to as field-oriented control (FOC) which was first proposed by Blaschke (Blaschke, 1972) controls the speed or torque of an AC motor by controlling the stator current space vectors, in manner similar to (but more complicated than) DC control methods (Das, 2016; Hannan et al., 2018). In the past such control techniques, were not possible because of the complex hardware and software required to solve the complex control problem. In contrast to a dc machine, in an ac machine, both the phase angle and the modulus of the current has to be controlled. In other words, the current vector has to be controlled precisely. This is the reason for the terminology “vector control” is used which requires the accurate control of both magnitude and direction instead of just magnitude in scalar control method. The merits of using vector control can be summarized as:

- The frequency of the drive is not directly controlled as in scalar control. The machine is essentially ‘self-controlled’, where the frequency as well as the phase are controlled indirectly with the help of unit vector.
- There is no fear of an instability problem by crossing the operating point beyond the breakdown torque as in a scalar control. Limiting the total current vector within the safe limit automatically which limits operation within the stable region.
- The transient response will be fast and dc machine-like because torque control by q – axis current does not affect the flux. However, it is to be noted that ideal vector control is impossible in practice because of delays in converter and signal processing and the parameter variation effect.
- Like a dc machine, speed control is possible in four quadrants without any additional control elements (like phase sequence reversing). In forward motoring condition, if the electromechanical torque is negative, the drive initially goes into regenerative braking mode, which slows down the speed. At zero speed, the phase sequence of the unit vector automatically reverses giving reverse motoring operation.

In FOC, the stator current is converted to DC-equivalent quantity (d, q –) axis currents with the help of forward Clarke and Park Transformation at synchronously rotating reference frame (Lftisi, George, & Rahman, 2017). The Park transformation has long been widely used in the analysis and study of synchronous and induction machines (Das, 2016). The transformation is by far the single most important concept needed for an understanding of how FOC works, the concept which was first conceptualized in a 1929 in paper authored by Robert H. Park (A. S. Muktar, R. Umale, & K. Kirpane, 2017). The novelty of Park's work involves his ability to transform any related machine's linear differential equation set from one with time varying coefficients to another with time invariant coefficients (Das, 2016). The invariant d, q – currents are controlled just like in the separately-excited DC motor. The d – component of current is responsible for controlling the flux and q – component of current is responsible in controlling the torque. They are orthogonally aligned (such that, when torque is controlled, the field flux is not affected, hence enabling dynamic torque response).

There are two vector control methods, direct or feedback vector control (DFOC) and indirect or feed-forward vector control (IFOC). Conventional direct field-oriented control (DFOC) algorithms provide more precision for torque control than scalar schemes, but require sensors for the speed control of the rotor and the magnetic flux to provide the data for the FOC algorithms. They also face challenges in the dynamic response and the dependence on measuring the parameters in the motor. On the other hand, an indirect field-oriented control (IFOC) method estimates the phase angle of the rotor magnetic field flux, eliminating the need for additional sensors but adding to

the complexity and the computation time of the control system. IFOC are being more commonly used because in closed-loop mode such drives more easily operate throughout the speed range from zero speed to high-speed field-weakening. The flux space angle feed forward and flux magnitude signals first measure stator currents and rotor speed for then deriving flux space angle proper by summing the rotor angle corresponding to the rotor speed and the calculated reference value of slip angle corresponding to the slip frequency.

The direct torque control (DTC) was proposed to replace the FOC in drives domain in order to achieve efficient decoupled control of flux and electromagnetic torque (Ammar, Bourek, Benakcha, & Ameid, 2017). DTC due to the fact that it doesn't require coordinate transformation or current regulation (Casadei, Profumo, Serra, & Tani, 2002), it has simpler control scheme with faster response and low dependence to the machine parameters compared to FOC. On the contrary, it produces high flux and torque ripples due to variable switching frequency (Alsofyani & Idris, 2016).

The difference between the scalar and vector control method is nicely reviewed by Hannan et al (Hannan et al., 2018) with extensive focus using space vector pulse width modulation techniques. A large number of papers on vector control are being published. Still, researchers find it difficult to follow this technique as most of the available literature does not detail the design of vector control (Divyasree & Binojkumar, 2017). The key features that differentiates vector control from scalar control are:

- Vector control is designed to operate with a standard a.c., squirrel-cage, asynchronous motor of known characteristics. The only addition to the motor is a rotary position encoder.
- A vector controller and its associated induction motor form an integrated drive; the drive and the motor have to be matched to achieve satisfactory operation.
- A vector-controlled induction motor and drive is capable of controlling in all four quadrants through zero speed, without any discontinuity. In addition, the drive is capable of holding a load stationary against an external applied torque.
- The vector-controlled-induction-motor's supply currents are controlled, both in magnitude and phase in real time, in response to the demand and to external disturbances.

Various Pulse Width Modulation (PWM) techniques are proposed to generate a variable voltage, variable frequency, three-phase AC using VSIs for variable speed AC drives (Divyasree & Binojkumar, 2017). PWM switching techniques used in the inverter fed induction motor includes Sine PWM (SPWM), space vector PWM (SVPWM/SVM), carrier-based PWM, selective harmonic elimination PWM, and harmonic based PWM (HBPWM), etc.

Sine PWM (SPWM) is a popular and widely used PWM strategy due to the simplicity in application. It has capability to reduce the low frequency harmonics in the output

waveform, low power consumption, high efficiency up to 90%, high power handling capacity, etc. (Kumar & Batra, 2016). However, Attenuation of the wanted fundamental component of the waveform, drastically increased switching frequencies that leads to greater stresses on associated switching devices and therefore de-rating of those devices, and generation of high-frequency harmonic components are major drawbacks of SPWM.

SVM provides higher DC bus utilization, lower switching loss and reduced harmonic distortion (THD) compared to SPWM (Hannan et al., 2018; Varma & Narayanan, 2006). It is proposed to replace the switching table by voltage vector selection (Ammar et al., 2017). If the switching frequency can be preserved at a constant value, then the flux and torque ripples can be reduced to a greater extent. Space-Vector modulation (SVM) was originally developed as a vector approach to pulse –width modulation (PWM) for three-phase inverter and the claims made for SVM include the following (Reney, 2011):

- It achieves the wider linear modulation range associated with PWM third – harmonic injection automatically without the need for distorted modulation.
- It has lower base band harmonics then compared to regular PWM or another sine-based modulation method, or otherwise optimizes harmonics.
- It is fast and convenient to compute.

The terminology “sensorless” refers to the fact that no conventional speed or position monitoring devices (e.g. tachometer-based speed sensors, optical incremental sensors or electromechanical resolvers) are used in these drives (Rashid, 2001). In recent years, various sensorless control schemes have been developed for variable-frequency AC drives (Comanescu & Xu, 2006; Tsuji, Shuo Chen, Izumi, & Yamada, 2001; Yuntao & Yan, 2011). The main reasons for the development of these sensorless drives are (Hule et al., 2014; Peter Vas, 1998; Zaky, Khater, Yasin, & Shokralla, n.d.): reduction of hardware complexity and cost, increased mechanical robustness and overall ruggedness, operation in hostile environments, higher reliability, decreased maintenance requirements, increased noise immunity, unaffected machine inertia, improvement of the vibration behavior, elimination of sensor cables etc. In sensorless drives, the speed and/or the position signal is obtained by using monitored voltages and/or currents and by utilizing mathematical models or artificial intelligence-based systems (Rashid, 2001),[17]. The state-of-the-art research in the field of sensorless AC drives is related to speed and position sensorless drives operating in the very low speed range [43].

An angular velocity of rotor-flux vector and slip calculation methods based on the rotor-flux-vector coordinates obtained from IM model are simplest sensorless speed estimator among many (Comanescu & Xu, 2006; Orłowska-Kowalska & Dybkowski, 2010). Although this method is simple and popular, the obtained accuracy is not so good due to sensitivity to motor-parameter uncertainties. Extended

Kalman filter or extended Luenberger observer are more robust to motor-parameter uncertainties but are much more complicated in practical implementation (Comanescu & Xu, 2006; Orłowska-Kowalska & Dybkowski, 2010). Another famous speed estimation method; Model reference adaptive system (MRAS) has advantage of its simplicity, better performance and thus the easy implementation and direct physical interpretation, compared to non-linear extended state observer or Kalman filter (Ammar et al., 2017; Hule et al., 2014; Orłowska-Kowalska & Dybkowski, 2010). In this scheme, the error vector is calculated from the output of reference and adaptive model, both dependent on different motor parameters. The error is driven to zero through adjustment of the parameter which influences one of the models. MRAS-based speed estimator developed so far can be classified into three types (Orłowska-Kowalska & Dybkowski, 2010). The first method is called the rotor-flux-error-based MRAS scheme (RF_MRAS), also called classical MRAS speed estimator. It was developed by Tamai et al (Tamai, Sugimoto, & Masao, 1987) and Schauder (Schauder, n.d.) which basically estimates the motor speed by synthesizing the stator and rotor fluxes of the motor. The modifications are done on classical MRAS by (Comanescu & Xu, 2006). This is one of the widely used method (Ammar et al., 2017). In this method, the voltage and current models of IM are used to generate the rotor flux error. PI controller is usually used in adjustable model to derive error signal to zero by varying P and I gain. The main drawback is it is highly sensitive to motor-parameter variation due to highly sensitive rotor-flux current and voltage models used for rotor-flux-vector estimation.

The second classification is called the back-electromotive force based MRAS (BEMF_MRAS) method is obtained by comparing the measured and calculated back-emf of the IM. The error is corrected as in rotor-flux-based MRAS. However, BEMF_MRAS is believed to have inferior performance (Comanescu & Xu, 2006).

The third method called the stator-current-error-based MRAS is not so popular. In this scheme, the speed is estimated by comparing the calculated stator-current to the measured stator-currents and then feeding to the adjustable model to make the error to zero. However, aforementioned novel MRAS based estimation methods fails to perform accurately at low or zero speed (Yuntao & Yan, 2011). Many literatures are present online which are proposed as an alternative or modifications in the in leu of native MRAS to combat the shortcomings. For instance, Yuntao and Yan (Yuntao & Yan, 2011) has proposed an intelligent novel fuzzy sliding-mode structure controller which combines the best of sliding-mode control (SLMC) and fuzzy logic-based control (FLBC). This system has the advantage of coping up with the dynamic response by enlarging the stability limit of the system by earlier and enhanced steady state performance by reducing chattering by latter. Maiti et al (Maiti, Chakraborty, Hori, & Ta, 2008) has proposed slip speed estimation using online rotor resistance estimation by utilizing the reactive power MRAS system. This method has various advantages: it maintains proper flux orientation in indirect vector-

controlled IM, independent of stator resistance, eliminates the requirement of flux estimation block, less sensitive to integrator related issues like drifts and saturation due to absence of integrator, and can quite satisfactorily estimate the speed at or near zero speed. Similarly, Mahanalakshmi et al (Comanescu & Xu, 2006) has proposed single and double-manifold sliding mode observer in conjunction to classical MRAS. The sliding-mode estimates the speed by algebraic calculation that do not exhibit underdamped poles and zeros on the right-hand plane. In addition, nonideal integrator problem is solved using low-pass filters. The proposed method is easy to implement; however, appropriate selection of the sliding-mode gains is required and introduction of LPF further complicates the system dynamics. Based on the discussions from literatures, fuzzy logic-based rotor-flux MRAS is proposed in this work for achieving sensorless speed control of IM.

The use of classical PI-controller requires a specific knowledge of control system modeling. Gain selection is another complex task. Moreover, it has limited performance when there is disturbance and uncertainties in the system which results in poor dynamic behavior and stability issue of the system (Ammar et al., 2017),[48],[49]. However, some conventional control theorists often argue that, it is not necessary to use FLC to replace classical controller in drives, because classical control theory is well developed; the implementations are straight forward, convenient and easy. However, ignoring the fact that recently emerging universal drives (a single drive, where software is used to implement various open-loop and closed drive configurations) and electronic motors (comprising of integrated motor and controller), the manufacturers of the power electronic devices and the motor are different and also there is no precise advance knowledge of the load or other changing operational conditions (P. Vas, 1999). In addition, there may not be enough information on the motor (parameters) to enable direct and fine tuning using mathematical model-based approaches. Thus, even if software and hardware implementations of tunable controllers are available, their tuning is not straightforward task and cannot be done in advance, but ideally it must be performed online.

The fuzzy theory was first introduced into the scientific literature as an extension to Boolean set theory that was multi-valued rather than binary in 1965 by Zadeh (Zadeh, 1965) who is also known as the founder of fuzzy logic. His fuzzy-logic set theory is a generalization of classical set theory; a generalization that deals excellently with imprecision. The idea of using fuzzy logic arose from a desire to incorporate logical reasoning and the intuitive decision making of an expert operator into an automated system (Zadeh, 1973). The power of fuzzy logic is that it enables the user to accurately describe a process or behavior without using mathematics. It is a tool for dealing with uncertainties and ambiguity in systems like “tall”, “short”, “few”, “many” etc. The aim is to make decisions based on a number of learned or predefined rules, rather than numerical calculations. Qualitative and heuristic considerations,

which cannot be handled by conventional control theory can be used for control purposes in a systematic form by applying fuzzy control concepts. In general, the fuzzy logic provides a decision-making capability that enables appropriate human reasoning capabilities. The theory of fuzzy logic is based upon the notion of relative graded membership and so are the functions of mentation and cognitive processes. The utility of fuzzy sets lies in their ability to model uncertain or ambiguous data (Sivanandam, Sumathi, & Deepa, 2007). The fuzzy logic incorporates a rule-base structure in attempting to make decisions [4],[42]. However, before the rule-base can be used, the input data should be represented in such a way as to retain meaning, while still allowing for manipulation.

FLC in last few years have attracted growing interest in motor control applications due to its ability to handle non-linearities and its independency of the plant model (Kimiaghalam, Rahmani, & Halleh, 2008). The FLC operates in a knowledge-based manner, and its knowledge relies on a set of linguistic if-then rules; similar to a human operator. Fuzzy logic defines some intermediate values between sharp appraisals like absolute or exact entities. It is more or less like human thinking because it is based on degree of truth and also uses linguistic variables. Due to its vagueness, fuzzy logic system was considered not acceptable theory in field of engineering that time, however from early 1970s, set theory has become very famous and was widely applied in engineering field (Kayacan, 2011). The first industrial application of fuzzy logic controller was in cement kiln in Denmark in 1975 followed by Fuji Electric for water purification process control in 1980. After fuzzy logic controller was used in Sendai Railway system for automatic train operation which was one of the challenging projects in 1987, fuzzy logic became a widely used control in trains like acceleration, breaking and stopping of it. Currently, not only the engineers but also social scientists apply fuzzy logic for different areas like air-conditioner, video cameras, televisions, washing machines, bus time tables, medical diagnoses, antilock braking system etc. (Kayacan, 2011). The number of membership functions and rules are selected based on trial and error approach in the conventional FLC structure. However, this method requires a lot of computation and time until the favorable solution is achieved (Hannan et al., 2018). The advantages of using fuzzy logic controller is summarized as (P. Vas, 1999):

- Conventional controllers require significant redesigning when plant characteristics, plant configuration, and plant environment change when there are parameter variations.
- Fuzzy logic is the solution if existing traditional controllers must be augmented or replaced to provide self-tuning, to give more flexibility of controller adaptivity, to monitor plant etc.
- It is easier to design and implement a fuzzy rule base that will control a complex plant (when the plant is highly non-linear, complex environment that is impossible, or at least cost prohibitive, to model efficiently)
- If sensor accuracy (or precise) is a problem, fuzzy logic can handle imprecise

measurements, uncertainties.

- FLC enables automated adaptive tuning, condition monitoring and diagnoses.
- To obtain solutions when inputs are uncertain or are conflicting or when solutions are not possible by using other techniques.
- To enable rapid development, simplifications, cost effectiveness, high competitiveness, new markets, decreased development and implementation time

According to Texas Instruments, the implementation of their fuzzy logic-controlled induction motor drive required only one fourth of the development time required for the implementation of the same drive using classical controllers. Same results were obtained for dc and ac machine drive implementations in SGS Thomson, Intelligent Motion Control Group at Aberdeen University (P. Vas, 1999). The application of FLC may also result in controllers, which are simpler than those using conventional, mathematical models.

The Table I below shows the proven advantages and applications of fuzzy logic controller used by many companies for different purposes.

Table I Various applications of FLC for different purposes by different companies

| | |
|---|--|
| Optimization | <ul style="list-style-type: none"> ◦ Mitsubishi fuzzy logic air-conditioner (power consumption reduction, improved temperature stability). ◦ Daimler Benz automatic transmission systems, ABS system. ◦ Siemens (home appliances, engine idle-speed controllers, traffic control) |
| Fewer, less expensive sensors | <ul style="list-style-type: none"> ◦ Fuzzy Logic incorporates imprecision and uncertainty. |
| Rapid product prototyping and development | <ul style="list-style-type: none"> ◦ Matsushita (Panasonic) automatic washing machine, vacuum cleaner, rice cooker, refrigerators, image-stabilized camcorders. ◦ Rockwell International Corp., engine idling control ◦ Omron temperature controller ◦ Canon autofocus camera, photocopier ◦ Sanyo, Mitsubishi tv (contrast, brightness control) ◦ Mitsubishi data compression ◦ SGS Thomson dc and ac drive applications ◦ Texas Instruments DSP-controlled induction motor drive |
| Inexpensive implementation in terms | <ul style="list-style-type: none"> ◦ Mitsubishi 8-bit μC-based air-conditioning control system |

| | |
|--|--|
| of μp memory | <ul style="list-style-type: none"> ◦ 4-bit μp for washing machine applications ◦ Sanyo-Fischer video camcorder (reduced μp). |
| Elimination of need to formulate sophisticated models of the process or plant to be modelled | <ul style="list-style-type: none"> ◦ Mamdani automated operation of cement kilns ◦ INFORM wastewater treatment |
| Support human decision making | <ul style="list-style-type: none"> ◦ Zimmerman & INFORM Corporation's bank decision support system |

Source: (P. Vas, 1999)

There are three main fuzzy logic inference systems viz. Mamdani-type, Sugeno-type and Tsukamoto-type. Mamdani -type fuzzy logic inference system; introduced to literature by Mamdani and Assilian in 1975 (Mamdani & Assilian, 1975), contains four main parts: fuzzifier, knowledge base, inference engine and defuzzifier. This is widely used method.

The Sugeno-type inference system which was first introduced into literature by Sugeno and Kang (Sugeno & Kang, 1988) is also popular type of fuzzy logic function approximator next to Mamdani-type. It has two main blocks (fuzzifier and inference engine), but there is no separate defuzzification block. The absence of defuzzification block makes this type more advantageous because it avoids to use a time-consuming defuzzification and thus was used extensively in Japan. The output membership function is not a distributed function but a single spike called singleton. Similarly, the third type Tsukamoto-type; proposed by Tsukamoto in 1979 also contains two blocks like in Sugeno-type. The difference in this type is, in the rule base, the consequent of each rule is represented by a fuzzy set with a monotonic output membership function. The inferred output of each rule (crisp value) is used to obtain the overall output, which is weighted average of each rule's output. This method also can avoid time-consuming defuzzification used in Mamdani-system.

Thailand is the only country in Southeast Asia that has maintained an energy efficiency labelling program since the 1990s as per M. Kojima and M. Watanabe (Kojima & Watanabe, 2016). ACs are listed as one of the specific methods of building energy efficiency in Part 2 of the Energy Conservation Promotion Act which was promulgated in 1992 which requires the government to create energy efficiency standards for various types of equipment. In the mid-1990s, Thailand began its labelling program for energy efficient products. This program was initiated by the Electricity Generating Authority of Thailand (EGAT). World Bank and Japan's Overseas Economic Cooperation Fund has also supported this move by promoting efficient lightings and cooling systems in the country (Kojima & Watanabe, 2016). This motivated many researchers and engineers to work on increasing energy efficiency in air conditioning system in line with improving the human comfort.

Different methods of measuring room temperature with maximum accuracy are proposed which leads to replacing the conventional bimetallic bar for temperature sensing like mobile phones, wearable devices etc. (Chengand & Lee, 2014). The methods of developing new energy-efficient equipment, applying complex control strategies, using solar energy as a new energy source, etc. are all being considered for saving energy in ACs. Among them, applying control strategies may be the more economical and efficient method. Energy-efficient control strategies for controlling variable speed pumps in a central AC are illustrated by Ma and Wang (Ma & Wang, 2009). The results show that the energy consumption of pumps can be lowered by using these control strategies. A feedback controller for ACs is designed and improves the energy efficiency of an ACs (Lin & Yeh, 2007). Zhao et al. (Zhao, Liu, Zhang, & Jiang, 2011) presented a temperature and humidity-independent control strategy to reduce the energy consumption of an ACs in an office building. The experimental results show that the strategy can provide a better coefficient of performance of the ACs and a comfortable indoor environment even in very hot and humid weather. For multi-unit ACs, a fuzzy logic control strategy is used to control the operational number of compressors and fans to enhance energy efficiency (Chiou, Chiou, Chu, & Lin, 2009). The previous researches of applying control strategies on ACs are based on the difference of parameters and cause the reaction. This is one kind of passive responses and may not be suitable for human comfort. Since, reducing energy consumption and to ensure thermal comfort are two important considerations for the designing an air conditioning system, an alternative approach to reducing energy consumption was proposed in (Nasution, Jamaluddin, & Mohd. Syeriff, 2011) by Nasution et al; to use a variable speed compressor using the fuzzy logic controller (FLC). Just for two hour of recording, energy saving achieved by running the system at various internal heat loads (0, 500, 700, and 1000 W) and various temperature settings (20, 22 and 24⁰C) are 21.86 to 51.73% saves in comparison with on/off controller; while, in comparison with PID control, the energy saving was 17.76 to 41.93% at setting temperature 20 and 22⁰C. This proves exceptional superiority in terms of energy saving. However, the measure of success cannot be based only on energy saving and methods used but also on some common indicators like harmonic distortions because this can affect whole power system network. Moreover, the paper lacks detail description of the methods.

Aim of Research

The air-conditioner has become the most important component in lives of people residing in lower altitude areas. Maximum energy is wasted in cooling system in Thailand. The need for more accurate control to the entire cooling or heating system has caused a simple switch, relay or contactor to control a motor speed is no longer sufficient. More effective with high performance control strategy is required if there is

need of the energy consumption to be reduced. Also, the Field-Oriented Control being a recent technological reform has put to a limited application. The time has come for new system to be place it into action in the field like controlling in compressor motor rather than just laboratory experiments. Moreover, sensed FOC structure would not be a feasible option for controlling compressor motor due to the fact that it is mounted outdoor and also have no moving shaft exposed out to mount speed encoder. Even if it is possible to mount encoder, the performance cannot guarantee the reliability due to the effect of moisture, pressure and temperature. So, sensorless (open loop) control strategy is the best option discovered. Thus, this project aims to improve the energy saving with improved efficiency in air-conditioners by providing the variable speed control of compressor motor. This method is going to guarantee improved human comfort as well. Variable-frequency drive (VFD) in HVAC system have evolved over the years as the demand for better use of energy. Employing this VFD system would be the best choice to combat the efficiency and power consumption issue in the AC machines.

Scope of Thesis

This thesis consists of five chapters, and are organized as follows: Chapter one covers introduction, background and literature review. Chapter two gives theoretical background of reference frame transformation, mathematical modelling of three phase induction motor and also development of software model in Simulink environment. The proposed architecture of sensorless vector control method is discussed in chapter three. The theoretical background on the space vector modulation-based voltage source inverter are also discussed in this chapter. Moreover, Fuzzy-based Rotor-flux model reference adaptive system for estimating rotor speed is also discussed with discretizing methods to implement in DSP. Chapter four walks you through the hardware development and programming technique in code composer studio. The experimental works (sensored control for 3-hp, 4-pole 3-phase induction motor and open loop control of 7 kW compressor motor) discussed separately are also included in this chapter. Furthermore, the simulation and hardware results are presented in this chapter. Finally, the chapter five includes discussion, conclusion and future work.

CHAPTER II

DYNAMIC MODELING OF INDUCTION MOTOR

Introduction

The modeling and simulation solve real-world problems safely and efficiently. It provides an important method to analysis which is easily verified, communicated and understood. modeling and simulation provide valuable solutions by giving clear insights into complex systems. Asynchronous motor models are classified into two: physical model and behavioral model. In physical model, the law of electromagnetism is used to describe the motor. These models vary in complexity and precision according to the methods adopted in modeling. On the other hand, behavioral model is modified version of physical model by introducing additional parameters. This model allows in the detection and localization of the motor faults. It can directly be used in the diagnosis purpose. In this chapter, the physical model is described using the reference frame transformation theory to ease and simplify the analysis.

Reference Frame Transformation

The electrical machines can be described using a first order differential equations of each windings. Each differential equation is related to each other by a mutual inductance. The stator to rotor mutual inductances, in particular, are functions of rotor position. When the rotor rotates, the mutual coupling terms vary with time which is the root cause of problem in computing transient behavior of the machine. Thus, a mathematical transformation can be used to facilitate the computation of transient solution of induction machine model by transforming the time-varying differential equations to time-invariant one (Ong, 1998). The change of variable in time-invariant reference frame offers the following major advantages:

- i. There is no magnetic coupling between phases, and
- ii. The mutual inductance can be made independent from rotor position by expressing both rotor and stator in the same reference frame, e.g. in the stationary reference frame.

The reference frame transformation was originally proposed by R.H. Park in the late 1920s (Kim, 2017). This transformation was used only for synchronous machines in the synchronous reference frame, which is commonly called Park's Transformation. Since then, several reference frame transformations have been developed for induction and synchronous machines. Later it was found that all known types of reference frame can be obtained from arbitrary reference frames by simply changing the reference speed. This arbitrary reference frame transformation is referred to as the generalized rotating transformation (Krause, Wasynczuk, & Sudhoff, 2002).

- control, the torque producing component of motor current or the back-EMF is aligned along this axis.
- c. zero-axis (neutral or n-axis): The direction of the 0 –variable, which is called 0 –axis, is defined as the direction that is orthogonal to both d –and q –axes. The 0 –axis has nothing to do with the mechanical output power but it is related to the losses in the motor.

Arbitrary Reference Frame

The reference frame transformation can be easily carried out by using the matrix form or complex vectors. The Figure 2 demonstrates the transformation of the three-phase a, b, c – to $d, q, 0$ – variables in the stationary reference frame. The reference frame transformation can be simply considered as the orthogonal projection of the three-phase a, b, c –variables v_a, v_b and v_c onto $d, q, 0$ –axis in the stationary reference frame $d^s - q^s$ axes. The $d, q, 0$ –in stationary reference frame are also called $\alpha, \beta, 0$ –reference frame.

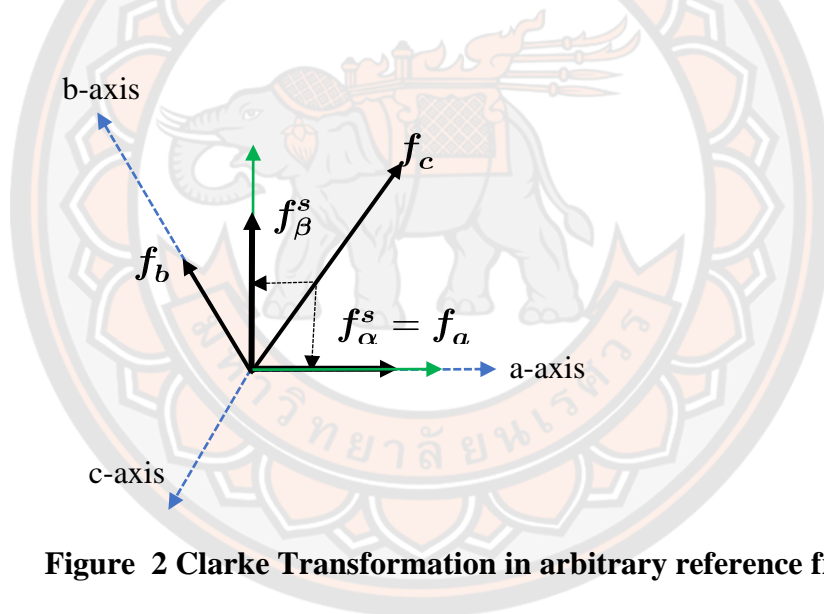


Figure 2 Clarke Transformation in arbitrary reference frame

The frame of reference can be rotated at any angular velocity ω . So, the transformation of the three-phase stationary a, b, c –variables into $d, q, 0$ –variables in the arbitrary reference frame rotating at speed ω can be generally formulated as:

$$f_{dq0}^{\omega} = [T_{dq0} \ \theta] f_{abc} \quad (1)$$

Here f can be used to denote either voltage, currents or flux linkage and superscript ω represents angular speed of reference frame. The $[T_{dq0} \ \theta]$ is the transformation matrix. The balanced three-phase time-domain stationary quantities (voltage, current and flux linkage) can be transformed to dq0-reference frame with the transformation matrix (Filizadeh, 2013; Kim, 2017; Ong, 1998):

$$[T_{dq0} \theta] = k \begin{bmatrix} \cos\theta & \cos\left(\theta - \frac{2\pi}{3}\right) & \cos\left(\theta + \frac{2\pi}{3}\right) \\ \sin\theta & \sin\left(\theta - \frac{2\pi}{3}\right) & \sin\left(\theta + \frac{2\pi}{3}\right) \\ \frac{1}{2} & \frac{1}{2} & \frac{1}{2} \end{bmatrix} \quad (2)$$

In electrical machine context, one of the frames may be chosen. For instance, one may choose the stationary reference frame with $\omega = 0$, a synchronously rotating reference frame with $\omega = \omega_e = 2\pi f_s$ (synchronous speed) or, a reference frame rotating with the rotor with $\omega = \omega_r$.

The matrix coefficient k can be chosen arbitrarily. The coefficient k can be chosen $2/3$ in which it means that the magnitude of $d, q, 0$ – variables are exactly identical to that of the a, b, c – variables. So, this transformation is called ‘magnitude invariance transformation’. However, the power and torque evaluated in $d, q, 0$ – variables become $2/3$ less than those evaluated in a, b, c – variables. On the other hand, when using the coefficient of $\sqrt{2/3}$, the power remains same in two reference frames. So, this transformation is called ‘power invariance transformation’. However, the magnitude of the $d, q, 0$ – variables is not equal to that of a, b, c – variables. The coefficient $2/3$ is mostly used when applying the transformation to motor variables (Kim, 2017). The arbitrary reference frame transformation is shown in Figure 3. The transformation between reference frame can be achieved in two steps. In the first step, the transformation of three-phase a, b, c – variables into $d, q, 0$ – variable in the stationary reference frame can be achieved by setting $\theta = 0$ in Eq. (2).

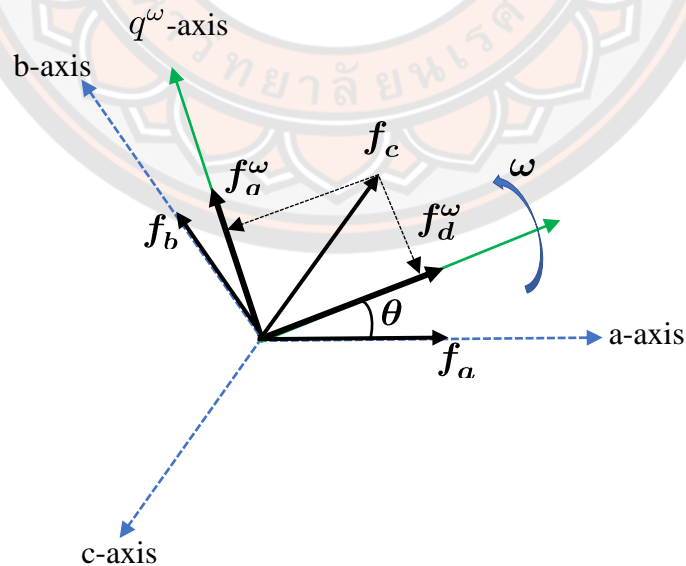


Figure 3 Park Transformation in arbitrary reference frame

Thus, the matrix equation for the reference transformation is:

$$f_{dq0}^s = [T_{dq0} \ 0] f_{abc} = \frac{2}{3} \begin{bmatrix} 1 & -\frac{1}{2} & -\frac{1}{2} \\ 0 & \frac{\sqrt{3}}{2} & -\frac{\sqrt{3}}{2} \\ \frac{1}{\sqrt{2}} & \frac{1}{\sqrt{2}} & \frac{1}{\sqrt{2}} \end{bmatrix} \begin{bmatrix} f_a \\ f_b \\ f_c \end{bmatrix} \quad (3)$$

In the stationary reference frame, the $d, q, 0$ –variables are arithmetically related to a, b, c –variables. In particular, if the sum of the a, b, c –variables in a balanced three-phase with no neutral connection is zero, then the 0 –axis variable is zero. Thus, $f_d^s = f_a$ i.e. the d^s –axis variable is always equal to the phase a-axis variable. This is known as Clarke's transformation.

The second step is the transformation of stationary reference frame into the rotating reference frame which can be formulated as:

$$f_{dq0}^e = [R_{dq0}(\theta)] f_{dq0}^s = \begin{bmatrix} \cos\theta & \sin\theta & 0 \\ -\sin\theta & \cos\theta & 0 \\ 0 & 0 & 1 \end{bmatrix} \begin{bmatrix} f_d^s \\ f_q^s \\ f_0^s \end{bmatrix} \quad (4)$$

This is known as Park's transformation. The vice versa can be achieved by simply rearranging the terms in Eq. (3) and (4). The reference frame transformation from one frame to another is summarized in Figure 4.

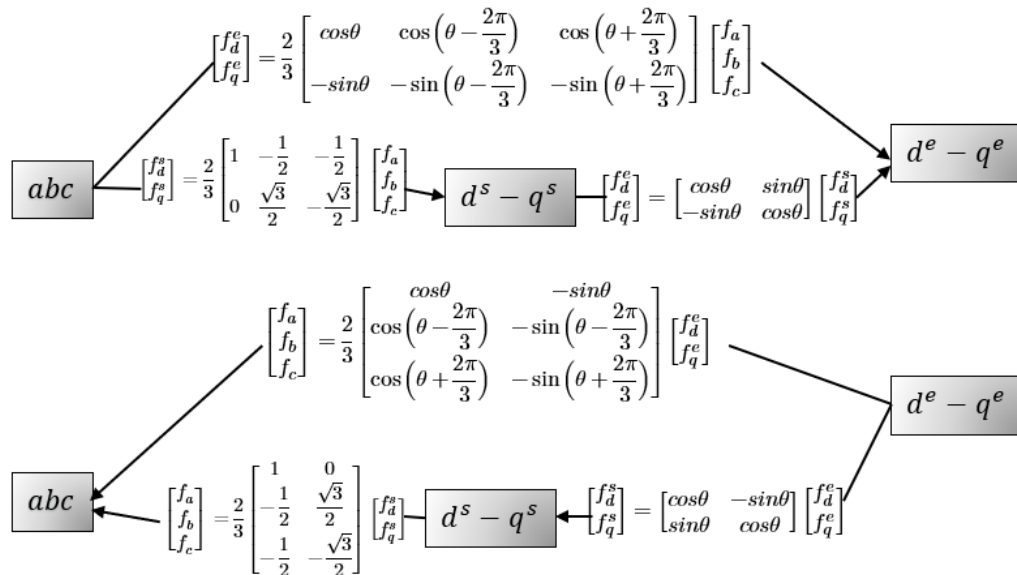


Figure 4 Reference Frame Transformation matrices

Source: (Kim, 2017)

The angle between the rotating reference frame and the stationary reference frame may vary over time. This angle θ_r is given by an integral of the angular velocity ω of the rotating reference frame as

$$\theta_r = \int \omega \tau d\tau + \theta_r(0) \quad (5)$$

Where, $\theta_r(0)$ is the initial angle at $t = 0$, and commonly, $\theta_r(0) = 0$.

Induction Motor Model

The analysis of the dynamic performance of induction motor has become a priority in addition to steady-state performance analysis in order to be able to achieve an appropriate control strategy. However, its dynamic stability study is complex because the AC IM is multivariable, non-linear with internal coupling effect, and discrete time in nature. In order to tackle this problem, the computer simulation study becomes useful and handy particularly when new control structure is being developed. Once the control structure and parameters of the control system are determined by the simulation study of acceptable performance, a prototype system can be designed and tested with further iteration of the controller parameters. This requires a mathematical model, which describes the behavior of a motor.

When describing a three-phase induction motor by a system of non-linear equations, following assumptions are made:

- i. The three-phase motor is symmetrical (Windings are identical within each three-phase set) with uniform airgap
- ii. Only the fundamental harmonics is considered, while the higher harmonics of the special field distribution and of the Magneto Motive Force (MMF) in the airgap are disregarded,
- iii. The spatially distributed stator and rotor windings are replaced by a concentrated coil, which are sinusoidally distributed
- iv. Effects of anisotropy, magnetic saturation, friction, windage losses, iron losses and eddy currents are neglected,
- v. Coil resistance and reactance are taken to be constant, which mean the skin and temperature effects are neglected
- vi. in many cases, especially when considering steady state, the current and voltages are taken to be sinusoidal.
- vii. Neutral of both the stator winding sets are separate. Thus, there is no fault propagation.

System Equations

Consider a three-phase induction motor as shown in Figure 5. Three-phase induction motor basically has three windings on stator and three windings on rotor. Therefore, the idealized machine is described by six first-order differential equations, one for each winding. The differential equations are coupled to each other through the mutual inductances between the windings.

The system equations of the magnetically coupled stator and rotor circuits shown in Figure 5 can be derived by the using Kirchoff's law from its equivalent circuit.

Stator Voltage Equations

$$\begin{aligned} v_{as} &= i_{as}r_s + \frac{d\lambda_{as}}{dt} \\ v_{bs} &= i_{bs}r_s + \frac{d\lambda_{bs}}{dt} \\ v_{cs} &= i_{cs}r_s + \frac{d\lambda_{cs}}{dt} \end{aligned} \quad (6)$$

Rotor Voltage Equations

$$\begin{aligned} v_{ar} &= i_{ar}r_{pr} + \frac{d\lambda_{ar}}{dt} \\ v_{br} &= i_{br}r_{pr} + \frac{d\lambda_{br}}{dt} \\ v_{cr} &= i_{cr}r_{pr} + \frac{d\lambda_{cr}}{dt} \end{aligned} \quad (7)$$

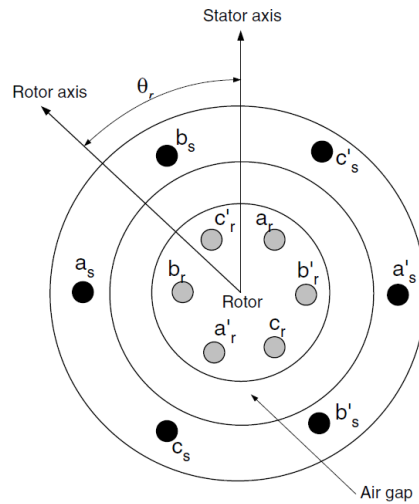


Figure 5 Cross-sectional representation of Induction Motor

Flux Linkage Equations

$$\begin{bmatrix} \lambda_s^{abc} \\ \lambda_r^{abc} \end{bmatrix} = \begin{bmatrix} L_{ss}^{abc} & L_{sr}^{abc} \\ L_{rs}^{abc} & L_{rr}^{abc} \end{bmatrix} \begin{bmatrix} i_s^{abc} \\ i_r^{abc} \end{bmatrix} \quad (8)$$

Where

$$\begin{aligned} \lambda_s^{abc} &= \lambda_{as}, \lambda_{bs}, \lambda_{cs}^t \\ \lambda_r^{abc} &= \lambda_{ar}, \lambda_{br}, \lambda_{cr}^t \\ i_s^{abc} &= i_{as}, i_{bs}, i_{cs}^t \end{aligned} \quad (9)$$

$$i_r^{abc} = i_{ar}, i_{br}, i_{cr} \quad t$$

The two types of fluxes produced by stator/rotor due to stator/rotor inductances are leakage flux (which links only its own winding) and magnetizing flux (which links its own and other winding as well). Let us look into each inductance individually one by one in following sections.

Stator Inductance

Stator inductance L_s consists of the self-inductances of each stator winding and the mutual inductance between stator winding as:

$$L_{ss}^{abc} = \begin{bmatrix} L_{asas} & L_{asbs} & L_{ascs} \\ L_{bsas} & L_{bsbs} & L_{bscs} \\ L_{csas} & L_{csbs} & L_{cscs} \end{bmatrix} \quad (10)$$

The diagonal elements of the matrix in (10) is stator mutual inductance and off-diagonal elements are mutual inductances. The self-inductances of the matrix consist of leakage inductance (L_{ls}) and magnetizing inductance (L_{ms}) as:

$$L_{asas} = L_{bsbs} = L_{cscs} = L_{ls} + L_{ms} \quad (11)$$

where,

$$L_{ms} = \mu_0 N_s^2 \left(\frac{r^l}{g} \right) \left(\frac{\pi}{4} \right) \quad (12)$$

Similarly, the mutual inductance between the stator winding, which are displaced from each other by 120° , are all same and are related to magnetizing inductance as

$$\begin{aligned} L_{asbs} = L_{ascs} = L_{bsas} = L_{bscs} = L_{csas} = L_{csbs} \\ = L_{ms} \cos\left(\frac{2\pi}{3}\right) = -\frac{1}{2}L_{ms} \end{aligned} \quad (13)$$

The negative sign in mutual-inductance indicates that each winding produces the flux in a direction opposite to one another. Thus (10) can be restated as:

$$L_{ss}^{abc} = \begin{bmatrix} L_{ls} + L_{ms} & -\frac{1}{2}L_{ms} & -\frac{1}{2}L_{ms} \\ -\frac{1}{2}L_{ms} & L_{ls} + L_{ms} & -\frac{1}{2}L_{ms} \\ -\frac{1}{2}L_{ms} & -\frac{1}{2}L_{ms} & L_{ls} + L_{ms} \end{bmatrix} \quad (14)$$

Rotor Inductance

The rotor inductance matrix L_{rr}^{abc} consists of also of self-inductances of each rotor windings and the mutual-inductances between these windings as

$$L_{rr}^{abc} = \begin{bmatrix} L_{arar} & L_{arbr} & L_{arcr} \\ L_{brar} & L_{brbr} & L_{brcr} \\ L_{crar} & L_{crbr} & L_{crer} \end{bmatrix} \quad (15)$$

As explained for stator inductance, the rotor self-inductance also consists of leakage inductance and magnetizing inductance as:

$$L_{arar} = L_{brbr} = L_{crer} = L_{lr} + L_{mr} \quad (16)$$

The rotor and stator magnetizing inductances are related as

$$L_{mr} = \mu_0 N_r^2 \left(\frac{rl}{g} \right) \left(\frac{\pi}{g} \right) = \left(\frac{N_r}{N_s} \right)^2 L_{ms} = n^2 L_{ms} \quad (17)$$

Similarly, the mutual-inductances between two rotor windings, which are displaced by 120° , are all same and related to the magnetizing inductance as

$$\begin{aligned} L_{arbr} &= L_{arcr} = L_{brar} = L_{brer} = L_{crar} = L_{crer} \\ &= L_{mr} \cos\left(\frac{2\pi}{3}\right) = -\frac{1}{2} L_{mr} = -\frac{1}{2} n^2 L_{ms} \end{aligned} \quad (18)$$

Therefore, the rotor inductance matrix of (15) can be restated as:

$$L_{rr}^{abc} = \begin{bmatrix} L_{lr} + n^2 L_{ms} & -n^2 \frac{1}{2} L_{ms} & -n^2 \frac{1}{2} L_{ms} \\ -n^2 \frac{1}{2} L_{ms} & L_{lr} + n^2 L_{ms} & -n^2 \frac{1}{2} L_{ms} \\ -n^2 \frac{1}{2} L_{ms} & -n^2 \frac{1}{2} L_{ms} & L_{lr} + n^2 L_{ms} \end{bmatrix} \quad (19)$$

Mutual Inductances

We can examine the flux linkage in two direction. First, the flux which is produced by the stator windings and links the rotor winding L_{rs}^{abc} and second is the flux is produced by rotor winding and links with stator winding, L_{sr}^{abc} . Let us derive for one and the other is simply a transpose of it. The inductance that leads to flux linkage of stator winding to rotor can be expressed in matrix form as:

$$L_{sr}^{abc} = \begin{bmatrix} L_{asar} & L_{asbr} & L_{ascr} \\ L_{bsar} & L_{bsbr} & L_{bscr} \\ L_{csar} & L_{csbr} & L_{cscr} \end{bmatrix} \quad (20)$$

The mutual inductance L_{sr}^{abc} represents the ratio of the flux linking in the stator to the rotor winding current generating flux. If the rotor winding is rotating at the speed ω_r , the relative position θ_r between the two windings will vary over time. Thus, the

mutual inductance varies sinusoidally with respect the displacement angle θ_r of the rotor. Thus,

$$\begin{aligned} L_{asar} &= L_{bsbr} = L_{cscr} = nL_{ms} \cos\theta_r \\ L_{asbr} &= L_{bscr} = L_{csar} = nL_{ms} \cos\left(\theta_r + \frac{2\pi}{3}\right) \\ L_{ascr} &= L_{bsar} = L_{csbr} = nL_{ms} \cos\left(\theta_r - \frac{2\pi}{3}\right) \end{aligned} \quad (21)$$

The mutual-inductance matrix of (20) can be restated with elements replaced with Eq. (21) as:

$$L_{sr}^{abc} = nL_{ms} \begin{bmatrix} \cos\theta_r & \cos\left(\frac{2\pi}{3} + \theta_r\right) & \cos\left(\frac{2\pi}{3} - \theta_r\right) \\ \cos\left(\frac{2\pi}{3} - \theta_r\right) & \cos\theta_r & \cos\left(\frac{2\pi}{3} + \theta_r\right) \\ \cos\left(\frac{2\pi}{3} + \theta_r\right) & \cos\left(\frac{2\pi}{3} - \theta_r\right) & \cos\theta_r \end{bmatrix} \quad (22)$$

The mutual-inductance L_{rs} which is related to amount of flux produced by stator winding and links the rotor windings are related as a transpose of L_{sr} as:

$$L_{rs}^{abc} = [L_{sr}^{abc}]^t \quad (23)$$

It is evident from Eq. (21) and Eq. (22) that the mutual inductances are function of the rotor position and thus vary over time except for at a standstill, which is undesirable characteristics. In order to make inductances constant, we transform the a, b, c –domain variables into so-called $d, q, 0$ –domain with help of the transformation matrices.

The equation for the shaft dynamics is as follows (Bose, 2006; Filizadeh, 2013; Krause et al., 2002):

$$T_{em} = J \left(\frac{2}{P} \right) p\omega_r - T_L + T_{damp} \quad (24)$$

The voltage, fluxes and torque equations for induction motor are derivation is complete with respect to the motor currents in each winding. However, all the quantities are in its physical units and it is difficult to establish good modeling aspect. So, it is always a wise step to convert all units into per unit system so that it is easy to implement in simulation and also solve numerous redundancies.

Per Unit System

It is always convenient to express machine parameters and variables by equivalent per unit system quantities. A per-unit system provides units or power, voltage, current, impedance, and admittance. With the exception of impedance and admittance, any two units are independent and can be selected as base values; power and voltage are typically chosen. All quantities are specified as multiples of selected base values.

Different types of quantities are labeled with the same symbol (p.u.); it should be clear whether the quantity is a voltage, current, or other unit of measurement. Only base power and base voltage have to be selected initially, and all parameters and variables are normalized using these base quantities. When the machine is being considered separately, the base power is generally selected as the horsepower rating of the machine in volt-amperes (i.e. horsepower times 746). If on the other hand, if the machine is a part of a power system and if it is desirable to convert the entire system to per unit quantities, then only one power base (VA base) is selected which would most likely be different from the rating of any machine in the system. The rms value of the rated phase voltage is generally selected as base voltage for the a, b, c – variables while the peak value is generally selected as base voltage for $d, q, 0$ – variables.

Base Quantities

The base quantities for motor apparent power, voltage, current, impedance, speed, flux and reactance are related to each other as

$$\begin{aligned}
 S_{bc} &= S_{rated} = \sqrt{3}V_{bc}I_{bc} \\
 V_{bc} &= \sqrt{\frac{2}{3}}V_{rated} = Z_{bc}I_{bc} = \omega_{bc}\lambda_{bc} \\
 I_{bc} &= \sqrt{2}I_{rated} = \frac{2}{3}S_{bc}/V_{bc} \\
 Z_{bc} &= \frac{V_{bc}}{I_{bc}} = \left(\frac{3}{2}\right)\frac{V_{bc}^2}{S_{bc}} \\
 \omega_{bc} &= 2\pi f_{rated} \\
 T_{bc} &= \frac{S_{bc}}{2/P \omega_{bc}}
 \end{aligned} \tag{25}$$

It is to be noted here that, if the S_{bc} is rated power output of the machine, then base torque T_{bc} will not be rated torque. This is because in induction machine, rated power output generally occurs at a speed (rated speed) slightly less than synchronous speed. Hence, T_{bc} will be less than the rated torque by the ratio of rated speed to synchronous speed. Moreover, oftentimes the machine equations are expressed in terms of the flux linkage per second, ψ , and reactance x , instead of fluxes, λ and inductances, L . These are related by base value of angular frequency of the system, ω_{bc} , as:

$$\begin{aligned}
 \psi &= \omega_{bc}\lambda \\
 x_{ls} &= \omega_{bc}L_{ls}
 \end{aligned} \tag{26}$$

Once the base quantities are derived, each motor parameters are to be converted to per unit system by using the relation:

$$p. u = \frac{\text{physical Quantity in actual unit}}{\text{Base Qunatity}} \tag{27}$$

The equations of a symmetrical induction machine in arbitrary reference frame in terms of flux linkages per second and reactance at the base frequency are summarized in Table II.

Table II Arbitrary Reference Equations in terms of ψ'_s and X's

| Stator and Rotor $d, q, 0$ –voltage equations | |
|--|---|
| v_{qs} | $= \frac{p}{\omega_{bc}} \psi_{qs} + \frac{\omega}{\omega_{bc}} \psi_{ds} + r_s i_{qs}$ |
| v_{ds} | $= \frac{p}{\omega_{bc}} \psi_{ds} - \frac{\omega}{\omega_{bc}} \psi_{qs} + r_s i_{ds}$ |
| v_{0s} | $= \frac{p}{\omega_{bc}} \psi_{0s} + r_s i_{0s}$ |
| v'_{qr} | $= \frac{p}{\omega_{bc}} \psi'_{qr} + \left(\frac{\omega - \omega_r}{\omega_{bc}} \right) \psi'_{dr} + r'_r i'_{qr}$ |
| v'_{dr} | $= \frac{p}{\omega_{bc}} \psi'_{dr} - \left(\frac{\omega - \omega_r}{\omega_{bc}} \right) \psi'_{qr} + r'_r i'_{dr}$ |
| v'_{or} | $= \frac{p}{\omega_{bc}} \psi'_{or} + r'_r i'_{or}$ |
| Stator and Rotor $d, q, 0$ –Flux equations | |
| $\begin{bmatrix} \psi_{qs} \\ \psi_{ds} \\ \psi_{0s} \\ \psi'_{qr} \\ \psi'_{dr} \\ \psi'_{or} \end{bmatrix} =$ | $\begin{bmatrix} x_{ls} + x_m & 0 & 0 & x_m & 0 & 0 \\ 0 & x_{ls} + x_m & 0 & 0 & x_m & 0 \\ 0 & 0 & x_{ls} & 0 & 0 & 0 \\ x_m & 0 & 0 & x'_{lr} + x_m & 0 & 0 \\ 0 & x_m & 0 & 0 & x'_{lr} + x_m & 0 \\ 0 & 0 & 0 & 0 & 0 & x'_{lr} \end{bmatrix} \begin{bmatrix} i_{qs} \\ i_{ds} \\ i_{0s} \\ i'_{qr} \\ i'_{dr} \\ i'_{or} \end{bmatrix}$ |
| Electromagnetic Torque equation in $d, q, 0$ – frame | |
| $\begin{aligned} T_{em} &= \frac{3}{2} \frac{P}{2\omega_r} \left[\frac{\omega}{\omega_{bc}} (\psi_{ds} i_{qs} - \psi_{qs} i_{ds}) + \left(\frac{\omega - \omega_r}{\omega_{bc}} \right) (\psi'_{dr} i'_{qr} - \psi'_{qr} i'_{dr}) \right] \\ &= \frac{3}{2} \frac{P}{2\omega_{bc}} (\psi'_{dr} i'_{qr} - \psi'_{qr} i'_{dr}) \\ &= \frac{3}{2} \frac{P}{2\omega_{bc}} (\psi_{ds} i_{qs} - \psi_{qs} i_{ds}) \end{aligned}$ | |

$$\begin{aligned}
&= \frac{3}{2} \frac{P}{2\omega_{bc}} x_m (i'_{dr} i_{qs} - i'_{qr} i_{ds}) \\
&= \frac{3}{2} \frac{P}{2\omega_{bc}} \frac{x_m}{x'_r} (\psi_{dr} i_{qs} - \psi_{qr} i_{ds})
\end{aligned}$$

Although the voltage and flux linkage per second equations do not change form when per unitizing, the torque equation is modified by per unitizing process. If the torque T_{em} expression in Table II is divided by base torque (T_{bc}) stated in Eq. (25) with base power (S_{bc}), the multiplier $3/2 P/2 1/\omega_{bc}$ is eliminated, and with all quantities expressed in per-unit, the per unit torque will appear as:

$$T_{em} = \psi_{dr} i_{qs} - \psi_{qr} i_{ds} \quad (28)$$

If the electrical variables are expressed in voltages, amperes, and watts, then the inertia of the rotor is expressed in MKS units. On the other hand, if the per unit system is used, the inertia is expressed in seconds. This can be shown by Eq. (24) that the inertia torque T_{iT} for a P-pole machine may be expressed as:

$$T_{iT} = J \left(\frac{2}{P} \right) p \omega_r \quad (29)$$

In order to express Eq. (29) in per unit system, it is divided by the base torque and the rotor speed is normalized to base speed (Krause et al., 2002). Thus,

$$T_{iT} = \frac{J}{T_{bc}} \frac{2/P \omega_{bc}}{p} \frac{\omega_r}{\omega_{bc}} \quad (30)$$

By definition, the inertia constant expressed in second is:

$$H = \left(\frac{1}{2} \right) \left(\frac{2}{P} \right) \frac{J \omega_{bc}}{T_{bc}} = \left(\frac{1}{2} \right) \left(\frac{2}{P} \right)^2 \frac{J \omega_{bc}^2}{S_{bc}} \quad (31)$$

Thus, in per unit, Eq. (24) becomes:

$$T_{em} = 2H p \frac{\omega_r}{\omega_{bc}} - T_L + T_{damp} \quad (32)$$

Induction Motor in Stationary Frame

Dynamic equivalent circuit for d and q axis is shown in Figure 6 and block diagram of induction machine in d - q coordinate system is shown in Figure 7.

The complete motor dynamic equation can be obtained by separating the real and imaginary components of the voltage and current complex space vector as:

$$\psi_{qs}^s = \omega_{bc} \int \left\{ v_{qs}^s + \frac{r_s}{x_{ls}} (\psi_{mq}^s - \psi_{qs}^s) \right\} dt$$

$$\psi_{ds}^s = \omega_{bc} \int \left\{ v_{ds}^s + \frac{r_s}{x_{ls}} \psi_{md}^s - \psi_{ds}^s \right\} dt \quad (33)$$

$$\psi_{0s}^s = \frac{\omega_{bc}}{x_{ls}} \int \{ v_{0s}^s + i_{0s}^s r_s \} dt$$

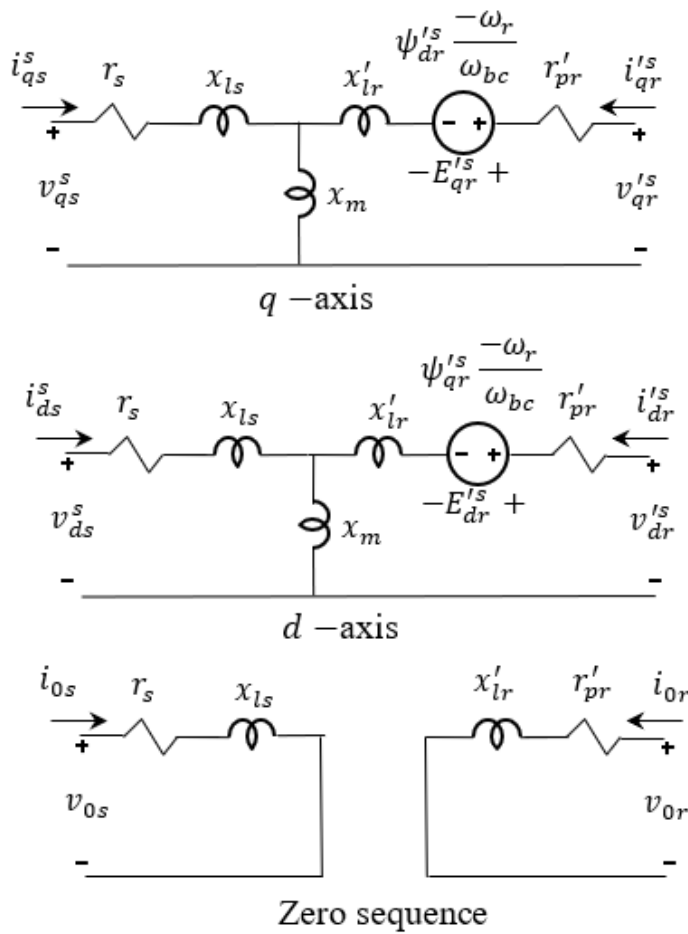


Figure 6 Dynamic Equivalent Circuit of Induction Motor

$$\psi_{qr}^s = \omega_{bc} \int \left\{ v_{qr}^s + \frac{\omega_r}{\omega_{bc}} \psi_{dr}^s + \frac{r'_r}{x'_{ls}} (\psi_{mq}^s - \psi_{qr}^s) \right\} dt$$

$$\psi_{dr}^s = \omega_{bc} \int \left\{ v_{dr}^s - \frac{\omega_r}{\omega_{bc}} \psi_{qr}^s + \frac{r'_r}{x'_{lr}} \psi_{md}^s - \psi_{dr}^s \right\} dt \quad (34)$$

$$\psi'_{0r} = \frac{\omega_{bc}}{x'_{lr}} \int \{v'_{0r} - i'_{0r} r'_r\} dt$$

Where,

$$\psi'_{mq} = x_m (i_{qs}^s + i'_{qr}) \quad (35)$$

$$\psi'_{md} = x_m i_{ds}^s + i'_{dr}$$

$$\begin{aligned} \psi_{qs}^s &= x_{ls} i_{qs}^s + \psi_{mq}^s & i_{qs}^s &= \frac{\psi_{qs}^s - \psi_{mq}^s}{x_{ls}} \\ \psi_{ds}^s &= x_{ls} i_{ds}^s + \psi_{md}^s & i_{ds}^s &= \frac{\psi_{ds}^s - \psi_{md}^s}{x_{ls}} \\ \psi'_{qr} &= x'_{lr} i'_{qr} + \psi_{mq}^s & i'_{qr} &= \frac{\psi'_{qr} - \psi_{mq}^s}{x'_{lr}} \\ \psi'_{dr} &= x'_{lr} i'_{dr} + \psi_{md}^s & i'_{dr} &= \frac{\psi'_{dr} - \psi_{md}^s}{x'_{lr}} \end{aligned} \quad (36)$$

Where,

$$\begin{aligned} \psi_{mq}^s &= x_M \left(\frac{\psi_{qs}^s}{x_{ls}} + \frac{\psi'_{qr}}{x'_{lr}} \right) \\ \psi_{md}^s &= x_M \left(\frac{\psi_{ds}^s}{x_{ls}} + \frac{\psi'_{dr}}{x'_{lr}} \right) \end{aligned} \quad (37)$$

And,

$$\frac{1}{x_M} = \frac{1}{x_m} + \frac{1}{x_{ls}} + \frac{1}{x'_{lr}} \quad (38)$$

The mechanical model of machine with its electromechanical torque expressed as following is used for rotor model.

$$T_{em} = \frac{3}{2} \frac{P}{2\omega_{bc}} (\psi_{ds}^s i_{qs}^s - \psi_{qs}^s i_{ds}^s) \quad (39)$$

Using the standard machine equations of Eq. (33) - (39), we can develop Simulink model of induction motor as shown in Figure 7. Each subsystems model is described individually from Figure 8 till Figure 13.

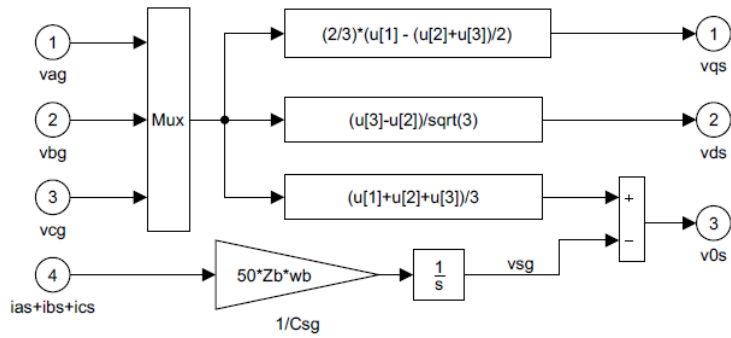


Figure 9 Clark Transformation of voltages

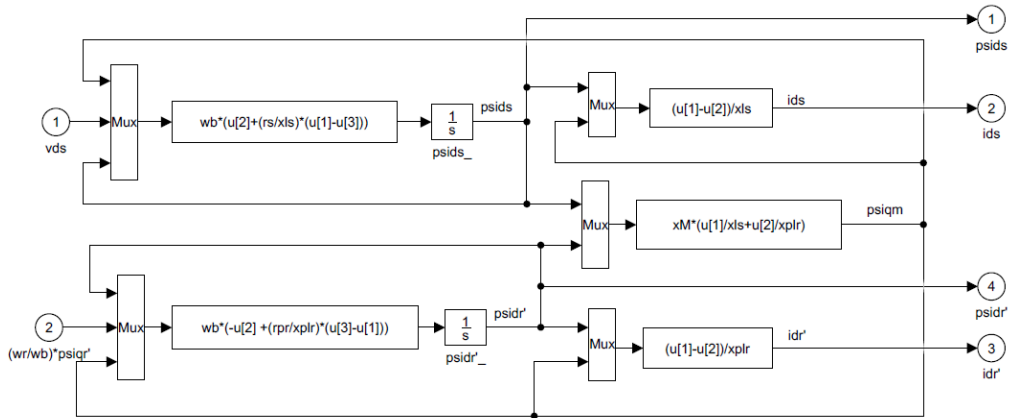


Figure 10 D-axis model

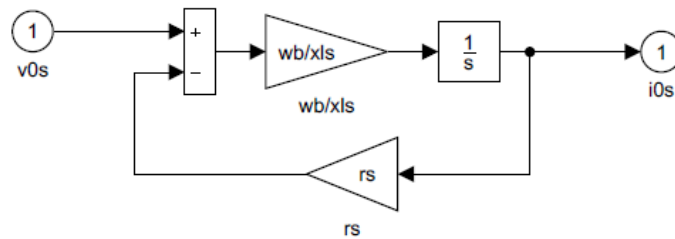


Figure 11 zero sequence model

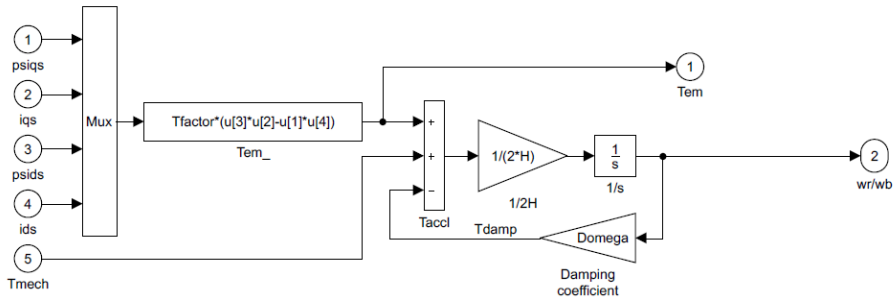


Figure 12 Rotor Model

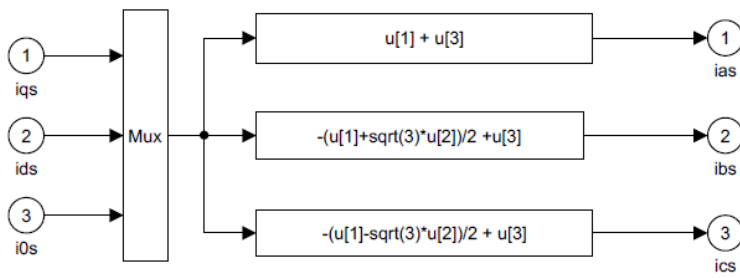


Figure 13 Inverse Clarke Transformation for motor currents

CHAPTER III

PROPOSED SENSORLESS VECTOR CONTROL ARCHITECTURE

Introduction

In this chapter, the principle of indirect FOC are presented. The simulation model of the induction motor drive developed using the principle of indirect FOC is used to apply FOC algorithm. Moreover, the sensorless method with Fuzzy-based Rotor-Flux MRAS is discussed. The Voltage Source Inverter (VSI) for AC/DC/AC conversion of supply for induction motor based on the Space Vector Modulation (SVM) based duty cycle generation technique is also presented. In the last part, the method of designing the controller and methods to discretize the controller for the implementation in DSP is presented.

Field Oriented Control

The variable frequency drive can be subdivided into several types as in Figure 14. It can be broadly classified into scalar and vector control. The scalar control is widely known as Volt per Hertz (V/F) control. It is easy to implement but the dynamic response is sluggish. The other is called vector control is known as Field Oriented Control (FOC). The main objective of FOC is to achieve decoupled control of flux and torque by control of the instantaneous current space vector.

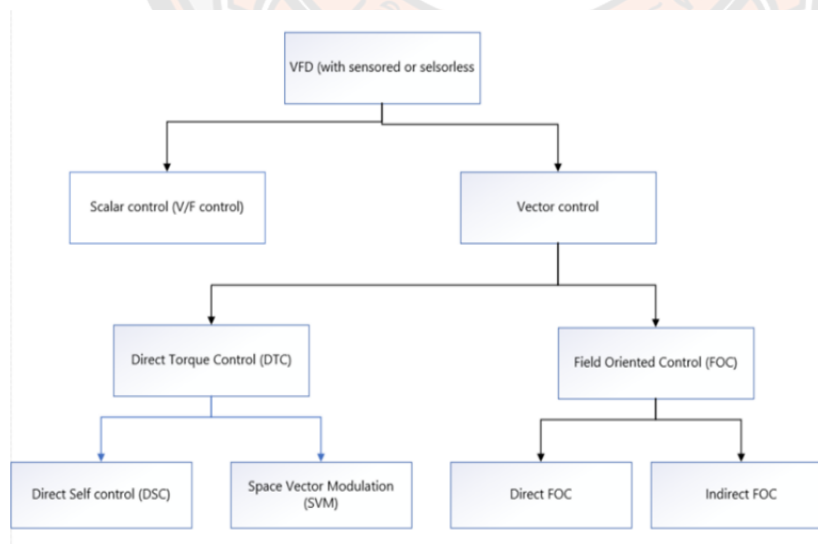


Figure 14 Types of Variable Frequency Drives (VFD)

$$T_e = \frac{3P}{2} \frac{x_m}{2x_{lr} + x_m} i_{qs}^\omega \psi_{dr}^\omega \quad (42)$$

As the result, the torque is seen to be function of the q –component of the stator current and the d –component of rotor flux linkage, which are perpendicular by nature. We further note that making $\psi_{qr}^\omega = 0$ yields the following expression for the d – component of rotor voltage:

$$v_{dr}^\omega = 0 = r_{pr} i_{dr}^\omega - \omega - \omega_r \psi_{qr}^\omega + p\psi_{dr}^\omega = r_{pr} i_{dr}^\omega + p\psi_{dr}^\omega \quad (43)$$

By substituting for ψ_{dr}^ω in Eq. (40), the below differential equation for i_{ds}^ω is obtained:

$$r_{pr} i_{dr}^\omega + x_{lr} + x_m p i_{dr}^\omega = -x_m p i_{ds}^\omega \quad (44)$$

It is to be noted that with constant i_{ds}^ω , the right-hand side of the differential equation becomes zero. This further implies that i_{dr}^ω will also tend to zero as time tends to infinity.

It can be further investigated the implications of keeping the i_{ds}^ω constant and thereby driving i_{dr}^ω to zero. With $i_{dr}^\omega = 0$, the d –component of the rotor flux linkage will be:

$$\psi_{dr}^\omega = \psi_r^\omega = x_{lr} + x_m i_{dr}^\omega + x_m i_{ds}^\omega = x_m i_{ds}^\omega \quad (45)$$

In other words, the rotor field becomes uniquely determined by i_{ds}^ω only. This is an important observation as it allows the d –component of the stator current to uniquely adjust ψ_{dr}^ω . The observation becomes even more significant when it is noted that i_{ds}^ω and ψ_{dr}^ω are along the same axis and that ψ_{dr}^ω is indeed the resultant rotor flux, as shown in Figure 15.

By combining Eq. (42) and Eq. (45), the following expression for electromagnetic torque is obtained:

$$T_e = \frac{3P}{2} \frac{x_m^2}{2x_{lr} + x_m} i_{ds}^\omega i_{qs}^\omega \quad (46)$$

This equation together with Eq. (45), forms the essence of field-oriented control, in which the rotor field and electromagnetic torque are uniquely determined by the two perpendicular components of the stator currents.

We have so far seen how to gain control over the rotor field by maintaining a constant i_{ds}^ω . However, the underlying assumption of the field-oriented control method is that the d –axis of the rotating reference frame is always kept aligned with the rotor field. This idea can be established by letting the $\psi_{qr}^\omega = 0$ in the q –axis rotor voltage equation due to the alignment of d –axis of the reference frame with the rotor flux linkage vector:

$$\begin{aligned} v_{qr}^\omega = 0 &= r_{pr} i_{qr}^\omega + \omega_e - \omega_r \psi_{dr}^\omega + p \psi_{qr}^\omega \\ &= r_{pr} i_{qr}^\omega + \omega_e - \omega_r \psi_{dr}^\omega \end{aligned} \quad (47)$$

Where, ω_e is the speed of the reference frame (in electrical radians per second) that causes the alignment of the d –axis with the rotor flux linkage. The angular position of this reference frame is denoted by θ_e . From Eq. (41), the following expression for ω_e is obtained:

$$\omega_e = \omega_r - r_{pr} \frac{i_{qr}^\omega}{\psi_{dr}^\omega} \quad (48)$$

This expression can be directly expressed in terms of the stator current's dq – components by noting that;

$$\begin{aligned} \psi_{qr}^\omega = 0 &= x_{lr} + x_m i_{qr}^\omega + x_m i_{qs}^\omega \\ \Rightarrow i_{qr}^\omega &= -\frac{x_m}{x_{lr} + x_m} i_{qs}^\omega \end{aligned} \quad (49)$$

And

$$\psi_{dr}^\omega = x_m i_{ds}^\omega$$

This equation yields the below expression for the speed of the desired reference frame:

$$\omega_e = \omega_r + \frac{r_{pr}}{x_{lr} + x_m} \frac{i_{qs}^\omega}{i_{ds}^\omega} = \omega_r + \frac{1}{T_r} \frac{i_{qs}^\omega}{i_{ds}^\omega} \quad (50)$$

The i_{ds}^ω and i_{qs}^ω are specified using a desired value of the rotor flux linkage and the electromagnetic torque, respectively. The actual location of the reference frame (θ_e) is obtained by integrating its angular speed ω_e . The second term in right hand side of Eq. (50) is called slip speed in rad/sec.

The aforementioned method of aligning the d –axis of the reference frame with the rotor flux linkage vector is thus, an indirect vector (FOC) control method because the rotor position is not measured directly and rather estimated indirectly by current components. This is shown in Figure 16. The Eq. (50) can be discretized using Tustin or Trapezoidal Approximation method which can be obtained simply by substituting $s = \frac{2}{T_s} \left(\frac{z-1}{z+1} \right)$ in the transfer function. The transfer function is:

$$\theta_e(s) = \int \omega_e dt + \omega_e 0 = \frac{1}{s} \omega_e(s) \quad (51)$$

Now, by applying approximation method on Eq. (50) in z-domain:

$$\theta_e z = \frac{T_s}{2} \left(\frac{z+1}{z-1} \right) \left(\omega_r + \frac{1}{T_r} \frac{i_{qs}^\omega(z)}{i_{ds}^\omega(z)} \right) \quad (52)$$

Multiplying and dividing right-hand-side by z will give:

$$\theta_e z = \frac{T_s}{2} \left(\frac{1 + z^{-1}}{1 - z^{-1}} \right) \left(\omega_r + \frac{1}{T_r} \frac{i_{qs}^\omega(z)}{i_{ds}^\omega(z)} \right) \quad (53)$$

Where, z^{-1} indicates the previous instance (In Simulink environment, this instance can be achieved by inserting delay block). Thus

$$\theta_e z (1 - z^{-1}) = \frac{T_s}{2} (1 + z^{-1}) \left(\omega_r + \frac{1}{T_r} \frac{i_{qs}^\omega(z)}{i_{ds}^\omega(z)} \right) \quad (54)$$

Or

$$\begin{aligned} \theta_e(k) - \theta_e(k-1) &= \frac{T_s}{2} \left(\omega_r(k) + \frac{1}{T_r} \frac{i_{qs}^\omega(k)}{i_{ds}^\omega(k)} + \omega_r(k-1) \right. \\ &\quad \left. + \frac{1}{T_r} \frac{i_{qs}^\omega(k-1)}{i_{ds}^\omega(k-1)} \right) \end{aligned} \quad (55)$$

The variable k indicates the current instance and the $k - 1$ indicates the past instance. The per unitized and discretized equation as shown in (55) is implemented in DSP. The vector control block diagram for induction motor is shown in Figure 16.

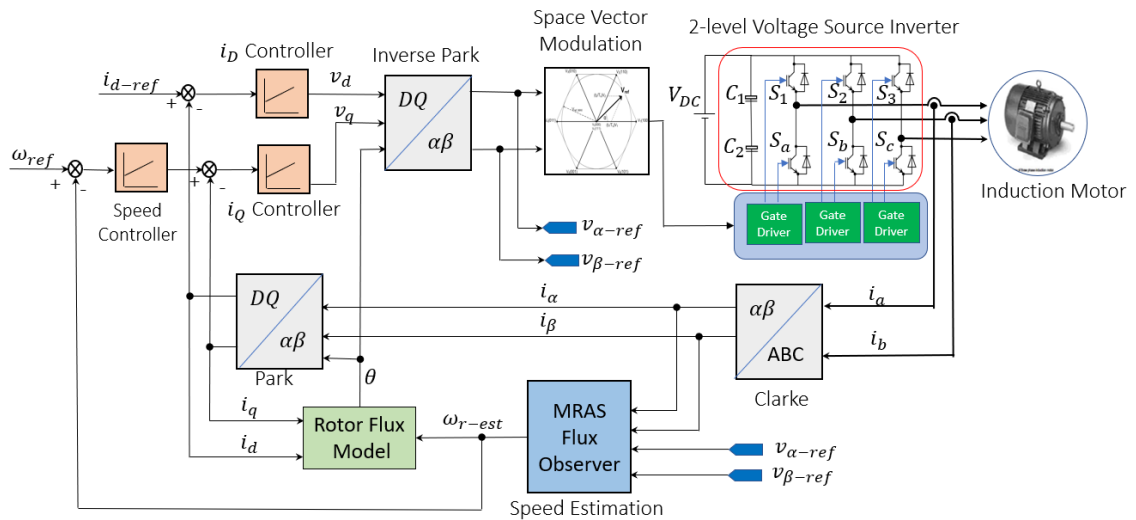


Figure 16 Block diagram of sensorless vector control method for IM

Voltage Source Inverter

The goal of inverter is to use a steady state DC-voltage by the means of six switches to emulate the three-phased sinusoidal waveform but both the frequency and the amplitude is made adjustable. While the basic hardware is the same in all VFDs, the

inverter can be one of several designs, depending on the application requirements like output, source, type of load etc. (Kansagara, 2018):

According to output characteristics

- Square Wave Inverter
- Sine Wave Inverter
- Modified Sine Wave Inverter

According to the source of inverter

- Current Source Inverter
- Voltage Source Inverter

According to type of load

- Single Phase Inverter
- Half Bridge Inverter
- Full Bridge Inverter
- Three-phase inverters
 - 180-degree mode
 - 120-degree mode

According to types of PWM technique used

- Simple Pulse Width Modulation (SPWM)
- Multiple Pulse Width Modulation (MPWM)
- Sinusoidal Pulse Width Modulation (SPWM)
- Modified sinusoidal Pulse Width Modulation (MSPWM)
- Space Vector Pulse Width Modulation (SVM)

According to number of outputs used

- Regular Two-Level Inverter
- Multi-Level Inverter

The two most common types of inverters are the current source inverter (CSI) and the voltage source inverter (VSI). As their names imply, current source inverters are fed with constant current, while voltage source inverters are fed with constant voltage. Consequently, the output of a CSI drive is adjustable, three-phase AC current, while a VSI drive produces three-phase AC voltage with adjustable magnitude and frequency. A most prominent difference between CSI and VSI is their energy storage method. CSI drives use inductive energy storage device (inductor) in their DC link to store DC energy and regulate current ripple between the converter and the inverter. Conversely, VSI drives use capacitive storage device (DC-link capacitor), which both stores and smooths the DC voltage for the inverter. This difference in storage method has a noticeable effect on drive performance.

A four-quadrant, full-bridge, three-phase voltage source inverter for the supply of AC-motor is shown in Figure 17. From left to right the following are shown:

- i. The fixed DC supply derived either from battery bank or the rectifier circuit.
- ii. A DC-link capacitor for energy storage and voltage stabilization
- iii. An inverter bridge with six IGBT switches

- iv. Three output terminals and a star connected (ungrounded) induction motor equivalent, and
- v. Gate driver for providing gate signals to IGBTs.

This kind of inverter is suitable for supplying induction as well as synchronous motors. There are six IGBT switches arranged in a bridge fashion. Two IGBT switches are arranged in each leg of the bridge and each leg corresponds to each phase of the three-phase system. Each leg has its own binary control signal $S_{a,b,c} \in \{1,0\}$, where 1 represents the ‘on’ state of the switch and 0 indicates ‘off’ state of switch. The semiconductor switches in one inverter leg are controlled with complementary signals to avoid:

- vi. both conducting at the same time
- vii. short-circuit the DC-link, and
- viii. to avoid both switches to be simultaneously opened and produce undefined output voltages.

Hence, when $s_x = 1$, phase x output node is connected to the positive rail of DC bus, generating a phase output voltage $v_x N = V_{DC}$, while with $s_x = 0$, phase x output node is connected to the negative rail of DC bus, generating a phase output voltage $v_x N = 0$. The voltage-source inverters described can be termed “two-level,” because each output terminal, temporarily connected to either of the two DC buses can assume only two voltage levels. This is the most widely used topology today because it is simple and cheap. Higher level converters are mostly used for high voltage applications but it will not be treated in this report.

All the inverter phase output voltages can be obtained by:

$$V_x N = S_x V_{DC}, \quad S_x \in \{1,0\}, \quad x = a, b, c \quad (56)$$

Since the inverter is controlled with three binary signals, it features $2^3 = 8$ different switching states S_a, S_b, S_c . Since the load is connected at the midpoint of the VSI, the three-phase output voltage has a DC component of $V_{DC}/2$. However, this DC offset is common to the three phases only and it is eliminated with the three-phase connection. Moreover, it does not appear in the line–line and load voltages.

For the IGBT switches, the switching frequency is usually selected above 16 kHz, i.e. beyond the audible range, so that there is no objectionable acoustic noise being produced by magnetic components (Leonhard, 1996). This practice has advantage of inverter exhibiting larger bandwidth for control. Moreover, if sufficient magnitude of DC-link voltage (V_{DC}) is provided, fast control loop can be designed which keep the stator currents close to the alternating reference value. This effectively results in near ideal current source for the stator current at the windings of the motor, thus eliminating the effects of stator voltage on dynamics of the drive. Consequently, considerable simplification of the control is achieved because the stator voltage interaction is now dealt with by the simple current controllers. These could either employ pulse-width modulator operating at constant frequency or simple On-Off comparators having a narrow hysteresis band.

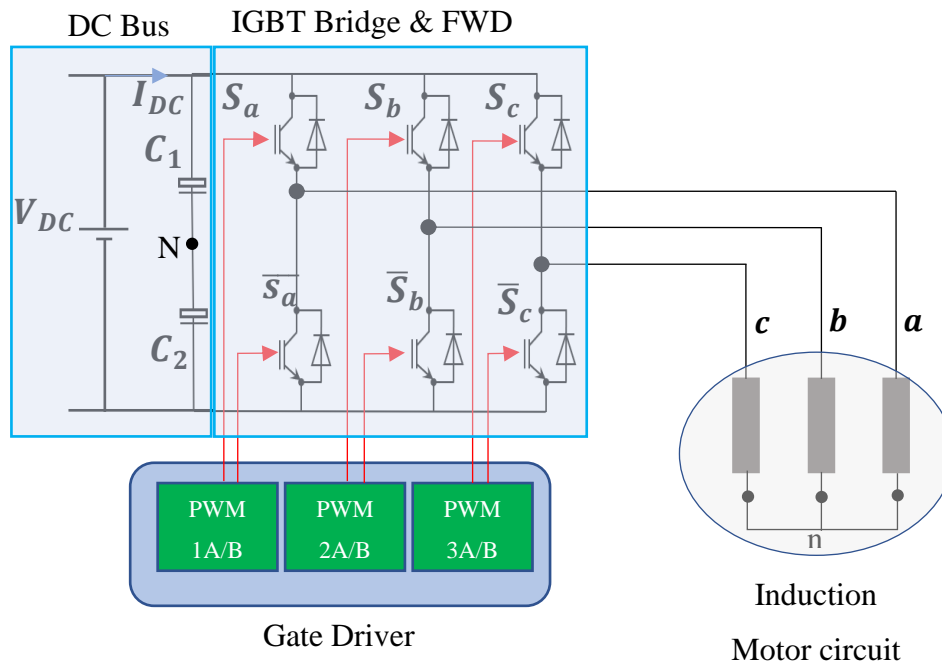


Figure 17 Two-Level Voltage Source Inverter Circuit

When extending the principle to three-phase loads like 3-phase induction motors, as shown in Figure 17, the tolerance band is helpful to avoid interactions between the controllers because, in view of the isolated neutral of the machine winding, one if the controllers is redundant and is only retained for symmetry.

The three-switching function: S_a, S_b and S_c , can be assigned to inverter; defining it as (P. Kazmierkowski, Blaabjerg, & Krishna, 2002):

$$\begin{aligned}
 S_a &= \begin{cases} 0 & \text{if } S_1 = ON, S_4 = OFF \\ 1 & \text{if } S_1 = OFF, S_4 = ON \end{cases} \\
 S_b &= \begin{cases} 0 & \text{if } S_3 = ON, S_6 = OFF \\ 1 & \text{if } S_3 = OFF, S_6 = ON \end{cases} \\
 S_c &= \begin{cases} 0 & \text{if } S_5 = ON, S_2 = OFF \\ 1 & \text{if } S_5 = OFF, S_2 = ON \end{cases}
 \end{aligned} \quad (57)$$

The line-to-line and line-to-neutral output voltages are given by

$$\begin{bmatrix} v_{ab} \\ v_{bc} \\ v_{ca} \end{bmatrix} = V_{DC} \begin{bmatrix} 1 & -1 & 0 \\ 0 & 1 & -1 \\ -1 & 0 & 1 \end{bmatrix} \begin{bmatrix} a \\ b \\ c \end{bmatrix} \quad (58)$$

And

$$\begin{bmatrix} v_{aN} \\ v_{bN} \\ v_{cN} \end{bmatrix} = \frac{V_{DC}}{3} \begin{bmatrix} 2 & -1 & -1 \\ -1 & 2 & -1 \\ -1 & -1 & 2 \end{bmatrix} \begin{bmatrix} a \\ b \\ c \end{bmatrix} \quad (59)$$

The line-to-line voltages at the motor terminals have three level waveforms, assuming the values V_{DC} , 0 , $-V_{DC}$, and each line-to-neutral voltage has five values, $-2V_{DC}/3$, $-V_{DC}/3$, 0 , $V_{DC}/3$, and $2V_{DC}/3$.

The output voltage can be expressed in terms of a , b and c as:

$$\begin{aligned} V_a &= \frac{V_{DC}}{3} (2S_a - S_b - S_c) \\ V_b &= \frac{V_{DC}}{3} (2S_b - S_a - S_c) \\ V_c &= \frac{V_{DC}}{3} (2S_c - S_b - S_a) \end{aligned} \quad (60)$$

Space Vector Modulation (SVM)

The Space Vector Modulation (SVM), is a technique to determine the pulse-width modulated signal for inverter switches in order to generate the desired three-phase voltage to the motor. SVM is the final step for FOC.

For understanding SVM, each leg of inverter can be simplified by replacing each IGBTs by a simple switch (NO/NC) as shown in Figure 18 (a). In the shown example, the switch combination is such that the leftmost has its upper switch closed and bottom switch open. The two other has upper switches are open and lower switches open. This will correspond to a positive voltage being applied to a -phase while the two other phases are negative. The current will thus take a-phase path from the positive DC link to motor and return to the negative DC link via other two phases. The line-to-ground voltage corresponding to all the switching states are summarized in Table III.

From the simplified schematics, it is understood that each switch can have two positions with total possible switch configuration of 8. Out of which there are six nonzero vectors; V_1 through V_6 , whose magnitude equals V_{DC} and are called *basic vectors*. Similarly, there are two zero vectors; V_0 and V_7 , whose magnitudes are zero, and are referred to as *zero vectors*. For the simple understanding, the reference voltage vector can be represented in a hexagonal space plane with six active voltage vectors lying on each vertex of the hexagon and two zero vectors on the center. This is illustrated in Figure 18(b). The desired resultant voltage vector can be simulated by an averaging effect between two adjacent active vectors and a zero vector.

The a -phase normally forms the basis for the basic vector's angles at 0° . The origin of the angles is the windings physical location inside the stator; installed around the circumference at 120° apart. Because each winding can have positive and negative voltage, it occupies two angles at 180° separation, for instance. 240° and 60° is c -phase in positive and negative state respectively.

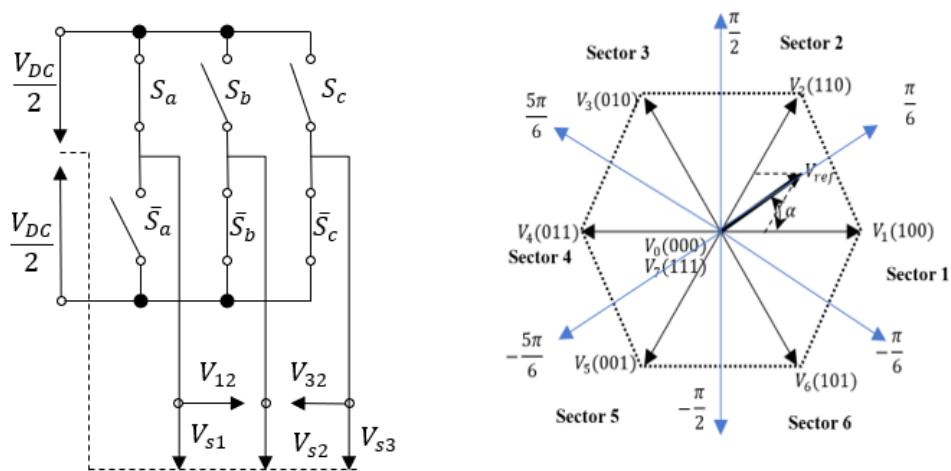


Figure 18 Switching algorithm for VSI. (a) switching states of inverter switches, (b) Hexagonal sectors for space vector

In binary, these vector combinations can be represented as eight different binary values, here named from V_0 to V_7 as shown in Table III. Each of the three binary digits refers to one bridge leg where the value 1 indicates that the top transistor is closed whereas the value 0 indicates that the bottom transistor is closed.

In the process of pulse width modulation, the space vector, V_{ref} , of fundamental output voltage is synthesized as (P. Kazmierkowski et al., 2002):

$$V_{ref} = \sum_{S=0}^7 D_S V_{DC} \quad (61)$$

Where, D_s denotes the duty ratio of sector ($S=0,1,2\dots6$).

In practice, only a zero vector and two non-zero vectors framing the output voltage are used. For instance, the vector V_{ref} in Figure 19(b), derived from Figure 18(b); is synthesized from vectors V_1 and V_2 and a zero vector, V_0 or V_7 . The radius of circular locus of the maximum available peak value of the fundamental line-to-line output voltage equals V_{DC} .

Denoting individual phase voltages of an inverter by v_{aN}, v_{bN}, v_{cN} (they can be line-to-line, line-to-ground, or line-to-neutral voltages), the voltage space vector, (V_{ref}), is defined in synchronously rotating reference frame as:

$$V_{ref} = v_d + jv_q = \frac{3}{2} V_p e^{j(\omega t + \phi)} \quad (62)$$

As the time (t), progresses, the voltage space vector, V_{ref} revolves with the angular velocity ω in a plane defined by a set of orthogonal coordinates d – and q – axis.

Table III Two-Level Three Phase VSI Switching Table

| Switching States | Switching Vector | | | Output Voltage (Line-to-neutral) | | | Space Vector | |
|------------------|------------------|-------|-------|----------------------------------|----------------------|----------------------|--|---------------|
| | S_a | S_b | S_c | V_{an} | V_{bn} | V_{cn} | | V_{sRef} |
| $V_0[000]$ | 0 | 0 | 0 | 0 | 0 | 0 | Zero vector | |
| $V_1[100]$ | 1 | 0 | 0 | $\frac{2}{3}V_{DC}$ | $-\frac{1}{3}V_{DC}$ | $-\frac{1}{3}V_{DC}$ | $\frac{2}{3}V_{DC}$ | Active vector |
| $V_2[110]$ | 1 | 1 | 0 | $\frac{1}{3}V_{DC}$ | $\frac{1}{3}V_{DC}$ | $-\frac{2}{3}V_{DC}$ | $\frac{2}{3}V_{DC}e^{j(\frac{\pi}{3})}$ | Active vector |
| $V_3[010]$ | 0 | 1 | 0 | $-\frac{1}{3}V_{DC}$ | $\frac{2}{3}V_{DC}$ | $-\frac{1}{3}V_{DC}$ | $\frac{2}{3}V_{DC}e^{j(\frac{2\pi}{3})}$ | Active vector |
| $V_4[011]$ | 0 | 1 | 1 | $-\frac{2}{3}V_{DC}$ | $\frac{1}{3}V_{DC}$ | $\frac{1}{3}V_{DC}$ | $\frac{2}{3}V_{DC}e^{j(\frac{3\pi}{3})}$ | Active vector |
| $V_5[001]$ | 0 | 0 | 1 | $-\frac{1}{3}V_{DC}$ | $-\frac{1}{3}V_{DC}$ | $\frac{2}{3}V_{DC}$ | $\frac{2}{3}V_{DC}e^{j(\frac{4\pi}{3})}$ | Active vector |
| $V_6[101]$ | 1 | 0 | 1 | $\frac{1}{3}V_{DC}$ | $-\frac{2}{3}V_{DC}$ | $\frac{1}{3}V_{DC}$ | $\frac{2}{3}V_{DC}e^{j(\frac{5\pi}{3})}$ | Active vector |
| $V_7[111]$ | 1 | 1 | 1 | 0 | 0 | 0 | Zero vector | |

In application to VSIs, the revolving voltage vector describes the fundamental output voltages. Each state of the inverter produces a specific stationary voltage space vector, and the revolving vector, V_{ref} , must be synthesized from the stationary vectors in a time-averaging process. The maximum possible value of V_{ref} determines the maximum voltage gain of the inverter.

The reference voltage vector V_{ref} can also be written in terms of $\alpha - \beta$ complex plane by:

$$v_{ref} = \frac{2}{3}[v_{aN} + av_{bN} + a^2v_{cN}], \quad (63)$$

Where $a = -\frac{1}{2} + j\frac{\sqrt{3}}{2}$.

It can be demonstrated that the space vector can be computed also using the load voltages v_{an}, v_{bn} , and v_{cn} without any difference, since the common mode voltage v_{nN} that relates both voltages ($v_{aN} = v_{an} + v_{nN}$) is common to the three-phases and when multiplied by $(1 + a + a^2)$ is eliminated in the space vector transformation given in Eq. (56).

As seen previously, the inverter phase output voltages are defined by the gating signals according to Eq. (56). By replacing Eq. (56) in Eq. (63), the voltage space vector can then be defined using the switching signals S_a, S_b , and S_c , which leads to

$$v_{ref} = \frac{2}{3}V_{DC}[S_a + aS_b + a^2S_c] \quad (64)$$

It is also good to note that all active vector has same magnitudes except for zeros vectors.

$$|V_s| = \frac{2}{3}V_{DC}, \quad \text{with } s = 1, 2, \dots, 6 \quad (65)$$

and different angles, which are rotated in $\pi/3$ (radians) with respect to each other

$$\angle\{V_s\} = s - 1 \frac{\pi}{3} \quad (66)$$

For balanced three-phase sinusoidal references, as is usual in power converter systems in steady state, the resulting reference vector is a fixed amplitude rotating space vector with the same amplitude and angular speed (ω) of the sinusoidal references, with an instantaneous position with respect to the real $\alpha -$ axis given by $\theta = \omega t$.

We can for time being assume that the inverter is switched at a basic clock frequency $f_0 = 1/T_0$, which may either be fixed or synchronized to the variable fundamental stator frequency. Also, assume that the current controllers have determined a command value V_{ref} for the next interval T_0 which may be inside the first sector, as shown in Figure 19 (b). Since this commanded voltage vector is not normally coinciding with one of the available 8 voltage vectors, $V_1 = V_s 100 = V_{DC}$ and $V_2 = V_s 110 = V_{DC}e^{j\pi/3}$ and filling up the rest of the interval with zero-vectors. The sub-intervals t_1 and t_2 for the two adjacent vectors are to be computed from the following equivalence

$$\begin{aligned}
V_{ref} &= V_{sa} + jV_{sb} \text{ }_{ref} = V_1 \frac{t_1}{T_0} + V_2 \frac{t_2}{T_0} \\
&= V_{DC} \left(\frac{t_1}{T_0} + e^{j\frac{\pi}{3}} \frac{t_2}{T_0} \right)
\end{aligned} \tag{67}$$

In addition, $t_1 + t_2 + 2t_0 = T_0$ holds, where t_0 is the zero-vector interval. Solving for t_1, t_2 results in

$$\begin{aligned}
\frac{t_1}{T_0} &= \frac{V_{saRef}}{V_{DC}} - \frac{1}{\sqrt{3}} \frac{V_{sbRef}}{V_{DC}} \\
\frac{t_2}{T_0} &= \frac{2}{\sqrt{3}} \frac{V_{sbRef}}{V_{DC}} \\
2\frac{t_0}{T_0} &= 1 - \frac{V_{saRef}}{V_{DC}} - \frac{1}{\sqrt{3}} \frac{V_{sbRef}}{V_{DC}} \geq 0
\end{aligned} \tag{68}$$

When a zero vector is omitted, i.e. $t_0 = 0$, the resulting equivalent voltage ends on the straight line connecting the two adjacent switching vectors according to

$$V_{ref} = V_1 - V_2 \frac{t_1}{T_0} + V_2 \tag{69}$$

The limits for $t_0 = 0$ and $t_1 = T_0$ confirms this result. Hence, with the inclusion of t_0 , any desired voltage vector inside the hexagon defined by six switching vectors may be realized. Of course, the adjoining switching vectors must be chosen according to the sectorial position of V_{ref} . If the switching frequency f_0 is high enough, fluctuations of the link voltage may be taken into account by replacing V_{DC} in the modulating equations by recent measurement of V_{DC} (Leonhard, 1996).

The switching sequence pertaining to the one shown in Figure 18, is plotted in Figure 19 depicting the potentials of the motor terminals. In order to remove the ambiguity with respect to which of the two adjoining switching states should be applied first, it is advantageous to repeat the same switching cycle with reverse sequence so that a symmetrical interval of length $2T_0$ is created. Sampling the motor currents in the center of the short circuit interval t_0 reduces the sampling noise.

From Figure 19,

$$V_{ref} = \frac{t_1}{T_0} V_1 + \frac{t_2}{T_0} V_2 \tag{70}$$

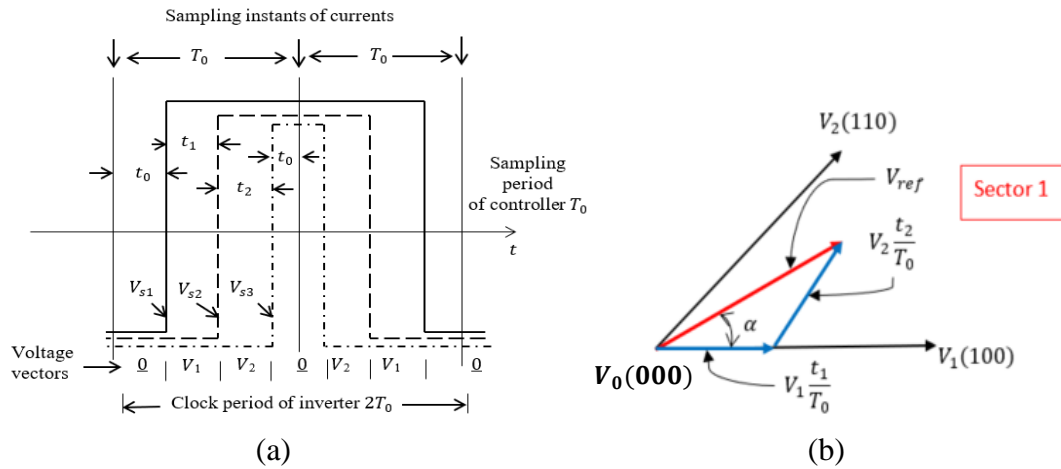


Figure 19 SVM with symmetrical switching sequence for sector 1. (a) Timing graph, (b) voltage synthesis to obtain reference voltage

The Eq. (67) describes an idealized situation, where the protective intervals and the inherent delays of the switching devices are neglected. For the actual design of modulators, these effects must be taken into account, particularly the differences between turn-on and turn-off times, which can cause considerable distortion of the inverter characteristics at low output voltage and frequency. The timing graph for PWM1A and PWM1B are just complimentary with short dead-band. The next sector will have another set of timing graph similar to discussed above and will have corresponding voltage vectors getting synthesized to generate resultant space vector. The most important steps left unexplained is the method/step to determine the sector number in which the resultant voltage vector must be residing. It is indeed simple. The sector number is selected based on the value of two orthogonal voltage vectors (v_d^s, v_q^s) in stationary reference frame. For instance if the magnitude of v_q^s is greater than zero, then the voltage vector must be lying on either sector 1, 2 or 3. So, to be sure on which sector does it lie exactly at particular instant of time, next comparison test has to be conducted. If magnitude of v_q^s is greater than $\sqrt{3}v_d^s$, then it confirms that the voltage vector lies in sector 2. Otherwise, the vector may be lying on either sector 1 or 3. So next comparative analysis has to be conducted. The way to determining the sector number based on the magnitude of d, q – voltage in stationary reference frame is illustrated clearly in Figure 20.

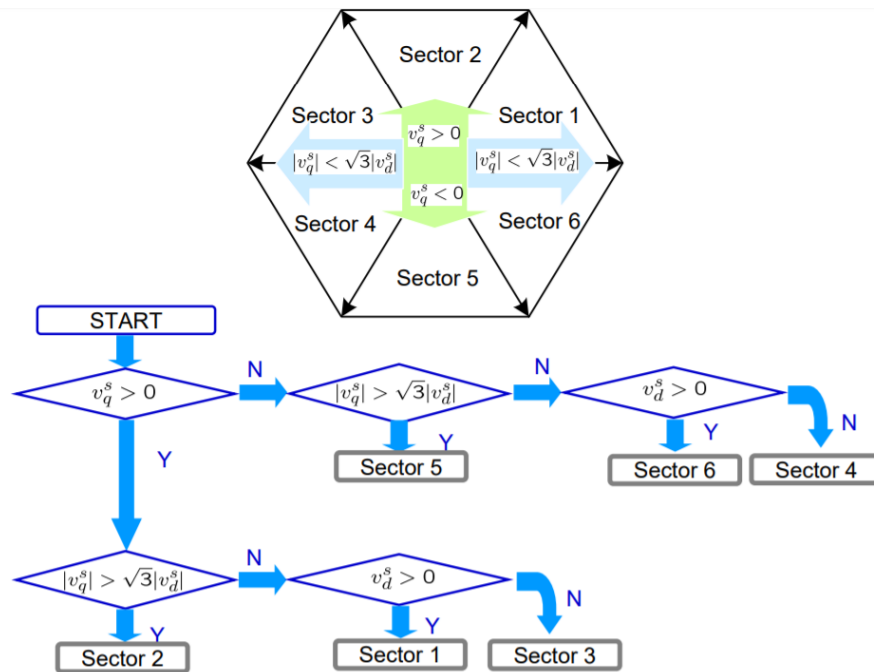


Figure 20 Technique to select the sector number.

Source: (Hee Nam, 2018).

In conclusion, the effective control techniques of machine depend widely on the types of inverter being chosen and the way its switches are operated notwithstanding the vector control or the precision in selecting the motor parameters.

Sensorless Vector Control Model

The vector model for induction motor control simulated in MATLAB/SIMULINK software is presented in Figure 21. The motor model is developed in stationary reference frame and the decouple control of torque and flux in the synchronous reference frame by transforming stator quantities using Clarke and Park transforms. The d – axis current which is field producing current is set to be equal to magnetizing current of the motor because when ignoring the field weakening, we assume the field flux to be constant. Furthermore, the magnetizing current can be considered to be equal to no load current by assuming core component of current is zero.

The q – axis current is the torque producing current and it is obtained from the outer speed loop. The rotor speed is estimated using MRAS algorithm and is compared with the reference speed. The error generated is then synthesized by the classical PI controller.

The rotor position is determined by indirect method. In this method, the synchronous speed is obtained by summing the estimated rotor speed and the slip speed. The precise establishment of rotor position is mandatory to obtain DC equivalent waveform in the d, q –axis current controller.

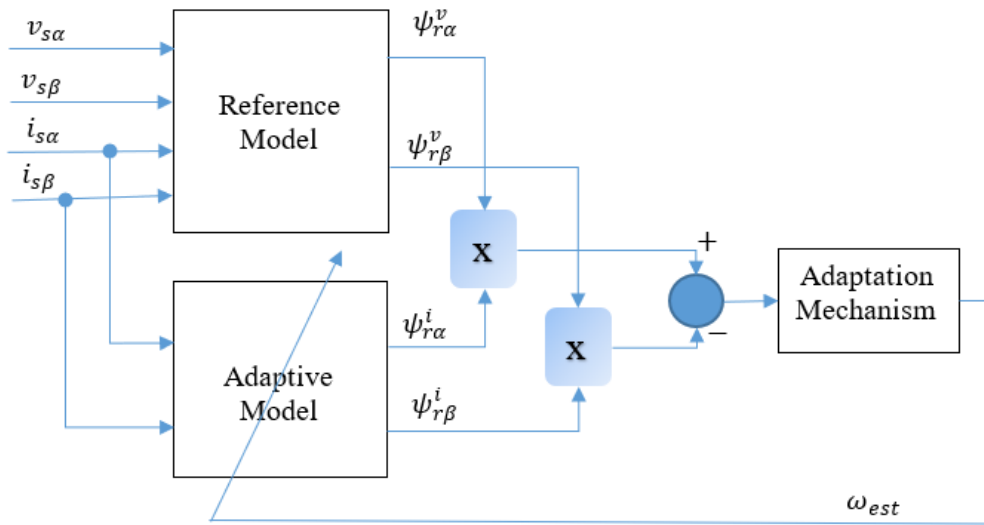


Figure 22 Rotor-Flux MRAS system

The inner current loop also employs classical PI controller with same controller gains for both d – and q –axis currents. The voltage reference obtained from the current controllers are transformed back to stationary reference frame and is used to generate reference voltage to determine the sector of the SVM. Based on the selected sector on the hexagon, the duty cycle for the IGBT switches are generated. This process can accurately generate voltage magnitude and frequency at the stator correspondingly to the torque and flux requirement for the motor to speed up/down to track the speed reference with smooth dynamics.

The comparative analysis between the sensed and sensorless model were conducted followed by the sensorless control comparison for fuzzy and PI controllers. This can be obtained by simply by selecting two manual switches (marked 1 and 2) as shown in Figure 21. Switch 1 is used to select the control mode between sensed and sensorless (currently sensorless is selected). Whereas, switch 2 is used to select the senseless model with PI or FLC (currently FLC is chosen).

Model reference Adaptive System (MRAS)

Model Reference Adaptive System (MRAS) is one of the famous speed observers usually used for sensorless induction motor drives. The block diagram of MRAS is presented in Figure 22. It is one of many promising techniques employed in adaptive control. The MRAS being a machine model-based speed estimator method, the mathematical equations for each block can easily be derived from the machine voltage and current equations.

First of all, the stator voltage in stationary reference frame are:

$$\begin{aligned} v_{s\alpha} &= R_s i_{s\alpha} + \frac{d}{dt} \lambda_{s\alpha} \\ v_{s\beta} &= R_s i_{s\beta} + \frac{d}{dt} \lambda_{s\beta} \end{aligned} \quad (71)$$

And, rotor voltage is,

$$\begin{aligned} v_{r\alpha} = 0 &= R_r i_{r\alpha} + \frac{d}{dt} \lambda_{r\alpha} + \omega_r \lambda_{r\beta} \\ v_{r\beta} = 0 &= R_r i_{r\beta} + \frac{d}{dt} \lambda_{r\beta} - \omega_r \lambda_{r\alpha} \end{aligned} \quad (72)$$

Where,

$$\begin{aligned} \lambda_{s\alpha} &= L_s i_{s\alpha} + L_m i_{r\alpha} \\ \lambda_{s\beta} &= L_s i_{s\beta} + L_m i_{r\beta} \end{aligned} \quad (73)$$

And

$$\begin{aligned} \lambda_{r\alpha} &= L_m i_{s\alpha} + L_r i_{r\alpha} \\ \lambda_{r\beta} &= L_m i_{s\beta} + L_r i_{r\beta} \end{aligned} \quad (74)$$

Reference Model

The reference model usually expressed by the voltage model, represents the stator equations. It generates the reference value of the rotor flux components in the stationary reference frame from the monitored stator voltage and current components. To obtain the reference model, we can replace $\lambda_{s\alpha}$ and $\lambda_{s\beta}$ by $\lambda_{r\alpha}$ and $\lambda_{r\beta}$ so that all the equations are referred to rotor side. To do that, first, Eq. (74) can be restated as:

$$\begin{aligned} i_{r\alpha} &= \frac{1}{L_r} \lambda_{r\alpha} - \frac{L_m}{L_r} i_{s\alpha} \\ i_{r\beta} &= \frac{1}{L_r} \lambda_{r\beta} - \frac{L_m}{L_r} i_{s\beta} \end{aligned} \quad (75)$$

Now, substituting Eq. (75) into Eq. (73) yields:

$$\begin{aligned} \lambda_{s\alpha} &= \sigma L_s i_{s\alpha} + \frac{L_m}{L_r} \lambda_{r\alpha} \\ \lambda_{s\beta} &= \sigma L_s i_{s\beta} + \frac{L_m}{L_r} \lambda_{r\beta} \end{aligned} \quad (76)$$

Further, substituting Eq. (76) into (71) results in:

$$\begin{aligned} v_{s\alpha} &= R_s i_{s\alpha} + \frac{L_m}{L_r} \frac{d}{dt} \lambda_{r\alpha} + \sigma L_s \frac{d}{dt} i_{s\alpha} \\ v_{s\beta} &= R_s i_{s\beta} + \frac{L_m}{L_r} \frac{d}{dt} \lambda_{r\beta} + \sigma L_s \frac{d}{dt} i_{s\beta} \end{aligned} \quad (77)$$

Or,

$$\begin{aligned} \frac{d}{dt} \lambda_{r\alpha} &= \frac{L_r}{L_m} \left(v_{s\alpha} - R_s i_{s\alpha} - \sigma L_s \frac{d}{dt} i_{s\alpha} \right) \\ \frac{d}{dt} \lambda_{r\beta} &= \frac{L_r}{L_m} \left(v_{s\beta} - R_s i_{s\beta} - \sigma L_s \frac{d}{dt} i_{s\beta} \right) \end{aligned} \quad (78)$$

Where, $\sigma = 1 - \frac{L_m^2}{L_s L_r}$ is called leakage coefficient.

Equation (78) is thus called reference model or voltage model since it is derived from machine voltage equation.

Adaptive Model

The adaptive model, usually represented by current model, describes the rotor equations where the rotor flux components are expressed in stator current components and the rotor speed. This model is dependent on the estimated speed. The current model can be established by substituting Eq. (75) into Eq. (72), so that the $i_{r\alpha}$ and $i_{r\beta}$ can be eliminated. The result is:

$$\begin{aligned} \frac{R_r}{L_r} \lambda_{r\alpha} - L_m \frac{R_r}{L_r} i_{s\alpha} + \frac{d}{dt} \lambda_{r\alpha} + \omega_r \lambda_{r\beta} &= 0 \\ \frac{R_r}{L_r} \lambda_{r\beta} - L_m \frac{R_r}{L_r} i_{s\beta} + \frac{d}{dt} \lambda_{r\beta} - \omega_r \lambda_{r\alpha} &= 0 \end{aligned} \quad (79)$$

Or,

$$\begin{aligned} \frac{d}{dt} \lambda_{r\alpha} &= \frac{L_m}{T_r} i_{s\alpha} - \frac{1}{T_r} \lambda_{r\alpha} - \omega_r \lambda_{r\beta} \\ \frac{d}{dt} \lambda_{r\beta} &= \frac{L_m}{T_r} i_{s\beta} - \frac{1}{T_r} \lambda_{r\beta} + \omega_r \lambda_{r\alpha} \end{aligned} \quad (80)$$

Thus, Eq. (80) is called Adaptive model or current model. The Eq. (78) and (80) are used to develop MRAS model in Simulink but to implement in the DSP, this is not enough. First, the fundamental quantities are converted into per units and then are discretized using either of the many discretizing methods available.

The voltage model in Eq. (78) can be per unitized by dividing by voltage base, $V_{bc} = Z_{bc} I_{bc} = \omega_{bc} \lambda_{bc}$ which yields:

$$\begin{aligned} \frac{1}{\omega_{bc}} \frac{d}{dt} \frac{\lambda_{r\alpha}}{\lambda_{bc}} &= \frac{L_r}{L_m} \left(\frac{v_{s\alpha}}{V_{bc}} - \frac{R_s}{Z_{bc}} \frac{i_{s\alpha}}{I_{bc}} \right) - \frac{\sigma L_s L_r}{L_m} \frac{1}{Z_{bc}} \frac{d}{dt} \frac{i_{s\alpha}}{I_{bc}} \\ \frac{1}{\omega_{bc}} \frac{d}{dt} \frac{\lambda_{r\beta}}{\lambda_{bc}} &= \frac{L_r}{L_m} \left(\frac{v_{s\beta}}{V_{bc}} - \frac{R_s}{Z_{bc}} \frac{i_{s\beta}}{I_{bc}} \right) - \frac{\sigma L_s L_r}{L_m} \frac{1}{Z_{bc}} \frac{d}{dt} \frac{i_{s\beta}}{I_{bc}} \end{aligned} \quad (81)$$

Or,

$$\begin{aligned} \frac{d}{dt} \psi_{r\alpha}^v &= \frac{\omega_{bc} L_r}{L_m} v_{s\alpha}^v - r_s i_{s\alpha}^v - \frac{\sigma L_r}{L_m} x_s^v \frac{d}{dt} i_{s\alpha}^v \\ \frac{d}{dt} \psi_{r\beta}^v &= \frac{\omega_{bc} L_r}{L_m} (v_{s\beta}^v - r_s i_{s\beta}^v) - \frac{\sigma L_r}{L_m} x_s^v \frac{d}{dt} i_{s\beta}^v \end{aligned} \quad (82)$$

Where, $\psi_{r\alpha}^v = \frac{\lambda_{r\alpha}}{\lambda_{bc}}, \psi_{r\beta}^v = \frac{\lambda_{r\beta}}{\lambda_{bc}}, v_{s\alpha}^v = \frac{v_{s\alpha}}{V_{bc}}, r_s = \frac{R_s}{Z_{bc}}, i_{s\alpha}^v = \frac{i_{s\alpha}}{I_{bc}}, i_{s\beta}^v = \frac{i_{s\beta}}{I_{bc}}, x_s^v = \frac{\omega_{bc}L_s}{Z_{bc}}$ are the per unit variables for rotor flux, stator voltages, resistances, currents and reactance; respectively. Similarly, adaptive model of Eq. (80) can be per unitized by dividing by voltage base as:

$$\begin{aligned} \frac{1}{\omega_{bc}} \frac{d}{dt} \frac{\lambda_{r\alpha}}{\lambda_{bc}} &= \frac{1}{T_r} \frac{L_m}{Z_{bc}} \frac{i_{s\alpha}}{I_{bc}} - \frac{1}{T_r} \frac{1}{\omega_{bc}} \frac{\lambda_{r\alpha}}{\lambda_{bc}} - \frac{\omega_r}{\omega_{bc}} \frac{\lambda_{r\beta}}{\lambda_{bc}} \\ \frac{1}{\omega_{bc}} \frac{d}{dt} \frac{\lambda_{r\beta}}{\lambda_{bc}} &= \frac{1}{T_r} \frac{L_m}{Z_{bc}} \frac{i_{s\beta}}{I_{bc}} - \frac{1}{T_r} \frac{1}{\omega_{bc}} \frac{\lambda_{r\beta}}{\lambda_{bc}} + \frac{\omega_r}{\omega_{bc}} \frac{\lambda_{r\alpha}}{\lambda_{bc}} \end{aligned} \quad (83)$$

Or,

$$\begin{aligned} \frac{d}{dt} \psi_{r\alpha}^i &= \frac{1}{T_r} x_m^i i_{s\alpha}^i - \frac{1}{T_r} \psi_{r\alpha}^i - \omega_r^i \omega_{bc} \psi_{r\beta}^i \\ \frac{d}{dt} \psi_{r\beta}^i &= \frac{1}{T_r} x_m^i i_{s\beta}^i - \frac{1}{T_r} \psi_{r\beta}^i + \omega_r^i \omega_{bc} \psi_{r\alpha}^i \end{aligned} \quad (84)$$

Where, $x_m^i = \frac{\omega_{bc}L_m}{Z_{bc}}, i_{s\alpha}^i = \frac{i_{s\alpha}}{I_{bc}}, i_{s\beta}^i = \frac{i_{s\beta}}{I_{bc}}, \psi_{r\alpha}^i = \frac{\lambda_{r\alpha}}{\lambda_{bc}}, \psi_{r\beta}^i = \frac{\lambda_{r\beta}}{\lambda_{bc}}, T_r = \frac{R_r}{L_r}, \omega_r^i = \frac{\omega_r}{\omega_{bc}}$ are per unit values of mutual inductance, stator stationary currents, rotor stationary fluxes, rotor time constant (in sec), and rotor speed; respectively.

The second step is to discretize the per unitized equations. The voltage model in Eq. (82) can be rearranged as:

$$\begin{aligned} \psi_{r\alpha}^v &= \psi_{r\alpha 1}^v - \frac{\sigma L_r}{L_m} x_s^v i_{s\alpha}^v \\ \psi_{r\beta}^v &= \psi_{r\beta 1}^v - \frac{\sigma L_r}{L_m} x_s^v i_{s\beta}^v \end{aligned} \quad (85)$$

Where,

$$\begin{aligned} \psi_{r\alpha 1}^v &= \frac{\omega_{bc}L_r}{L_m} \int v_{s\alpha}^v - r_s i_{s\alpha}^v dt \\ \psi_{r\beta 1}^v &= \frac{\omega_{bc}L_r}{L_m} \int (v_{s\beta}^v - r_s i_{s\beta}^v) dt \end{aligned} \quad (86)$$

Discretizing the voltage model by Tustin/Trapezoidal Approximations yields:

$$\begin{aligned} \psi_{r\alpha}^v(k) &= \psi_{r\alpha 1}^v(k) - \frac{\sigma L_r}{L_m} x_s^v i_{s\alpha}^v(k) \\ \psi_{r\beta}^v(k) &= \psi_{r\beta 1}^v(k) - \frac{\sigma L_r}{L_m} x_s^v i_{s\beta}^v(k) \end{aligned} \quad (87)$$

$$\begin{aligned} \psi_{r\alpha 1}^v(k) &= \frac{\omega_{bc}L_r T_s}{L_m} \frac{1}{2} (v_{s\alpha}^{v1}(k) - v_{s\alpha}^{v1}(k-1)) \\ \psi_{r\beta 1}^v(k) &= \frac{\omega_{bc}L_r T_s}{L_m} \frac{1}{2} (v_{s\beta}^{v1}(k) - v_{s\beta}^{v1}(k-1)) \end{aligned} \quad (88)$$

Where,

$$\begin{aligned} v_{s\alpha}^{v1} k &= v_{s\alpha}^v(k) - r_s i_{s\alpha}^v(k) \\ v_{s\beta}^{v1} k &= v_{s\beta}^v - r_s i_{s\beta}^v \end{aligned} \quad (89)$$

Similarly, discretizing current model using Tustin or Trapezoidal Approximation methods in Eq. (97) gives:

$$\begin{aligned} \psi_{r\alpha}^i k &= \frac{T_s}{2} \left(\frac{1}{T_r} x_m^i i_{s\alpha}^i k - \frac{1}{T_r} \psi_{r\alpha}^i k - \omega_r^i \omega_{bc} \psi_{r\beta}^i k \right. \\ &\quad \left. + \frac{1}{T_r} x_m^i i_{s\alpha}^i(k-1) - \frac{1}{T_r} \psi_{r\alpha}^i(k-1) \right. \\ &\quad \left. - \omega_r^i \omega_{bc} \psi_{r\beta}^i(k-1) \right) + \psi_{r\alpha}^i(k-1) \end{aligned} \quad (90)$$

$$\begin{aligned} \psi_{r\beta}^i k &= \frac{T_s}{2} \left(\frac{1}{T_r} x_m^i i_{s\beta}^i k - \frac{1}{T_r} \psi_{r\beta}^i k + \omega_r^i \omega_{bc} \psi_{r\alpha}^i k \right. \\ &\quad \left. + \frac{1}{T_r} x_m^i i_{s\beta}^i(k-1) - \frac{1}{T_r} \psi_{r\beta}^i(k-1) \right. \\ &\quad \left. + \omega_r^i \omega_{bc} \psi_{r\alpha}^i(k-1) \right) + \psi_{r\beta}^i(k-1) \end{aligned}$$

Combining the like terms,

$$\begin{aligned} \psi_{r\alpha}^i k \left(1 + \frac{T_s}{2T_r} \right) &= \frac{T_s}{2T_r} x_m^i (i_{s\alpha}^i k + i_{s\alpha}^i(k-1)) \\ &\quad - \frac{T_s}{2} \omega_r^i \omega_{bc} (\psi_{r\beta}^i k + \psi_{r\beta}^i(k-1)) \\ &\quad + \left(1 - \frac{T_s}{2T_r} \right) \psi_{r\alpha}^i(k-1) \end{aligned} \quad (91)$$

$$\begin{aligned} \psi_{r\beta}^i k \left(1 + \frac{T_s}{2T_r} \right) &= \frac{T_s}{2T_r} x_m^i (i_{s\beta}^i k + i_{s\beta}^i(k-1)) \\ &\quad + \frac{T_s}{2} \omega_r^i \omega_{bc} (\psi_{r\alpha}^i k + \psi_{r\alpha}^i(k-1)) \\ &\quad + \left(1 - \frac{T_s}{2T_r} \right) \psi_{r\beta}^i(k-1) \end{aligned}$$

After modification yields:

$$\begin{aligned}
\psi_{r\alpha}^i k &= \left(\frac{T_s}{2T_r + T_s} \right) x_m^i (i_{s\alpha}^i k + i_{s\alpha}^i k - 1) \\
&\quad - \frac{T_s T_r}{2T_r + T_s} \omega_r^i \omega_{bc} (\psi_{r\beta}^i k + \psi_{r\beta}^i k - 1) \\
&\quad + \left(\frac{2T_r - T_s}{2T_r + T_s} \right) \psi_{r\alpha}^i k - 1 \\
\psi_{r\beta}^i k &= \left(\frac{T_s}{2T_r + T_s} \right) x_m^i (i_{s\beta}^i k + i_{s\beta}^i k - 1) \\
&\quad + \frac{T_s T_r}{2T_r + T_s} \omega_r^i \omega_{bc} (\psi_{r\alpha}^i k + \psi_{r\alpha}^i k - 1) \\
&\quad + \left(\frac{2T_r - T_s}{2T_r + T_s} \right) \psi_{r\beta}^i k - 1
\end{aligned} \tag{92}$$

The voltage model due to the presence of pure integrator in classical MRAS causes initial value and drift problems. This problem will affect precision in the rotor position. Thus, to compensate that, a first order high-pass filter (HPF) is used. To avoid phase and amplitude problems brought up by the HPF in voltage model, HPF in current model are used simultaneously. Thus, the HPF also has to be discretized in a similar manner. The HPF is described by a transfer function:

$$G_s = \frac{v_0}{v_i} = \frac{T_f s}{T_f s + 1} \tag{93}$$

Where, reciprocal of T_f is the cut-off frequency of HPF.

By applying Tustin approximation method, Eq. (93) can be restated as:

$$\frac{v_0 z}{v_i z} = \frac{T_f \left(\frac{2}{T_s} \frac{z-1}{z+1} \right)}{T_f \left(\frac{2}{T_s} \frac{z-1}{z+1} \right) + 1} \tag{94}$$

$$\Rightarrow \frac{v_0 z}{v_i z} = \frac{\frac{2T_f}{T_s} z - 1}{\frac{2T_f}{T_s} z - 1 + z + 1}$$

$$\Rightarrow \frac{v_0 z}{v_i z} = \frac{\frac{2T_f}{T_s} 1 - z^{-1}}{\frac{2T_f}{T_s} 1 - z^{-1} + 1 + z^{-1}}$$

$$\Rightarrow \frac{v_0 z}{v_i z} = \frac{\frac{2T_f}{T_s} 1 - z^{-1}}{\left(\frac{2T_f + T_s}{T_s} \right) - \left(\frac{2T_f - T_s}{T_s} \right) z^{-1}}$$

Therefore,

$$v_0(k) = \frac{2T_f}{T_f + T_s} v_i(k) - v_i(k-1) + \left(\frac{2T_f - T_s}{2T_f + T_s} \right) v_0(k-1) \quad (95)$$

Adaptation Mechanism

The adaption block generates the value of estimated speed by synthesizing the error generated by comparing voltage and current model. In the classical MRAS, this is performed by defining a speed tuning signal, ϵ_ω to be minimised by a classical PI controller which generates the estimated speed which is fed back to the adaptive model. The expression for the error is

$$\epsilon_\omega = \psi_{r\alpha}^i \psi_{r\beta}^v - \psi_{r\alpha}^v \psi_{r\beta}^i \quad (96)$$

And the estimated speed can be derived by

$$\omega_r = \left\{ K_p + \frac{K_i}{s} + k_d \frac{d}{dt} \right\} \epsilon_\omega \quad (97)$$

To improve the dynamic performance of the classical MRAS, the fuzzy logic controller is used to adopt the cut-off frequency of HPF on-line and replace conventional PID controller.

Fuzzy Logic Controller

There are various types of fuzzy logic controllers, depending on the number of inputs and also on form of output signal. When a classical (PI or PID) are used, the input to the controller is the error signal. For example, for a PI speed controller, the input is speed error: $e = (\omega_{set} - \omega_r)$, which is the difference between reference or commanded speed to the actual rotor speed. However, when fuzzy logic controller is used, usually two inputs and sometimes more depending on the requirement and desire of the developer are used. For instance, if two inputs are considered, it can be described as the error and the derivative of the error. The derivative or change in error can be defined as $ce(k) = e(k) - e(k-1)$. This type of fuzzy logic controller is called Fuzzy-PI controller because it is analogous to classical PI controller which can be described by $u = K_p e + K_i \int e dt$, where u is the output of classical controller. Differentiating the classical PI controller would yield $du/dt = K_p de/dt + K_i e$.

It can be thus concluded that the change of the output depends on the error and also on the derivative of the error. The Simulink model of Fuzzy-PI controller is presented in Figure 23. The error and change in error inputs are first normalized and are mapped to the input membership function. Then, the fuzzified linguistic variables are synthesized by the IF-THEN rule. The process is followed by fuzzification process and finally is denormalized to physical value. From the figure, the red circled components are: (1) Normalizing gain for error ϵ , (2) derivative of the error (ce) and

normalizing gain for ce, (3) fuzzy logic controller and de-normalizing gain for output u, and (4) is controlled derivative of output (cu).

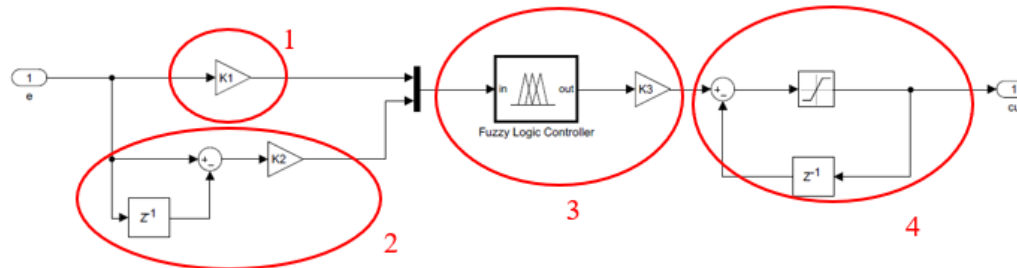


Figure 23 Fuzzy-PI controller model.

Membership functions

Various type of membership functions is present of which some are smooth membership functions like bell-shaped, sigmoid, Gaussians etc. while others are non-smooth which includes triangular, trapezoidal, etc. The choice of type of membership functions for specific problem is not unique. Thus, it is reasonable to specify parametrized membership function, which can be fitted to a practical problem. For example, to measure speed of motor or temperature of the room has large numbers of elements in universe, it is always useful to have a parametrized membership functions, where the parameters are adjusted according to the given problem.

Membership functions which contain straight line segments like triangular and trapezoidal membership functions are used extensively in various implementations due to their simple form and higher computational efficiency. However, it is good to note that when membership functions are constructed by straight line segments, they are not smooth at the switching points specified by parameters (P. Vas, 1999). This is the main reason for using other membership functions sometimes for some applications. In nutshell, in many applications both cost-effectiveness and performance play an important role, however, some systems demand cost as the major factor and satisfactory performance does not mean the highest possible performance. In such cases, simple membership functions are again proved to be useful.

The triangular membership function can be defined by lower limit as 'a', upper limit as 'b' and mid value as 'm', where $a < m < b$ can be defined as:

$$\mu_A x = \begin{cases} 0, & x \leq a \\ \frac{x-a}{m-a}, & a < x < m \\ \frac{b-x}{b-m}, & m < x < b \\ 0, & x \geq b \end{cases} \quad (98)$$

Similarly, trapezoidal membership function can be defined by a lower limit 'a', an upper limit 'd', a lower support limit 'b', and an upper support limit 'c', where $a < b < c < d$.

$$\mu_A x = \begin{cases} 0, & x < a \\ \frac{x-a}{b-a}, & a \leq x \leq b \\ 1, & b \leq x \leq c \\ \frac{b-x}{b-m}, & c \leq x \leq d \\ 0, & x > d \end{cases} \quad (99)$$

The membership definition in Eq. (98) and Eq. (99) can be graphically be represented as shown in Figure 24.

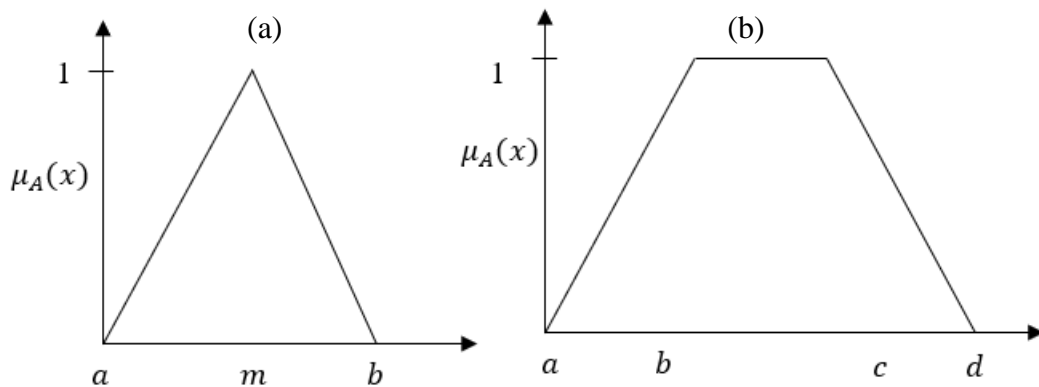


Figure 24 Membership function definition. (a) Triangular membership function, (b) Trapezoidal membership function

Other types of membership functions are not defined here but are described in many literatures. A mixture of triangular and trapezoidal membership functions proposed for this work is presented in Figure 25. Same membership functions are used for the two inputs (e and ce) and output.

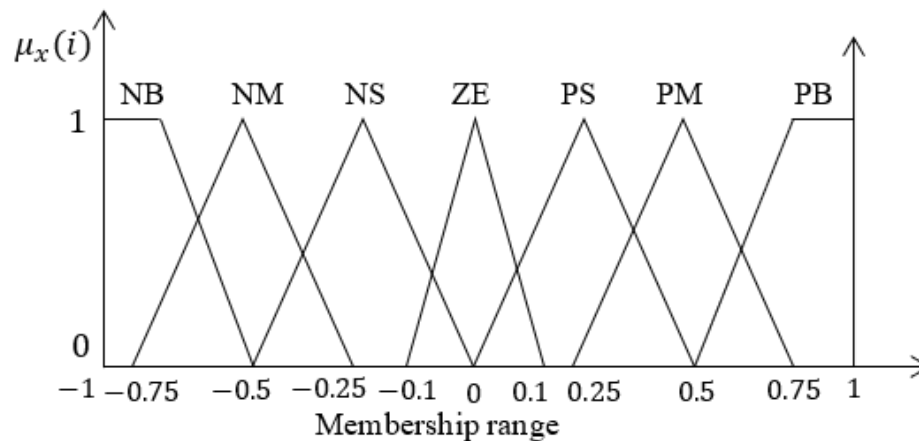


Figure 25 Membership Functions

The linguistic variables are Negative Big (NB), Negative Medium (NM), Negative Small (NS), Zero (ZE), Positive Small (PS), Positive Medium (PM) and Positive Big (PB) respectively defined in range of:

- i. NB = [-1.5 -1.25 -0.75 -0.5] – trapezoidal MF
- ii. NM = [-0.75 -0.5 -0.25] – triangular MF
- iii. NS = [-0.5 -0.25 0] - triangular MF
- iv. ZE = [-0.1 0 0.1] - triangular MF
- v. PS = [0 0.25 0.5] - triangular MF
- vi. PM = [0.25 0.5 0.75] - triangular MF
- vii. PB = [0.5 0.75 1 1.25 1.5] - trapezoidal MF

Fuzzy Inference Engine

Mamdani -type fuzzy logic inference system contains four main parts as shown in Figure 26. These parts are: fuzzifier, knowledge base, inference engine and Defuzzifier.

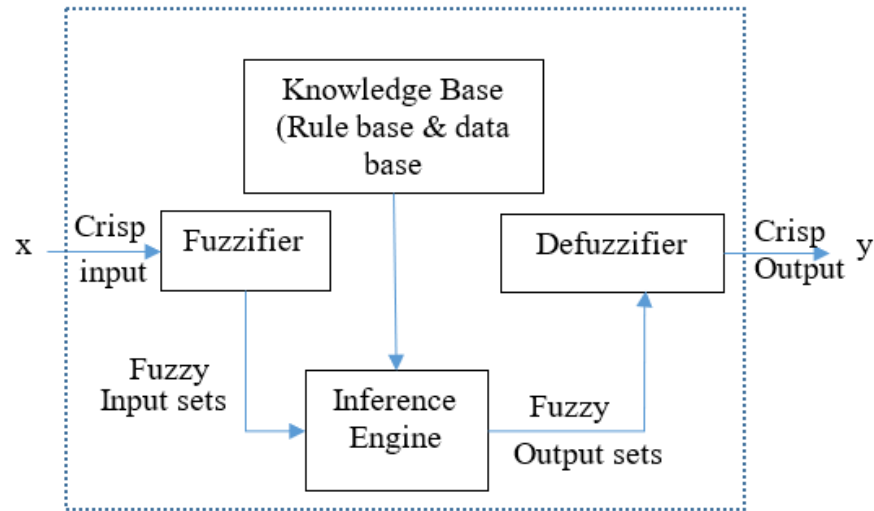


Figure 26 Schematic of Fuzzy Logic Controller

Fuzzifier perform measurement of the input variables, scale mappings and perform fuzzification process. Fuzzification is the process of converting a numerical variable (real number) to a linguistic variable or fuzzy number (antecedent). Each input(s) to fuzzy controller is mapped to a set of membership functions. The fuzzification process can be summarized as (Iancu, 2012):

- measures the values of inputs variables,
- performs a scale mapping that transfers the range of values of inputs variables into corresponding universes of discourse,
- performs the function of fuzzification that converts input data into suitable linguistic values which may be viewed as label of fuzzy sets.

The *knowledge base* consists of data base and the linguistic control rule base. The information used to define linguistic control rules and fuzzy data manipulation is provided by data base. The data base for the proposed controller is shown in Table IV. The rule base, on other hand, contains set of IF-THEN rules. The number of rules depends on number of input and membership functions. For instance, for the proposed method, there are 49 rules (7 x7) for two inputs. The 49 IF-THEN rule for the proposed controller can be evaluated as:

$$\begin{aligned}
 R_1: & \text{IF } e \text{ is NB AND } ce \text{ is NB THEN } u \text{ is NB} \\
 R_2: & \text{IF } e \text{ is NM AND } ce \text{ is NB THEN } u \text{ is NB} \\
 R_3: & \text{IF } e \text{ is NS AND } ce \text{ is NB THEN } u \text{ is NB} \\
 & \dots \dots \dots \dots \dots \dots \dots \\
 R_{21}: & \text{IF } e \text{ is PB AND } ce \text{ is NS THEN } u \text{ is PM} \\
 R_{22}: & \text{IF } e \text{ is NB AND } ce \text{ is ZE THEN } u \text{ is NB} \\
 & \dots \dots \dots \dots \dots \dots \dots \\
 R_{48}: & \text{IF } e \text{ is PM AND } ce \text{ is PB THEN } u \text{ is PB}
 \end{aligned} \tag{100}$$

$$R_{49}: IF e \text{ is } PB \text{ AND } ce \text{ is } PB \text{ THEN } u \text{ is } PB$$

The rule base is developed using the steps described as (P. Vas, 1999):

- Experience and expert knowledge for the application and control goals
- Modelling the control action of the expert operator.
- Modelling the system and the process.
- By using self-organized or artificial intelligence methods like neural networks.

Moreover, the rule base development should also be guided by the three important objectives to be achieved by fuzzy logic controller. The objectives are:

- Any significant errors in the process output should be removed by suitable adjustments in the control output.
- Smooth control action is to be ensured near the reference values by blocking the minimal oscillations produced by process output to the control input.
- To have good controller behavior with rise time, settling time and overshoot withing the permissible limits.

The *fuzzy inference engine* is the brain of fuzzy logic controller. It is popular computing framework based on the concept of fuzzy set theory, fuzzy IF-THEN rules and fuzzy reasoning. It has capability of both simulating human decision-making and inferring fuzzy control actions. The linguistic variables obtained from fuzzification of input variables are evaluated using the IF-THEN rules by the inference engine and the output (linguistic variable) is generated.

Table IV Linguistic Rule for speed error and change-in-error

| $e \rightarrow$ ce | NB | NM | NS | ZE | PS | PM | PB |
|-----------------------|----|----|----|----|----|----|----|
| NB | NB | NB | NB | NB | NM | NS | ZE |
| NM | NB | NB | NB | NM | NS | ZE | PS |
| NS | NB | NB | NM | NS | ZE | PS | PM |
| ZE | NB | NM | NS | ZE | LP | PM | PB |
| PS | NM | NS | ZE | LP | P | PB | PB |
| PM | NS | ZE | LP | P | VP | PB | PB |
| PB | ZE | PS | PM | PB | PB | PB | PB |

Defuzzifier performs scale mapping as well as defuzzification. Defuzzification is the process of producing a quantifiable result in crisp value, given output linguistic variables (also called consequent) and corresponding membership degrees. It is the process that maps a fuzzy set to a crisp set. The defuzzification interface performs the following functions (Iancu, 2012):

- scale mapping; which converts the range of values of output variables into corresponding universes of discourse.
- Defuzzification; which yields a non-fuzzy control action from an inferred fuzzy control action.

There are many different methods of defuzzification available, not limited to the following (Iancu, 2012; Leekwijck & Kerre, 1999; P. Vas, 1999):

- Center of Sums Method (COS)
- Center of gravity (COG) / Centroid of Area (COA) Method
- Center of Area / Bisector of Area Method (BOA)
- Weighted Average Method
- Maxima Methods
 - First of Maxima Method (FOM)
 - Last of Maxima Method (LOM)
 - Mean of Maxima Method (MOM)

The maxima methods are good candidates for fuzzy reasoning systems. The area methods exhibit the property of continuity that makes them suitable for fuzzy controllers (Leekwijck & Kerre, 1999). The center of gravity (COG) also known by names like centroid of area method, center of area method. The COG defuzzification is more commonly used method (Sugeno & Kang, 1988).

The Center of Gravity (COG) defines the output as corresponding to the abscissa of the center of gravity of the surface of the membership function characterizing the fuzzy set resulting from the aggregation of the implication results. This method provides a crisp value based on the center of gravity of the fuzzy set. For continuous membership function, the defuzzified crisp output value denoted by z^* using COG is defined as:

$$z^* = \frac{\int z \cdot \mu(z) dz}{\int \mu(z) dz} \quad (101)$$

Where, $\mu(z)$ is the aggregated output membership functions, z is the output quantity. For the discrete membership function, it can be obtained by discretizing at instant k from continuous membership function as (Iancu, 2012; Ross, 2010):

$$z^* = \frac{\sum_{k=1}^n z_k \cdot \mu(z_k)}{\sum_{k=1}^n \mu(z_k)} \quad (102)$$

where, z_k indicates the sample element, $\mu(z_k)$ is the membership function, and n represents the number of elements in the sample.

The fuzzy inference system in the MATLAB/Simulink can be designed using the steps described below.

1. Open fuzzy logic GUI can be launched by typing the key word 'fuzzy'. You will be prompted to GUI window similar to the (1) in figure.
2. From the File dropdown menu, we can select type of inference engine (Mamdani or Sugeno). Mamdani is chosen for this work.
3. Set number of inputs and outputs from the dropdown menu in GUI window. For instance, two inputs namely e and ce is set and output, u .
4. Double click on the input, e to set membership function and membership range. Another window as in (2) will be prompted. Here we can set membership functions and its range as shown in Figure 25. Also, the

linguistic variables are renamed to use during setting rules. Repeat the step for the other input and output.

5. Double clicking on the middle block seen in (1) will take us to rule editor as shown in (3). Here, we can set 49 rules which are listed in Table IV.
6. After setting the rule, we can check verify our rules by two types of view window. First is surface window. It will show 3-D surface. For instance, the rules for this project looks like in (4). Another verification can be done by providing arbitrary inputs to see the output the FLC can generate as in (5). Also, rule viewer can also show the mapping of input MFs to output.
7. The whole setup can be exported to either workspace or to file to be implemented in the Simulink for the purpose of simulating the model or to be implemented into DSP board.
8. On the other hand, the Fuzzy Logic library in Simulink contains fuzzy logic controller block as shown in Figure 23, which can be used to implement the fuzzy inference developed through GUI.

There is no proper tuning method proposed for fuzzy logic controller, so, the tuning method for the gains K_1 , K_2 and K_3 are through trial and error method by observing the estimated speed. The C program for the DSP implementation was developed in a similar way as in MATLAB GUI.

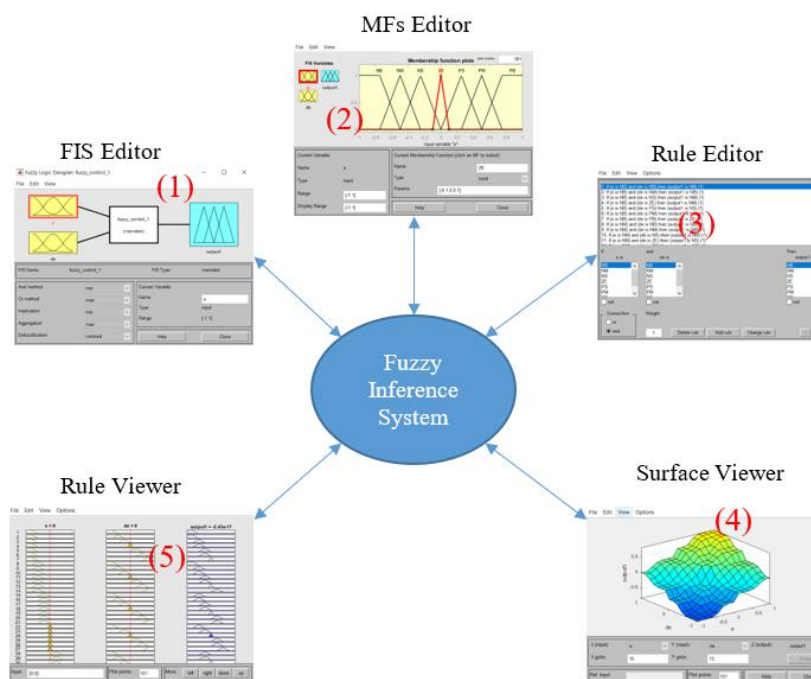


Figure 27 Fuzzy Inference System

Normalizing Factor

The conventional methods of designing fuzzy logic controller is to have membership function whose range cover all possible range of inputs and outputs but it is inefficient method. This is not a normalized form of fuzzy membership functions. The fuzzy inputs are first normalized using a normalizing factor or scaling factor and later transformed back to physical value using de-normalizing transformation factor as shown in Figure 28. Thus, the membership functions are set in range of $[-1 \ 1]$. If the FLC's applied in the normalized/denormalized process, the identical control algorithm can be convenient to all operating conditions (Bose, 2002).

The normalization process is a scale transformation, which maps the physical values of speed variable into a normalized universe of discourse (UoD). Meanwhile, the denormalization process maps the normalized UoD into physical values of the speed variable, which is also performed by a scale transformation (Isa et al., 2017). Since the UoD remains normalized/denormalized, the system can be tuned at its input and output scaling factors only, which may not affect the FLC system. Hence, the design becomes easier to be tuned due to its flexibility.

Two inputs (error and change in error) with single output are common in motor control because two different inputs lead to more accurate and faster response (Asgharpour-Alamdari, Alinejad-Beromi, & Yaghoobi, 2016).

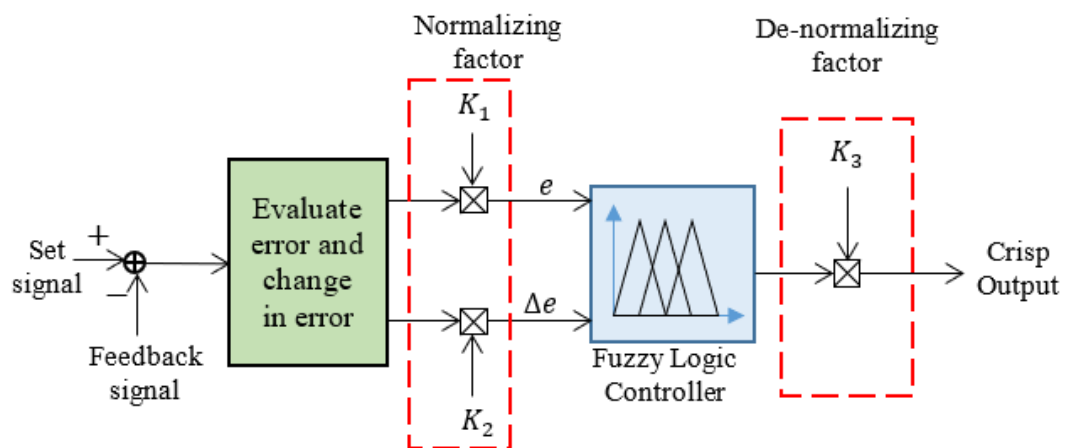


Figure 28 Scaling factors for fuzzy controller

The scaling factor makes the input fits the appropriate Universe of Discourse (UoD) instead of dealing with different operating conditions (Maamoun, Alsayed, & Shaltout, 2013). Scaling factor is one of the fuzzy logic parameters, which contributes significant effect on motor performance. Experimental investigations are conducted by Isa et al (Isa et al., 2017) based on the methods proposed in Sulaiman et al. (Sulaiman et al., 2015) on a performance analysis on the scaling factor of fuzzy logic speed control for vector-controlled induction motor drives. Since the input scaling factors have significant effect the motor performance, the scaling factors of rotor-flux error and change in error are to be determined through a systematic approach. Once the initial guess is set, the values are then tuned manually in order to achieve best motor performance. In the literatures, there is formula derived to achieve the initial

guesses of the scaling factors for speed controller but for rotor-flux controller for MRAS, there is no set of rules derived. For this reason, the scaling factors for this research are obtained purely through manual; trial and error methods. Therefore, a simple and systematic approach for obtaining the input scaling factors is feasible for the motor drive system.

Indirectly, the scaling factor shows a vital role for the FLC which influences the stability of the system. If the scaling factors are not well-tuned, the normalization for UoD, domain and the membership function of input or output can be affected. Other than that, unsuitable scaling factor also can influence transient and steady state response. An inappropriate initial choice for the scaling factors can also damage the plant process. Therefore, the scaling factor needs to be selected wisely.

Controllers

There are four controllers employed in the proposed project as shown in Figure 21: two inner current controllers, an outer speed controller and a rotor-flux controller in MRAS adaptation mechanism system. The rotor-flux controller as discussed in previous section uses fuzzy logic controller. So, the cascaded control loop for outer speed loop and inner current loop both employs classical PI controller. The outer speed loop also consists of PI controller. This controller will generate torque producing current i_q . This precise control of speed loop is of utmost importance to have accurate torque and speed control.

Precise control of motor current is a mandatory prerequisite for accurate torque and speed control. Thus, a current regulation plays an important role in modern power electronics systems like in variable speed drives. The key targets of the current controllers are summarized as (Holmes, Lipo, McGrath, & Kong, 2009):

- Achieve steady-state error by minimizing the steady-state magnitude and phase errors.
- Establish as high bandwidth as possible to achieve accurate reference tracking even at transient conditions.
- Avoid overload conditions by limiting the peak currents.
- Achieve minimal low-order harmonics in load currents, and
- Compensate for dc-link voltage ripples, deadtime delays, semiconductor device voltage drops and related second order effects associated with inverter.

For the simple first-order system, classical linear control theory suggests that the simple PI control should be enough (Holmes et al., 2009). The proportional action will manage the high frequency system response and the integral action will minimize the steady-state error. This control algorithm can achieve excellent DC current control, with minimal steady-state error because of large DC gain provided by integral action. The detail is described excellently by Holmes et.al in (Holmes et al., 2009). Here, the discussion will be focused on the controller transfer functions and its tuning method derived from their work.

The forward transfer function $G_c(s)$ for the PI controller would be defined as:

$$G_c(s) = k_p V_{DC} \left(1 + \frac{1}{sT_i} \right) \quad (103)$$

However, sampling and transport delay also has to be considered while designing controller for the modern converter system because of the use of DSP to implement the modulation process. The combined sampling and transport delay can be represented as:

$$G_d s = e^{-sT_d} \quad (104)$$

The principal objective of the current Pi controller is to maximize the proportionate gain k_p and also the integral gain k_i (by minimizing the integrator time constant, T_i). In addition, the sampling and transport delays are taken into account with phase margin, ϕ_m is retained while forward path open loop gains track through unity. The greater proportionate gain would be achieved if the system crossover frequency, ω_c (the frequency at which the unity gain occurs with required phase margin) is made as high as possible. The desired phase margin is firstly fixed and based on that the crossover frequency is approximated as:

$$\phi_m \approx \tan^{-1} \omega_c T_i - \omega_c T_d \quad (105)$$

Which produces,

$$\omega_c = \frac{\tan^{-1} \omega_c T_i - \phi_m}{T_d} \quad (106)$$

Thus, the maximum crossover frequency for given phase margin is achieved when $\tan^{-1} \omega_c T_i = \pi/2$. Therefore, maximum crossover frequency would be:

$$\omega_{c(max)} = \frac{\pi/2 - \phi_m}{T_d} \quad (107)$$

Based on the parameters available, now the controller gains are approximated as:

$$k_p \approx \frac{\omega_{c(max)} L}{V_{DC}} \quad (108)$$

Which is dependent only on plant series inductance, the crossover frequency and the DC bus voltage. Similarly, the integral time constant can be approximated by making $\tan^{-1}(\omega_{c(max)} T_i) \approx \pi/2$, which gives:

$$T_i \approx \frac{10}{\omega_{c max}} \quad (109)$$

However, practically the numerator in Eq. (109) needs to be bigger than 10 (for example 20, 30 or even 40).

Next, for the DSP implementation, the PI controller can also be discretized using Tustin or Trapezoidal approximation method.

The general form of PI controller is shown in Eq. (97). This can be discretized as in the MRAS as:

$$\omega_r(z) = K_p \epsilon_\omega(z) + \frac{K_i}{T_s} \left(\frac{z+1}{z-1} \right) \epsilon_\omega(z) \quad (110)$$

$$\begin{aligned}
\Rightarrow \omega_r z &= K_p \epsilon_\omega z + \frac{T_s K_i \epsilon_\omega z (1 - z^{-1})}{1 + z^{-1}} \\
\Rightarrow \omega_r z (1 + z^{-1}) &= K_p \epsilon_\omega z (1 + z^{-1}) + \frac{T_s K_i \epsilon_\omega z (1 - z^{-1})}{1 + z^{-1}} \\
\Rightarrow \omega_r k &= \omega_r (k-1) + K_p \epsilon_\omega (1 + z^{-1}) + \frac{T_s K_i \epsilon_\omega (1 - z^{-1})}{1 + z^{-1}}
\end{aligned}$$

Therefore,

$$\begin{aligned}
\omega_r k &= \omega_r (k-1) + \left(K_p + \frac{T_s K_i}{2} \right) \epsilon_\omega k \\
&\quad + \left(K_p - \frac{T_s K_i}{2} \right) \epsilon_\omega (k-1) \quad (111)
\end{aligned}$$

Open-loop Control of Compressor Motor

The compressor is one of the simplest applications which can be optimized using the variable frequency drive to improve the energy efficiency and also the thermal comfort. This is because the conventional air conditioner employing constant speed induction motor which as just ON/OFF capability has lots of energy wastage (when motor turns ON, the starting current is > 3 times the full load current which leads to more power consumption) and unbalance created in the power grid due to frequent switching of large motors. Moreover, this action will lead to discomfort/annoyance to the people residing in the room.

The cost and complexity in implementation of VFD technology for any induction motor drive depends on the type of system used to control the duty cycle/ratio of the IGBT switches in the VSI. For instance, the system would be very expensive and complex if speed signal is estimated in sensorless manner and the closed loop vector control algorithm is applied. The focus area is to control the old CarrierTM make air conditioner with compressor motor manufactured in 1987. The motor is enclosed in the cabinet creating impossible to conduct tests also to obtain equivalent circuit parameters.

This work employs open-loop control algorithm to control the speed of compressor motor in turn controls the temperature of the room. The overall block diagram of the control algorithm is presented in Figure 29. The motor speed is directly proportional to the room temperature measured by temperature sensor. The degree at which the motor will spin is decided by the fuzzy logic controller. Based on the measured temperature, the compressor motor speed is varied by varying the duty cycle of the IGBT switches in VSI. The voltage source inverter can have both frequency and magnitude of the voltage varied, thus achieving the speed control of motor.

The Figure 30 shows the arrangement for the measurement with the proposed algorithm. The real-time temperature and pressure measurements are taken using high accuracy testoTM smart probe (testo 805i and testo 549i) respectively; which has capability to send real-time data to smart phone via Bluetooth every 2 seconds.

The temperature sensor (RTD pt-100) is used to measure room temperature for the control algorithm. The point of temperature measurement is chosen at the back of Evaporator as shown in Figure 31 because that is the point which measures highest temperature and also last place to get cooled. The RTD temperature measured output is fed to ADC in F28069M via temperature transmitter. The ADC output is used as input to fuzzy logic controller to generate motor speed command.

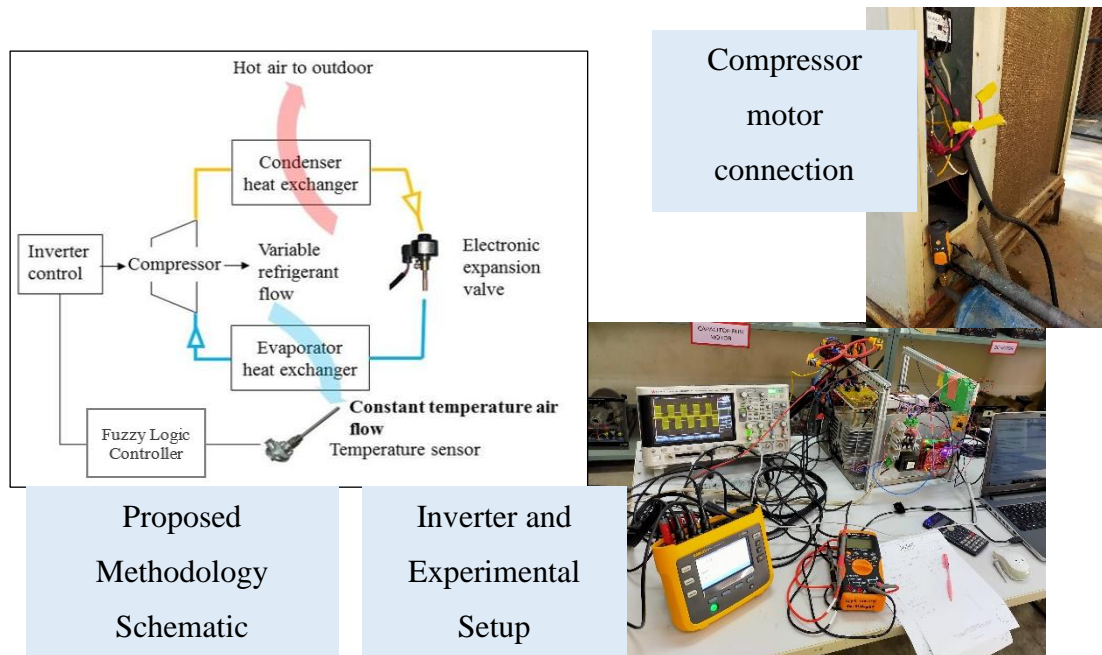


Figure 29 Control Algorithm and setup with Proposed method

The temperature sensor continuously monitors the room temperature. The fuzzy logic controller is used to decide the percentage of duty cycle to be generated through the expert decision-making technique used based on the room temperature. The Sugeno method of FLC is used in this experiment as it has easiest form compared to Mumdari method due to absence of requirement of defuzzification of output. This can increase execution time, decrease the requirement of memory and also cheap. The degree of output is instantly generated by the fuzzification block and it is mapped to the singleton output. The input triangular membership function for the air conditioning system is designed as shown in Figure 32.

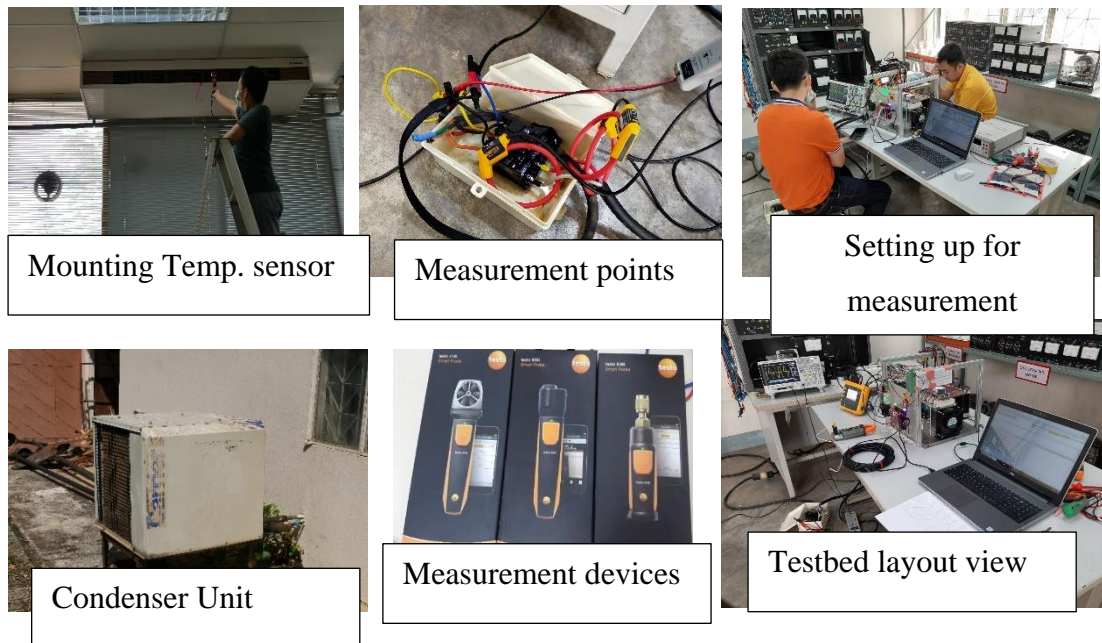


Figure 30 Setup for the proposed algorithm

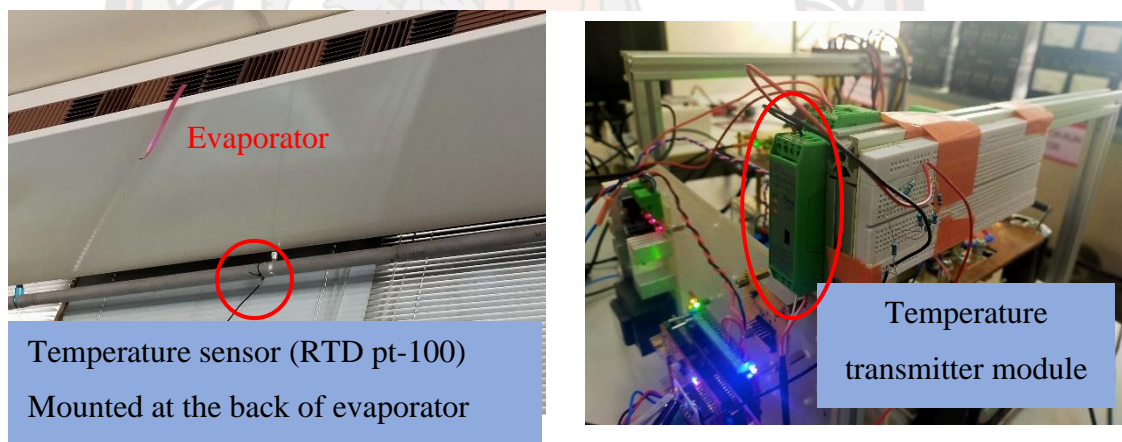


Figure 31 Temperature Measurement Unit

The linguistic variables are Very Cold (VCOLD), Cold (COLD), cool (COOL), Moderate (MOD), warm (WARM), Hot (HOT) and Very Hot (VHOT) which corresponds to the numerical values:

1. VCOLD: [0 16 18];
2. COLD: [17 20 22];
3. COOL: [20 22 25];
4. MOD: [22 25 28];
5. WARM: [25 27.5 29];

6. HOT: [28 29.5 31];
7. VHOT: [30 32 40].

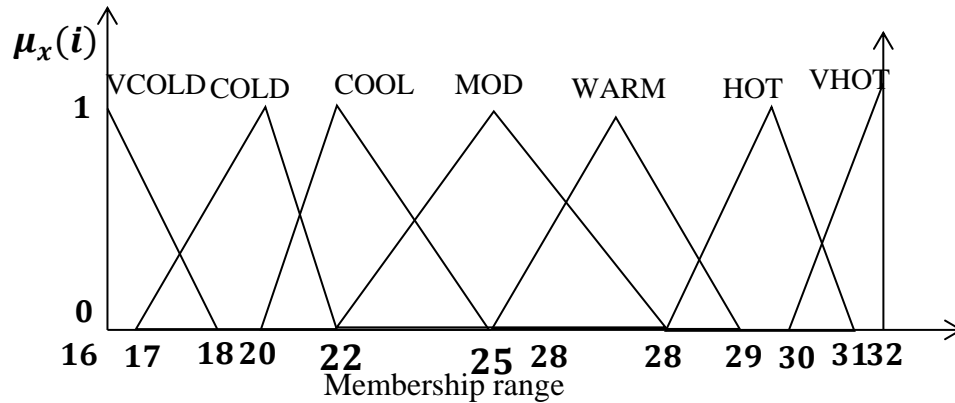


Figure 32 Membership Functions for temperature controller

Similarly, the output singleton can be defined for motor speed as: Very Fast (VFAST), Fast (FAST), Little Fast (LFAST), Moderate (MOD), Little Slow (LSLOW), Slow (SLOW), Very Slow (VSLOW) with membership value of 1, 0.95, 0.9, 0.85, 0.8, 0.75 and 0.7 %; respectively. The generated output from FLC is used to drive the inverse Clarke transformation by varying the d – and q – axis voltages. This generates the voltage space vector responsible to generate duty cycle of IGBT switches using SVM techniques.

CHAPTER IV

HARDWARE DEVELOPMENT, EXPERIMENTAL WORKS AND RESULTS

Introduction

Two different control techniques are discussed in this chapter. First one is the closed-loop control of induction motor of 3-hp, 4-pole and the second part comprises of sensorless control of 7 kW compressor motor. The VFD based vector control technique for the motors are accomplished with laboratory developed VSI with IGBTs controlled by SVM technique. The DSP used is Texas Instrument's motor control TMS320F28069M launchpad and the control algorithm was developed in Code Composer Studio (CCS™) IDE.

Practical Implementation of Proposed Method

The schematics of the practical setup is presented in Figure 33. It consists of the 3-phase commercial supply, uncontrolled 3-phase rectifier, voltage source inverter with DC-link capacitor, and the induction motor. On the control side, there is current measurement devices, speed sensor (encoder), DSP board, and PC with CCS installed.

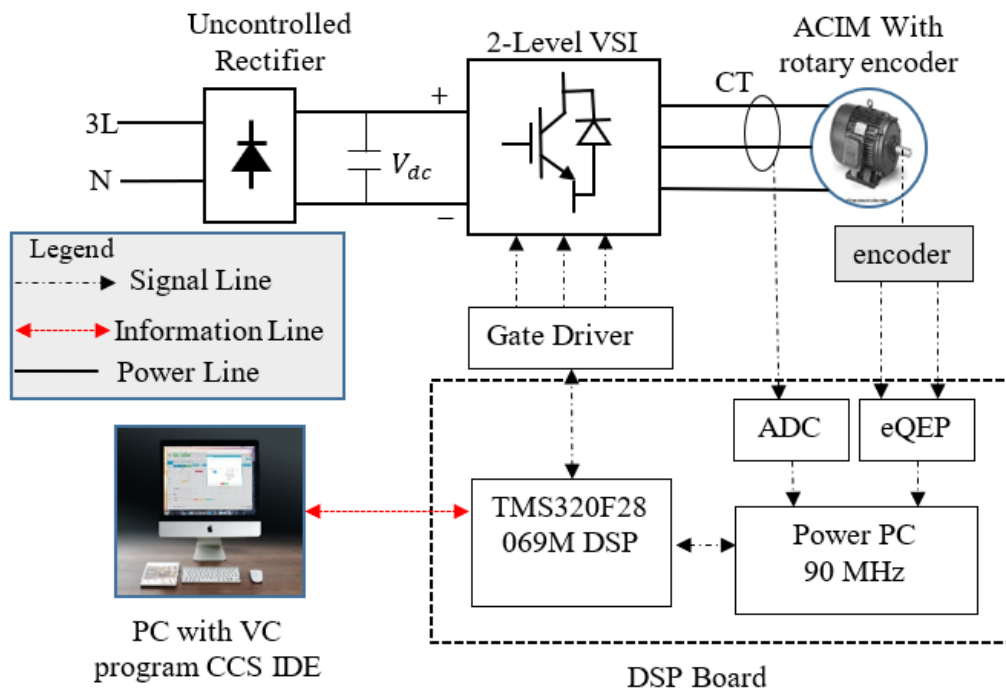


Figure 33 Laboratory Hardware Arrangement

The 3-phase supply is obtained from the commercial national grid supply which is maintained at 380V, 50 Hz. The supply along with the neutral point from the grid is tapped and is first connected to the 3-phase 4 pole molded-case circuit breaker (MCCB) of 15 A. The timer relay gets activated and thus after the set time is struck, the contactor coil is activated to close the contacts. The commercial supply with the protection circuit is arranged as shown in Figure 34.

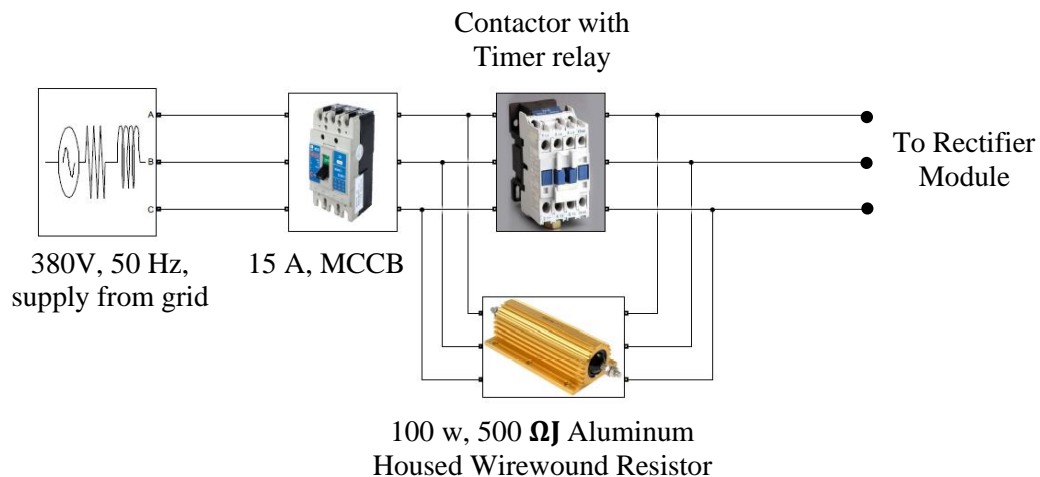


Figure 34 Power supply and protection layout

Three 100 w, 500ΩJ aluminum housed wire-wound power resistors are connected across each phase of contactor for the protection purpose. It is extremely stable, high quality wire wound resistors capable of dissipating high power in a limited space with relatively low surface temperature. The power is rapidly dissipated as heat through the aluminum housing to a specified heatsink.

Rectifier

The bridge rectifier converts 3-phase AC signals into equivalent DC signals. The ‘Vishay VS-130MT120KPBF’ is a Vishay make power rectifier module as shown in Figure 35 (a). It has 6-pin connections outlets. The first three pins are for 3-phase supply and next three are for positive and negative terminal for rectified DC output. The schematic is shown in Figure 35 (b). A range of extremely compact, encapsulated three phase bridge rectifier offers efficient and reliable operation. They are intended for use in general purpose and heavy-duty applications like inverter. For the multi-purpose applications, the inverter is developed with 1.2 kV rectifier module with maximum DC output current of 130 A.

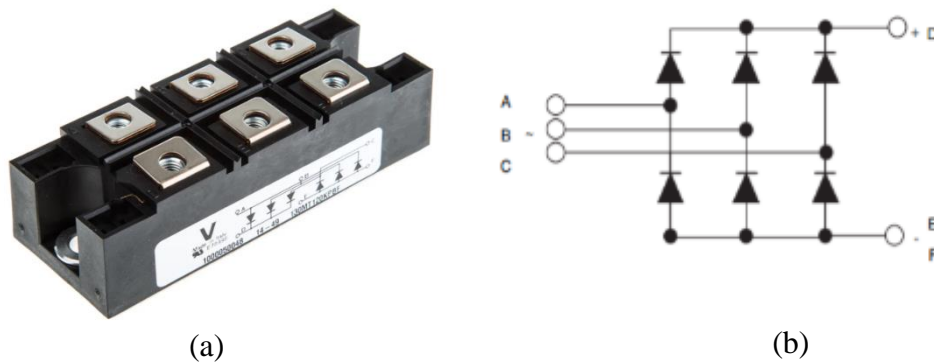
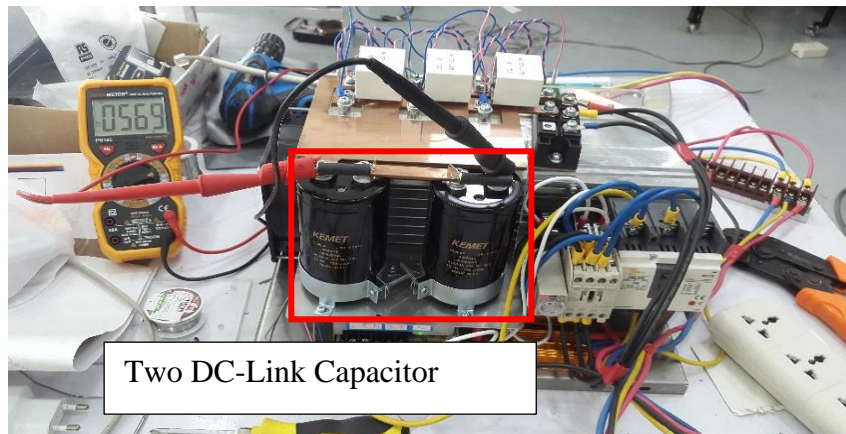


Figure 35 Three-phase rectifier. (a) 3-phase rectifier module, (b) circuit configuration of the module

DC-Link Capacitor

A 'DC-link' capacitor is fitted in between the rectifier (input stage) and the inverter (output stage) circuit to provide a low impedance path for high frequency switching currents and to provide energy storage. The two DC-link capacitors are shown presented in Figure 36 which is connected across the DC bus of inverter. As the inverter operation demands pulsed currents from the DC link side, DC-link capacitors are required to deliver these currents so that they do not reflect on the source side. Also, during abnormal conditions insufficient DC-link energy storage can result in high DC-link voltages if energy in inductors subjected to overload level currents dump into the DC-link. Moreover, the DC-link capacitor acts as the power factor correction (PFC) stage output filter, absorbing switching currents for minimum ripple voltage.

However, the capacitor has to be sized to meet specifications for ripple voltage at the DC-link and energy storage between mains cycles or when input power is lost. It should have a low equivalent series resistance (ESR) and a minimum capacitance and ripple current rating at the required operating voltage, temperature, power output, line and switching frequencies, and target lifetime.



Two DC-Link Capacitor

Figure 36 Inverter circuit showing DC-link Capacitor

For low power AC-DC converters with no PFC stage, minimum capacitance is normally set by the allowed mains ripple voltage on the DC-link. This gives a capacitance value of approximately $2 \mu\text{F}/\text{watt}$ for a universal mains input supply. For higher power AC-DC converters with PFC, the value is set by 'hold-up' or 'ride-through' time on input power loss and a much lower capacitance is possible with energy stored at high voltage, values of less than $1 \mu\text{F}/\text{watt}$ being normal. However, for AC output inverters, hold-up may not be an issue and a minimum capacitance is just needed to be low enough impedance at the inverter switching frequency to minimize voltage ripple.

In practical circuits, the ripple current that the capacitor must handle without overheating by dissipation in the ESR is often the overriding factor. The current can be so high that for a given voltage, a minimum physical size of capacitor is required to achieve low ESR, high dissipation and long lifetime. From calculation, experiment or simulation, headline capacitor specifications can be found but then practical considerations of size, cost, lifetime and reliability matters. In nutshell, it is up to the designer to choose. There are several types of capacitor which are available for the application, splitting between aluminum electrolytic, film and ceramic types. The choice is not easy to make and depends strongly on the application but the general trade-off is that electrolytic are cheaper and smaller than film and ceramic types for a given combination of voltage rating and capacitance (CV ratio) but have lower ripple current rating. They also have higher variation of capacitance, ESR and ripple current rating with time and temperature and have a shorter lifetime, heavily dependent on temperature and applied voltage. Electrolytic are only available up to about 600 VDC rating compared with several kV for film types, requiring series connection of electrolytic with balancing networks in high voltage applications.

Voltage Source Inverter

The motor control board developed in laboratory is shown in Figure 37. The control board comprises of voltage source inverter, current sensors and F28069M launchpad. The commercial 3-phase supply is fed to 3-phase bridge rectifier module which converts 3-phase alternating current to fixed direct current. The IGBT bridge derives

supply from fixed DC bus and the three-phase alternating voltage is generated which has change in magnitude as well as in frequency compared to the supply voltage. The magnitude and frequency of the output voltage depends on the duty cycle of the IGBT bridge generated by the gate driver. The duty cycle of IGBTs are generated by SVM technique which has superiority over other types of modulation techniques. The voltage required for the calculation of SVM is derived from the d-axis and q-axis voltages which flux and torque controlling components of the motor. The main components of VSI will be discussed briefly.

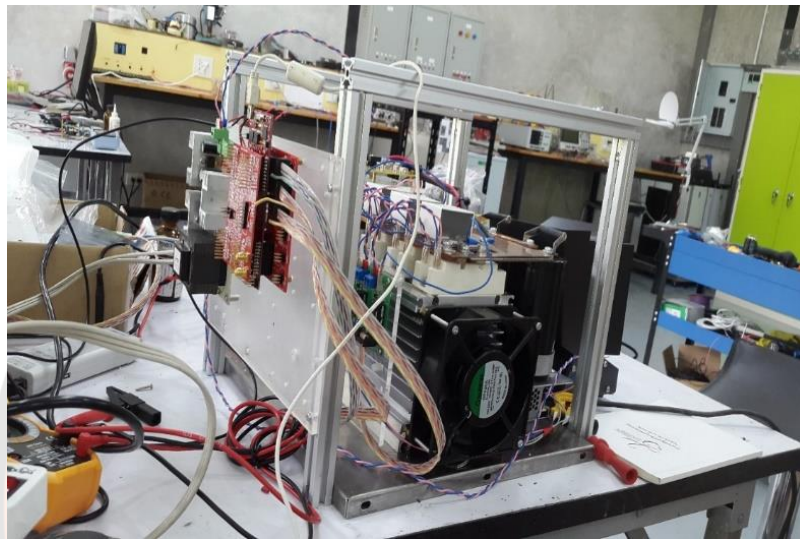


Figure 37 Inverter circuit

IGBT

An insulated-gate bipolar transistor (IGBT) is a three-terminal power semiconductor device primarily used as an electronic switch which, as it was developed, came to combine high efficiency and fast switching. It consists of four alternating layers (P-N-P-N) that are controlled by a metal–oxide–semiconductor (MOS) gate structure without regenerative action. Although the structure of the IGBT is topologically the same as a thyristor with a 'MOS' gate (MOS gate thyristor), the thyristor action is completely suppressed and only the transistor action is permitted in the entire device operation range. Since it is designed to turn on and off rapidly, the IGBT can synthesize complex waveforms with pulse-width modulation and low-pass filters, so it is also used in switching amplifiers in sound systems and industrial control systems. In switching applications modern devices feature pulse repetition rates well into the ultrasonic range—frequencies which are at least ten times the highest audio frequency handled by the device when used as an analog audio amplifier. As of 2010, the IGBT is the second most widely used power transistor, after the power MOSFET. The IGBT module shown in Figure 38 has two IGBTs embedded together in a module with three power terminal and two signal terminals. The power terminals are common terminal, The IGBT combines the simple gate-drive characteristics of the MOSFETs with the high-current and low–saturation-voltage capability of bipolar transistors by

combining an isolated gate FET for the control input, and a bipolar power transistor as a switch, in a single device.

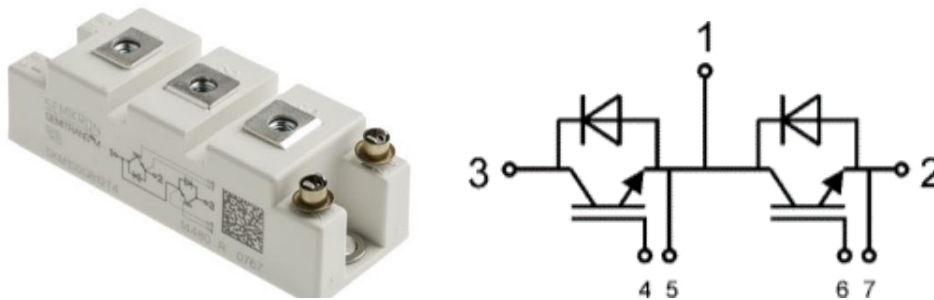


Figure 38 IGBT Module. Semikron SKM100GB12T4, SEMITRANS2, N-Channel Dual Half Bridge IGBT Module, 160 A max, 1200 V, Panel Mount

The Figure 39 (a) shows the arrangements of different components of inverter. The power electronic components are assembled and mounted on the heat-sink unit. The heat sink serves two main purpose. The first one is the heat sink can be used as the mounting support for different components. And the second is to assist the power electronic devices such as IGBTs to dissipate heat faster as it the heat dissipation capability by itself is very low. If the heat generated by power electronic components are not removed, it will lead to premature failure and may cause failure to entire circuit or system's performance.

The two DC-link capacitors of $2200 \mu F$ (400 V DC) each are connected in series to have voltage capacity of 800 V DC. The functions of DC-link capacitor are explained in chapter 3. The combination is in turn connected in parallel to the DC bus bar. Two copper plates are used as a connector to extend bus-bar terminal to be connected to link capacitor. Three $1 \mu F$ coupling capacitors (1200 V) are connected across each leg of IGBT bridges. The coupling capacitor transfers energy within the electrical network by means of displacement current between circuit nodes. The reactive nature of a capacitor allows it to respond to different frequencies uniquely. In coupling applications, a capacitor filters out low frequency DC components and allows only higher frequency AC components. Otherwise, if the DC components enter into the AC side of the inverter, it will affect the quality of the desired signal by introducing noise. The gate driver circuit for each leg of IGBT bridge attached at the backside of heat-sink accepts PWM signal from the DSP in range of 0 or 3.3 V and amplifies to 0 or 9 V (0 V for ON state and 9 V for OFF). The gate driver is powered by 12 V fixed DC supply. The gate driver also provides protection to the inverter apart from its main function of delivering the PWM gate pulse to IGBTs. The common terminal of each leg of inverter is tapped and is taken out as a supply to the motor. To achieve vector control of motor, the stator currents are required to be measured in real time. This is obtained by using a voltage and current sensor board as shown in Figure 39 (b). This board has possibility to have three voltage sensors and three current sensors. However, for this project, only two current sensors are used because the requirement for vector control is i_a and i_b only.

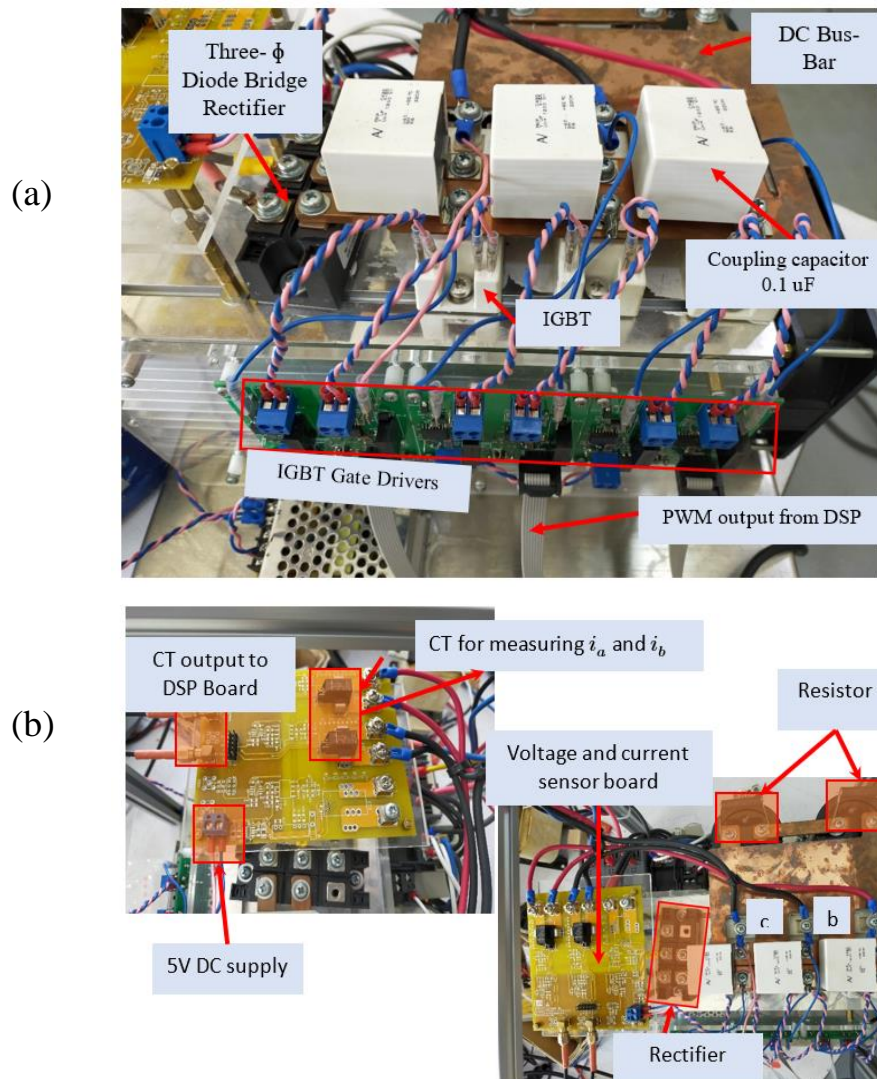


Figure 39 Voltage Source Inverter circuit. (a) Inverter accessories and (b) sensor and rectifier

The DSP board comprises of three other boards stacked on each other as shown in Figure 40. The first layer on the stack is power supply board. It has two level of DC voltages. The 5 V supply for powering board and other accessories and second is 3.3 v for ADC, DAC or any other signal conversion purposes. Second layer on stack is main F28069M board. The third layer is called the signal conditioning board. As name suggests, it consists of filters and buffers to obtain signal conditioning. And, the top layer is DAC board which is used to generate analog signal from the DSP.

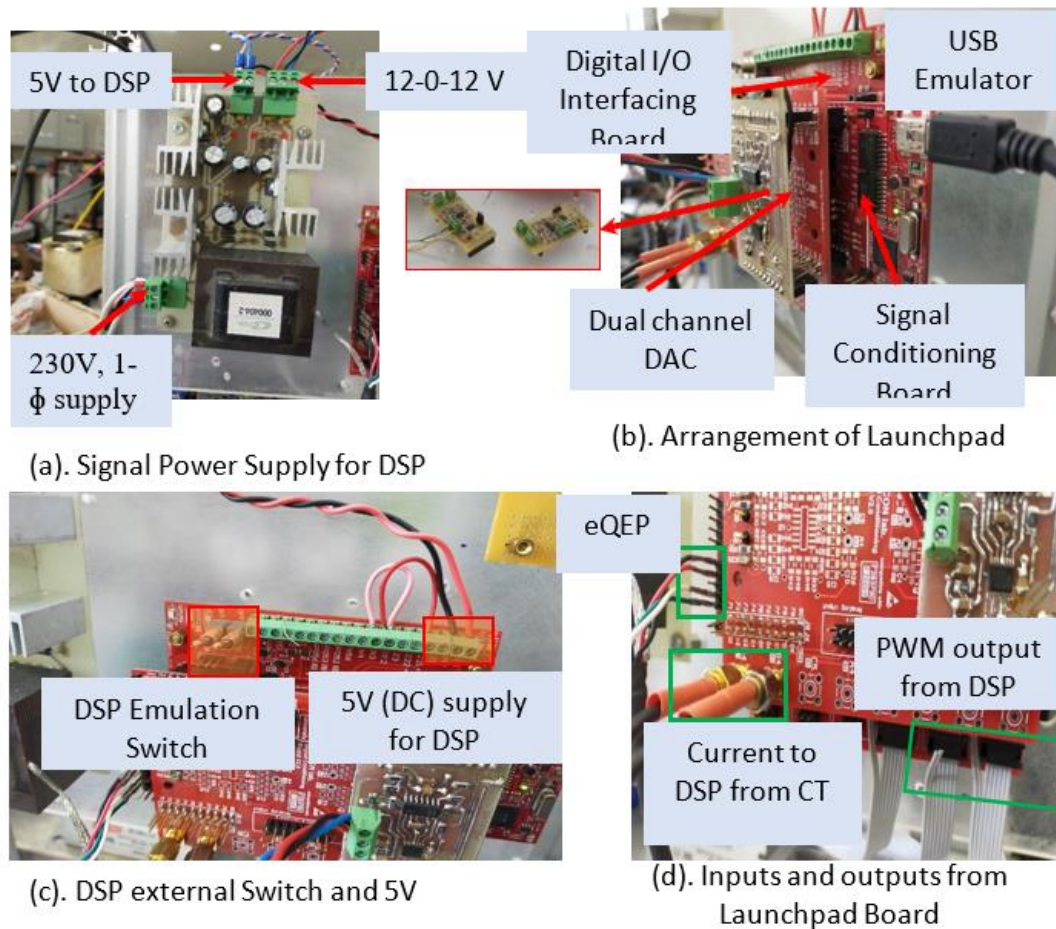


Figure 40 DSP Layout

TMS320F28069M TI's Launchpad and CCS Programming

The high-efficiency 32-bit TMS320F28069M piccolo microcontroller with InstaSPIN MOTION is the F2806x Piccolo family of microcontrollers (MCUs). This MCU is particularly developed for motor control applications. Some of the special features of this F280x MCU are:

1. High-Efficiency 32-Bit CPU (TMS320C28x)
 - 90 MHz (11.11-ns Cycle Time)
 - Fast Interrupt Response and Processing
 - Unified Memory Programming Model
 - Code-Efficient (in C/C++ and Assembly)
2. Embedded Memory
 - Up to 256KB of Flash
 - Up to 100KB of RAM
 - 2KB of One-Time Programmable (OTP) ROM
3. 6-Channel Direct Memory Access (DMA)

4. Low Device and System Cost
 - Single 3.3-V Supply
 - No Power Sequencing Requirement
 - Integrated Power-on Reset and Brown-out Reset
 - Low-Power Operating Modes
 - No Analog Support Pin
5. Clocking
 - Two Internal Zero-Pin Oscillators
 - On-Chip Crystal Oscillator/External Clock Input
 - Watchdog Timer Module
 - Missing Clock Detection Circuitry
6. Peripheral Interrupt Expansion (PIE) Block That Supports All Peripheral Interrupts
7. Three 32-Bit CPU Timers
8. Advanced Control Peripherals
9. Up to 8 Enhanced Pulse-Width Modulator (ePWM) Modules
 - 16 PWM Channels Total (8 HRPWM-Capable)
 - Independent 16-Bit Timer in Each Module
10. Up to 2 Enhanced Quadrature Encoder Pulse (eQEP) Modules
11. 12-Bit Analog-to-Digital Converter (ADC), Dual Sample-and-Hold (S/H)
 - Up to 3.46 MSPS
 - Up to 16 Channels
12. Up to 54 Individually Programmable, Multiplexed General-Purpose Input/output (GPIO) Pins with Input Filtering
13. Advanced Emulation Features
 - Analysis and Breakpoint Functions
 - Real-Time Debug Through Hardware

Fixed-Point Programming and Q-format Representation

To lower the cost of the implementation, many digital signal processors are designed to perform arithmetic operations only on integer numbers. To represent fractional numbers on these processors, we can use an implied binary point. For example, the eight-bit word $a = 01010110_2$ represents 86_{10} when interpreted as an integer number; however, we can consider an implied binary point for a and interpret it as a fractional number. However, if there is binary point in a fifth place: $a = 0101.0110_2$, the equivalent decimal value of this number is

$$\begin{aligned}
 a &= 0 \times 2^3 + 1 \times 2^2 + 0 \times 2^1 + 1 \times 2^0 + 0 \times 2^{-1} + 1 \times 2^{-2} + 1 \times 2^{-3} + 0 \times 2^{-4} \\
 &= 5.375
 \end{aligned}$$

With this interpretation, eight-bit word is used to represent four bits integer part of the number and another four bits to represent the fractional part. It is vivid that the first bit position to the right of the binary point has a weight of 0.5, the second bit position

has a weight of 0.25, and so on. It is good to note that this implied binary point is not specified in the hardware. Thus, the programmer needs to consider an appropriate scaling factor to interpret the result of the calculations correctly. For the above example, the hardware uses eight storage elements to represent the eight-bit word $a = 01010110_2$. Now, if the programmer aims to represent 5.375 with a , one should remember that a scaling factor of 2^{-4} must be appropriately applied to the result of any calculation using the variable a .

Depending on where the binary point is assumed to be, a given number can be interpreted as several different values. To make programming simpler, we generally use a fixed binary point throughout the algorithm. To easily specify how many bits are used to represent the integer and fractional parts of the number, we use a notation called the Q-format. For example, to specify that we are using three bits for the integer part and four bits for the fractional part, we may say that the numbers are in Q3.4 format.

Another possible notation is to specify only the length of the fractional part. This is based on the assumption that the word-length is known for a given processor. For example, when working with a processor which has a word-length of 16-bits, we may simply say that we are using the Q15 format to represent the numbers. This means that we are putting 15 bits to the right of the binary point and one bit to its left. In this case, the Q15 format is equivalent to the Q1.15 format. The latter notation is used by Texas Instrument for programming in its CCS IDE. However, note that, apart from using an implied scale factor, the Q format has nothing new compared to the well-known concept of representing numbers on a digital computer. As a result, we can use the Q format to represent signed two's complement numbers, too. In this case, we only need to allocate the most significant bit (MSB) to the sign and use the two's complement form for the negative numbers.

To choose the position of the binary point, it is critical to consider two main factors:

- The largest number that we may need to represent in a given algorithm
- The tolerable quantization noises

The former specifies how many bits must be used for the integer part and the latter determines the length of the fractional part.

When adding two signed numbers, the addend and augend may have different lengths. In this case, we have to extend the sign bit of the shorter number otherwise the result may not be correct. For example, extending the sign of 1011_2 by two bits, we obtain 111011_2 . How is this replication of the sign bit justified? We know that putting zeros at the left of a positive number will not change its value. To understand why sign extension does not change the value of a negative number, we should remember that, in the two's complement representation, a negative number is defined with regard to a complementation constant. Working with k -bit numbers, the complementation constant of the two's complement representation is $M = 2^k$. Similarly, to add two numbers in Q format, we should first align the binary point of the two numbers and sign extend the number that has shorter integer part. When using fixed-point representation to perform arithmetic operations, we must be careful about the range of the values that can be represented with a given Q format. As an example, assume that we add a in $Q_{na.ma}$ format to b in $Q_{nb.mb}$ format. Similar to the above example, we can sign extend the number with a shorter integer part and represent the

result in Q_{nc}.mc format where $nc = \text{maximum}[na, nb]$ and $mc = \text{maximum}[ma, mb]$. However, we should note that there are chances for overflow because adding two N-bit numbers can lead to an (N+1)-bit result. With the mentioned Q_{nc}.mc format for the result, we would have to make sure that overflow has not occurred.

Many digital signal processors choose the size of the output register of the accumulator larger than its input registers by several bits. These extra bits are called the guard bits. The guard bits allow the programmer to avoid overflow while accumulating a number of values without even scaling the accumulator inputs. You can easily verify that an accumulator with n guard bits allows us to accumulate $2n$ values without overflow. While we can use larger adders to prevent overflow, we cannot generally allow the word length to grow without limit. Hence, somewhere in our calculations, we have to truncate or round the addition results to a shorter word length. This generally means that we would have to allocate more bits to the integer part of the addition result so that we can represent larger values. In other words, we would have to change the position of the binary point.

For this project, Q₂₆ is chosen as the global Q value. This means, all the calculations will be performed at the Q₂₆ fixed-point number. However, if there are some calculation requiring higher precision or range, the other Q-formats are chosen explicitly and the results are converted back to global Q-format to normalize the calculation.

The IQmath library for CCS supports math functions for different calculations and conversions. The details can be accessed from the TI's C28x IQmath Library documentations.

DSP Programming

Programming DSPs in a high-level language such as C provides for portability and maintainability. A program can be rapidly prototyped and proven in C and then optimized to a particular processor architecture. Often, the real-time or time-critical portions of the code are hand assembled in this optimization process, resulting in high-performance code that is also efficient and readable.

Code Composer Studio is an integrated development environment (IDE) that supports TI's Microcontroller and Embedded Processors portfolio. Code Composer Studio comprises a suite of tools used to develop and debug embedded applications. It includes an optimizing C/C++ compiler, source code editor, project build environment, debugger, profiler, and many other features. Code Composer Studio combines the advantages of the Eclipse software framework with advanced embedded debug capabilities from TI resulting in a compelling feature-rich development environment for embedded developers.

The program flow for the closed-loop speed control of induction motor can be described as in Figure 41. The standard library functions are linked the program just the way it is done in standard C programming software as shown in code snippet below:

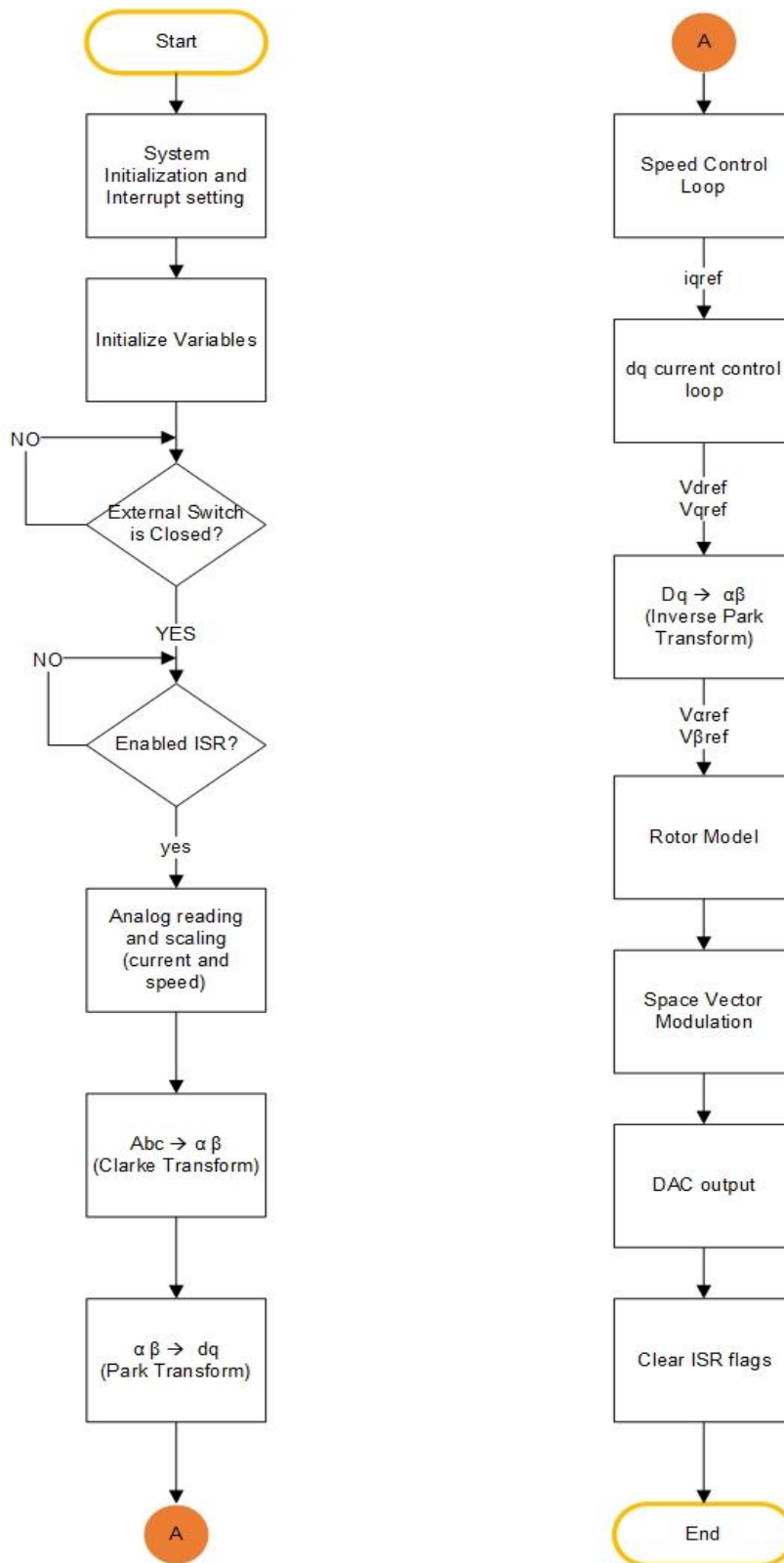


Figure 41 Flowchart for the program execution in CCS

```

88#include "IQmathLib.h"
49#include "DSP28x_Project.h" // Device Headerfile and Examples Include File
50#include <stdio.h>
51#include <stdlib.h>

```

Almost all the required library header files can be linked through the device header file and the IQmath library is used for low-cost fixed-point Q-format system. The Q26 is set as the global Q-format for the project (see definition in code snippet below). It is important to set global Q value to have uniform and standard numbering range and precision throughout the program, otherwise, it may lead to redundancy and overflow. Once the global Q-format is set, the programming has to just use the keyword `_IQ(x)` where x is the value to be converted to Q26 and not `_IQ26(x)`. However, if another Q-format is used in the program, then the Q-format has to be used in program to make the distinction from the global format.

```

54#define GLOBAL_Q    26
--

```

Generation of PWM

The f28069M has 16 Enhanced Pulse-Width Modulator (ePWM) modules with 8 HRPWM capability. However, for this project, we use only three-ePWM modules are used in this project. Each ePWM channel generates ePWMxA and ePWMxB which are nearly complimentary to each other. This means when the IGBT on positive rail of DC bus is ON, the IGBT on the negative rail should be OFF.

The rising and falling dead time (see code snippet below) makes sure to create some time delay in turning one switch on and another off in same rail to prevent dead-shot circuit of the system.

```

56#define PWMprd  4500 //fsw = 90 MHz/PWMprd for up-down count
57#define PWM_RED 90  //Rising edge dead time = (PWM_RED/90) us
58#define PWM_FED 90  //Falling edge dead time = (PWM_FED/90) us
59#define PWM_mode 1  //"0" for Bipolar and "1" for Unipolar

```

In this project the PWM module is configured in up-down count mode. In up-down count mode, the time-base counter (TBCTR), which is directly based on the CPU clock, counts up from zero and increments until the period (TBPRD) value is reached. Once the period value is reached, the time-base counter decrements until it reaches zero. At this point the counter will repeat the pattern and begin to count up again. The shape of the generated PWM waveform is determined by how the actions of the Action Qualifier Module are configured to behave at certain counter events. For this project, the following action/event pairs are used:

- Set PWM1A on event TBCTR= CMPA - up counting (CAU)
- Clear PWM1A on event TBCTR=CMPA - down counting (CAD)
- Set PWM1B on event TBCTR= CMPB - up counting (CBU)

- Clear PWM1B on event TBCTR=CMPB - down counting (CBD)

The code for this configuration is shown below and is illustrated in Figure 42.

```
EPwm1Regs.AQCTLA.bit.CAU = AQ_SET; // set actions for EPWM1A
EPwm1Regs.AQCTLA.bit.CAD = AQ_CLEAR;
EPwm2Regs.AQCTLA.bit.CAU = AQ_SET; // set actions for EPWM2A
EPwm2Regs.AQCTLA.bit.CAD = AQ_CLEAR;
```

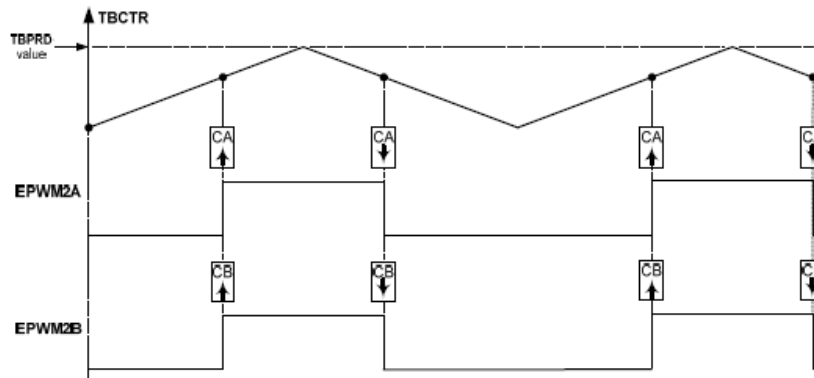


Figure 42 Action qualifier Module configuration and resultant PWM waveform

Source: TI ControlSUITE

The PWM frequency for up or down count is calculated as follows:

$$T_{PWM} = (2 \times TBPRD) \times T_{TBCLK}$$

$$F_{PWM} = \frac{1}{T_{PWM}} \quad (112)$$

where TBPRD is initialized as PWMprd = 4500 and T_{TBCLK} is set to 1/90MHz (90 MHz is system frequency of F28069M). Therefore, in this project the generated PWM frequency (FPWM) is 10kHz.

The user can observe the waveforms by putting an oscilloscope probe at the ePWM1A and ePWM1B pins as shown in Figure 43(a). The waveform in Figure 43(b) can be obtained by use of an external first-order low-pass RC filter to filter out the high frequency components. The selection of R and C value (or time constant, τ) is based on the cut-off frequency (f_c). For this type of filter, the variables are related to each other as:

$$\tau = RC = 1/2\pi f_c \quad (113)$$

It should be noted that the cut-off frequency, f_c has to be below the PWM frequency. Using the formula above, one can customize low pass filters used for signal being monitored.

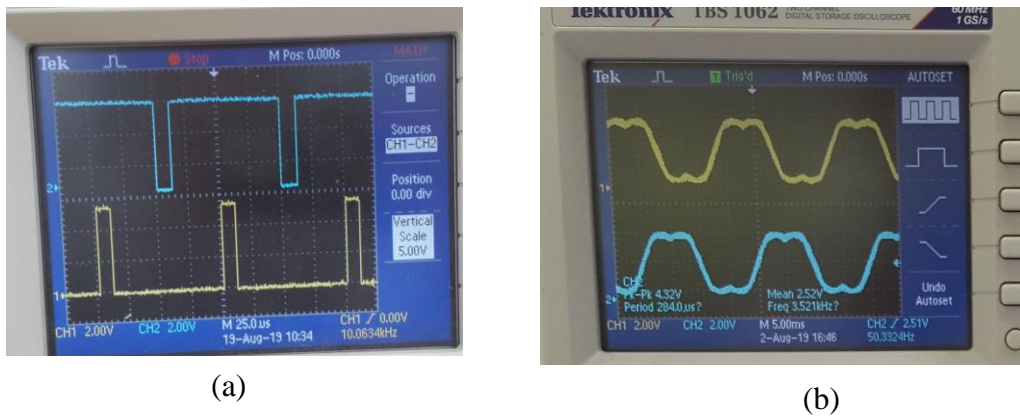


Figure 43 PWM outputs. (a) complementary waveform of PWM1A and PWM1B, (b) SVM wave obtained from low-pass RC-filter.

In order to change the PWM frequency, the user should change the value of 'PWMprd'. The shape of the PWM waveforms can be re-configured by editing the code under 'set actions' (see code snippet below). The individual PWM clocks and GPIO MUX can be configured in symmetrical mode (up-down mode).

```

600  /**EPWM Module 1 config**//
601  EPwm1Regs.TBPRD = PWMprd;
602  EPwm1Regs.TBPHS.half.TBPHS = 0; // Set Phase register to zero
603  EPwm1Regs.TBCTL.bit.CTRMODE = TB_COUNT_UPDOWN; // Symmetrical mode
604  EPwm1Regs.TBCTL.bit.PHSEN = TB_DISABLE; // Master module
605  EPwm1Regs.TBCTL.bit.PRDL = TB_SHADOW;
606  EPwm1Regs.TBCTL.bit.SYNCSEL = TB_CTR_ZERO; // Sync down-stream module
607  EPwm1Regs.TBCTL.bit.HSPCLKDIV = TB_DIV1; // Clock ratio to SYSCLKOUT
608  EPwm1Regs.TBCTL.bit.CLKDIV = TB_DIV1;
609  EPwm1Regs.CMPCTL.bit.SHDWAMODE = CC_SHADOW;
610  EPwm1Regs.CMPCTL.bit.SHDWBMODE = CC_SHADOW;
611  EPwm1Regs.CMPCTL.bit.LOADAMODE = CC_CTR_ZERO_PRD; // load on CTR=Zero
612  EPwm1Regs.CMPCTL.bit.LOADBMODE = CC_CTR_ZERO_PRD; // load on CTR=Zero
613  EPwm1Regs.AQCTLA.bit.CAU = AQ_SET; // set actions for EPWM1A
614  EPwm1Regs.AQCTLA.bit.CAD = AQ_CLEAR;

```

A trip-zone signal is used to halt, perhaps temporarily, a subset of PWM signals via hardware. The trip-zone signals at pins TZA and TZB are active low input signals. When one of these pins goes low, it indicates that a trip event has occurred. Each ePWM module can be individually configured to use or ignore each of the trip-zone pins. This configuration is determined by the TZSEL register for that specific ePWM module.

Each TZ input can be individually configured to provide either a cycle-by-cycle or one-shot trip event for an ePWM module. When a one shot or cycle-by-cycle trip event occurs (TZ pin is pulled to low), the action specified in the TZCTL register is carried out immediately on the ePWMxA and/or ePWMxB output. In the case of cycle-by-cycle the specified condition on the pins is automatically reset when the

ePWM time-base counter reaches zero if the trip event is no longer present. Therefore, in cycle-by-cycle, the trip event is reset every PWM cycle.

- ePWM1 will react as a one-shot trip and won't change the status when "OSHTx=1"
- ePWM1 will react as a cycle by cycle trip when "one_shot=0" and will be cleared if TZ1 pulled back high. The ePWM1 configurations are shown but other two PWMs are configured in similar manner.

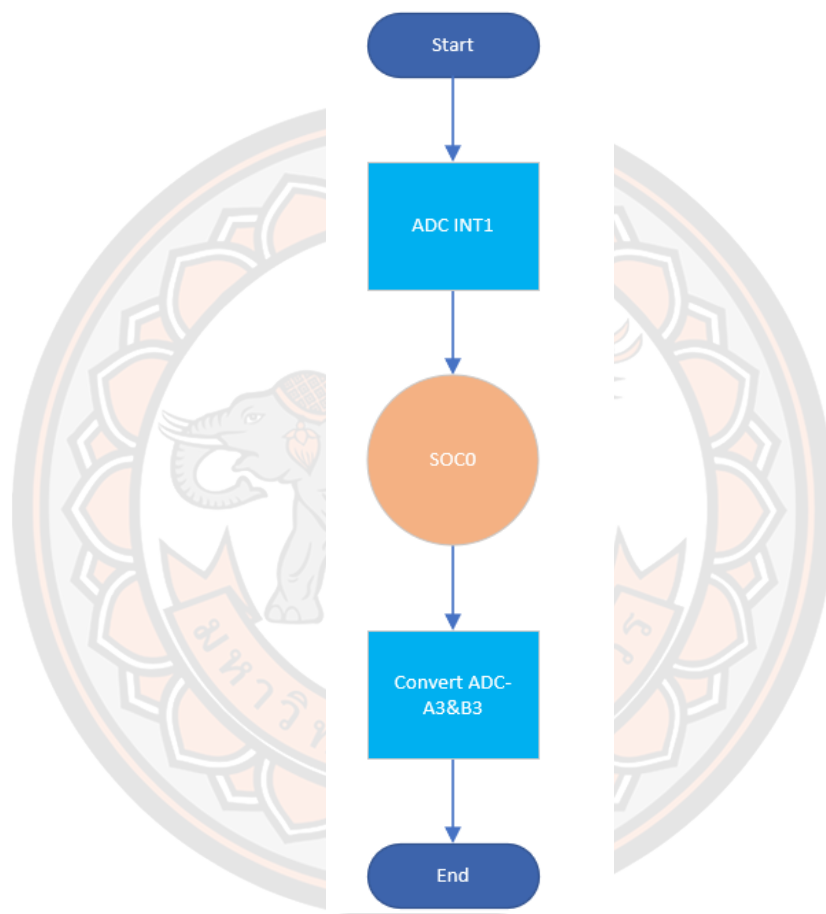


Figure 44 Flow chart for ADC conversion

ADC Configuration

This project is configured to simultaneously convert 2 ADC channels ADC-A3 and ADC-B3 for current i_a and i_b . This is achieved by configuring an ADC's end of conversion (EOC) event to create an ADC interrupt. This ADC interrupt is then configured to start the conversion of an ADC channels (SOC0 and SOC1). The Figure 44 illustrates the ADC conversion sequence used in this project. The ADC conversion results are stored in hexadecimal format. These values range from 0x0000 to 0x0FFF, which linearly scale to the equivalent of 0 to 3.3 volts respectively.

In this project, ADCInterrupt1 is used exclusively. For greater configurability, ADCInterrupt2 could be used to begin some subset of ADC SOC triggers. This would

effectively allow there to be two separate ADC conversion sequences with a configurable set of ADC channel conversions. There are various sources triggering start of ADC conversion (SOC) such as ePWM, S/W- software immediate start, external signals etc. In this project, only ePWM1 is configured to trigger ADC. Each time the CMPA is equal to PWM1 counter, ADC-A3 and ADC-B3 starts conversion. This process is illustrated in Figure 45.

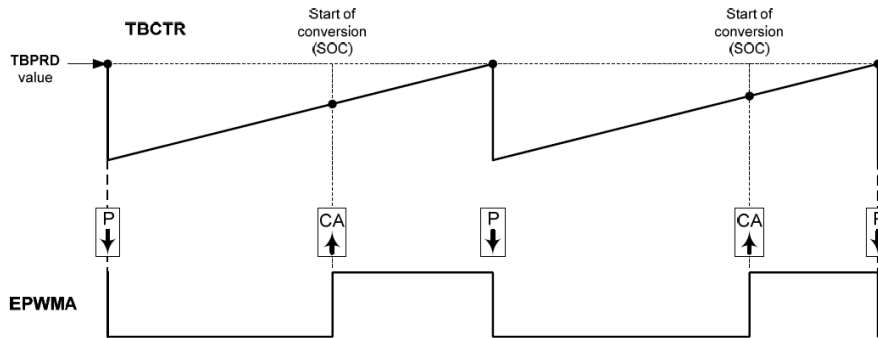


Figure 45 Action Qualifier Module and resultant PWM waveform.

Source: TI ControlSuite

An ADC channel 1 (ADC-A3 and ADC-B3) end of conversion event (EOC) causes the ADCInterrupt1 interrupt to fire. A write to the INTPULSEPOS field of the ADCCTL1 register allows the ADCInterrupt1 interrupt to be generated one cycle prior to output latch ADCInterrupt1. See the code snippet below:

```

707
708 AdcRegs.ADCCTL1.bit.INTPULSEPOS = 1; //ADCINT1 trips after AdcResults latch
709
710 AdcRegs.INTSEL1N2.bit.INT1SEL = 1; //setup EOC1 to trigger ADCINT1 to fire
711 AdcRegs.INTSEL1N2.bit.INT1CONT = 0; //Disable ADCINT1 Continuous mode
712 AdcRegs.INTSEL1N2.bit.INT1E = 1; //Enabled ADCINT1
713

```

Next, ADCInterrupt1 is configured to generate a start of conversion (SOC) events using the ADCINTSOCSEL3 register corresponding to ADC-A3 and ADC-B3. These ADC SOC events is then configured to begin the conversion of a specific ADC channel via the CHSEL field of the ADCSOC0CTL register. The CHSEL field has a value 3 which corresponds to ADC channels ADCA3 and ADC-B3.

If the INT1E field of the ADCINTSEL1N2 is set to 0, no interrupt will cause an ADC start of conversion (SOC) interrupt. Setting this field to 1 or 2 allows the ADCInterrupt1 or ADCInterrupt2 respectively to cause an ADC SOC0 trigger. Moreover, INT1CONT field has to be disabled to allow simultaneous conversion of ADC channel because F28069M allows simultaneous conversion only. Refer the code snippet for the setting below:

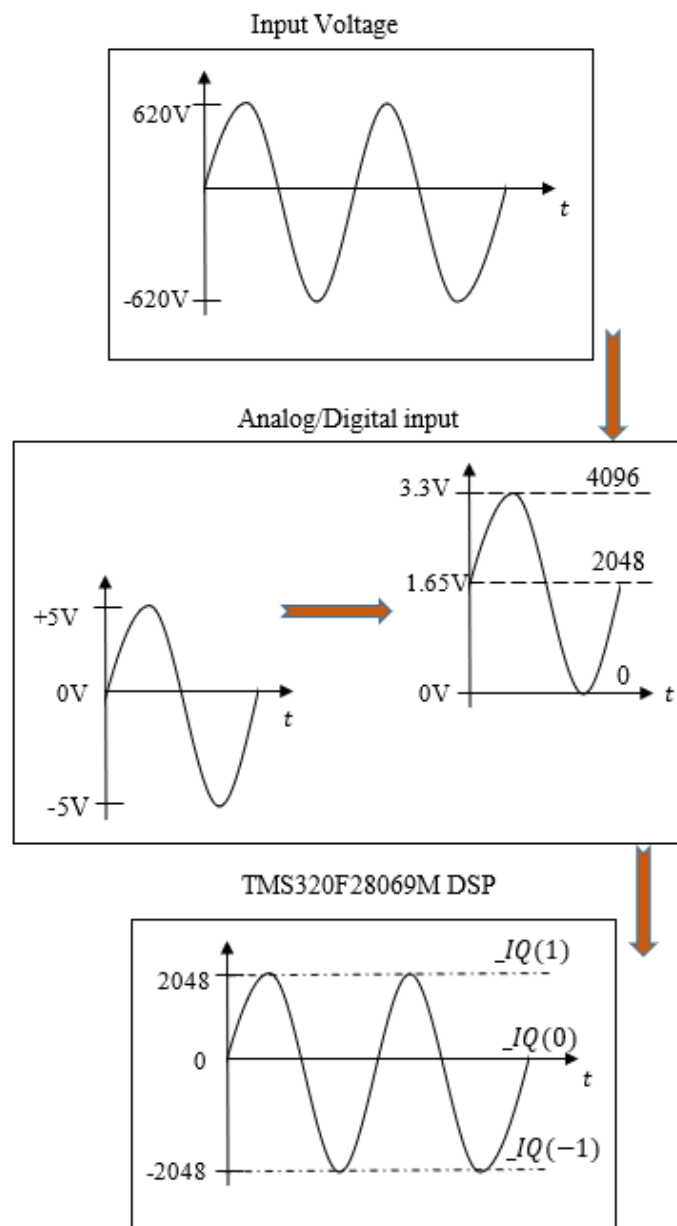


Figure 46 ADC logic Layout Diagram

```

AdcRegs.ADCCTL1.bit.INTPULSEPOS = 1; //ADCINT1 trips after AdcResults latch
AdcRegs.ADCCTL2.bit.ADCNONOVERLAP = 1; //Nonoverlap
AdcRegs.SOCPRCTL.bit.SOCPRORITY = 1; //SOC0 is the highest priority
AdcRegs.INTSEL1N2.bit.INT1E = 1; //Enabled ADCINT1
AdcRegs.INTSEL1N2.bit.INT1CONT = 0; //Disable ADCINT1 Continuous mode
AdcRegs.INTSEL1N2.bit.INT1SEL = 1; //setup EOC1 to trigger ADCINT1 to fire
AdcRegs.ADCSAMPLEMODE.bit.SIMULEN0 = 1; //Simultaneous sampling SOC0 and SOC1

AdcRegs.ADCSOC0CTL.bit.CHSEL = 3; //set SOC0 channel select to ADCINA3 and
AdcRegs.ADCSOC0CTL.bit.TRIGSEL = 5; //set SOC0 start trigger on EPWM1A-SOCA
AdcRegs.ADCSOC0CTL.bit.ACQPS = 6; //set SOC0 S/H Window to 7 ADC Clock Cyc

```

The stator currents from motor terminal is measured by CT and is converted to digital value and are assigned to i_a and i_b variables. The datasheet of the current sensor showed the sensitivity of 80mV/A. The scaling factor of CT is calculated by illustrating the ADC as shown in Figure 46.

The analog to digital conversion happens in three steps. (a) from physical measured value from output of inverter, (b) CT measures the physical value and sends in range of ± 5 V to Analog-to-digital converter, and (c) the offset correction and scaling to suit DSP.

```

while (AdcRegs.ADCINTFLG.bit.ADCINT1 == 0) {asm(" NOP");} //Wait for ADC conversion
temp = _IQ12toIQ(AdcResult.ADCRESULT0); // - _IQ(0.5); //get ADC in Q12 to Global_Q
ia = _IQmpy(_IQ(1),temp); //Ib=7.0711Arms Khall=0.08 V/A

temp = _IQ12toIQ(AdcResult.ADCRESULT1) - _IQ(0.5); //get ADC in Q12 to Global_Q
ib = _IQmpy(_IQ(5.833604390),temp); //Ib=7.0711Arms Khall=0.08 V/A

```

The scaling factor is calculated as:

$$K_{scaling} = \frac{3.3(v)}{I_{bc}K_H(v)} \quad (114)$$

Where, I_{bc} is the base current and K_H is the C.T sensitivity factor. In this project, the base current value was 7.0710 and C.T sensitivity factor is 0.008 (From datasheet). Therefore, the scaling factor is 5.8336.

Hardware Interrupt Service Routine (ISR)

One of the inherent differences between a digital signal processor (DSP) and other processors is the DSP's ability to receive and service multiple sources of interrupts very quickly. These interrupt sources can be timers for setting up different time bases, external analog-to-digital converters for converting analog audio signals into digital data, or on-chip coprocessors indicating a task is complete. The main steps for setting up interrupts for TMS320F28069M DSPs are:

- Create the interrupt service routines.
- Initialize the vector table and set up the vectors in the memory map.
- Enable the interrupts to the CPU.
- Enable the interrupt sources.

Typically, when an interrupt occurs, ordinary processing stops and an interrupt service routine (ISR) starts executing. The ISR's function is to store the contents of critical registers, perform the processing required by the interrupt, restore the register contents, and restart the interrupted process (Brenman, 1995). The first step in setting up interrupts in C is to define the ISR. The ISR is no different from an ordinary C subroutine except for the name of the routine (see the definition in code snipped below).

```
235 interrupt void epwm1_isr(void)
```

In the second step, the interrupt service routines need to save and restore every register that is used by the ISR. This is achieved by appropriately loading the vector (or table) of the ISR into the memory. This can be observed in snipped code below.

```
InitPieVectTable();
```

```
Interrupts that are used in this example are re-mapped to
ISR functions found within this file.
EALLOW; // This is needed to write to EALLOW protected registers
PieVectTable.EPwm1_INT = &epwm1_isr;
EDIS; // This is needed to disable write to EALLOW protected registers
```

The third step of enabling the interrupt to the CPU is established as shown in snipped code below.

```
Enable CPU INT3 which is connected to EPWM1-3 INT:
IER |= M_INT3;

Enable EPWM INTn in the PIE: Group 3 interrupt 1
PieCtrlRegs.PIEIER3.bit.INTx1 = 1;

Enable global Interrupts and higher priority real-time debug events:
EINT; // Enable Global interrupt INTM
ERTM; // Enable Global realtime interrupt DBGM
```

Finally, the last step is achieved by setting ePWM1 as the interrupt source. The ADC interrupt is triggered by the ePWM1 at the interval of 10 kHz which gets triggered at either zero or period. The setting is shown in snipped code below.

```
582 /***Interrupt enable setting ***/
583 EPwm1Regs.ETSEL.bit.INTSEL = ET_CTR_PRDZERO; // Select INT on Zero or PRD
584 EPwm1Regs.ETSEL.bit.INTEN = 1; // Enable INT
585 EPwm1Regs.ETPS.bit.INTPRD = ET_1ST; // Generate INT on 1st event
586
```

EQEP

An incremental encoder disk is patterned with a track of slots along its periphery. This is shown in Figure 47. These slots create an alternating pattern of dark and light lines. The disk count is defined by the number of dark and light line pairs that occur per revolution (lines per revolution). Therefore, every rotary encoder is defined by its pulse per revolution/lines per revolution (PPR). Index signal or zero reference is

added to generate a signal that occurs once per revolution (index signal: QEPI), which can be used to indicate an absolute position.

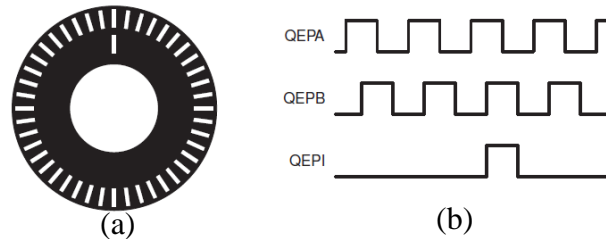


Figure 47 Rotary encoder disk. (a) rotary encoder disk, and (b) alternating pulse generated by encoder

Source: F280x reference technical manual

Since two photo-element reads the disk pattern to derive the direction information with a mechanical shift of 1/4 the pitch of a line pair between them, the PPR is multiplied by 4 to get total counts per revolution of the encoder. As the disk rotates, the two photo-elements generate signals that are shifted 90° out of phase from each other. These are commonly called the quadrature QEPA and QEPB signals. The clockwise direction for most encoders is defined as the QEPA channel going positive before the QEPB channel and vice-versa. F28069M has two eQEP channels, here, eQEP channel 1 is used. Therefore, only registers of eQEP1 is defined as evident from the snipped code below.

```
EQep1Regs.QUPRD=900000; // Unit Timer for 100Hz at 90 MHz SYSCLKOUT
EQep1Regs.QDECCTL.bit.QSRC=00; // QEP quadrature count mode

EQep1Regs.QEPCTL.bit.FREE_SOFT=2;
EQep1Regs.QEPCTL.bit.PCRM=00; // PCRM=00 mode - QPOSCNT reset on index event
EQep1Regs.QEPCTL.bit.UTE=1; // Unit Timeout Enable
EQep1Regs.QEPCTL.bit.QCLM=1; // Latch on unit time out

EQep1Regs.QOSMAX= 0x960; //set at 2^16
EQep1Regs.QEPCTL.bit.QPEN=1; // QEP enable
EQep1Regs.QCAPCTL.bit.UPPS=5; // 1/32 for unit position
EQep1Regs.QCAPCTL.bit.CCPS=6; // 1/64 for CAP clock
EQep1Regs.QCAPCTL.bit.CEN=1; // QEP Capture Enable
```

Once the settings and definition are completed, the rotor is calculated using the formula

$$v_k = \frac{x_k - x_{k-1}}{T} = \frac{\Delta X}{T} \quad (115)$$

Where, $v(k)$ is velocity at instant k , $x(k)$ is position at instant k , x_{k-1} is position at instant $k-1$, and T is fixed unit time or inverse of velocity calculation rate, and ΔX is increment position movement in unit time.

It is very important to do correct setting in the eQEP registers, otherwise unexpected results might be generated. For instance, I have chosen value of $QOSMAX = 6553$

which is decimal equivalent of Q16. This made the counter to overflow and caused motor to jerk every interval. This kind of issue is always possible if not taken care. The detail of eQEP settings can be accessed from eQEP section under TI TMS320F28069M technical reference manual.

RESULTS

Software Simulation Results

The model is validated by simulating it to see the dynamic tracking behavior of the machine according to the set speed. This is the first step to development of hardware system. The closed loop control behavior of the 5-hp, induction motor is simulated in MATLAB/SIMULINK software. The simulation results are presented in the following sections.

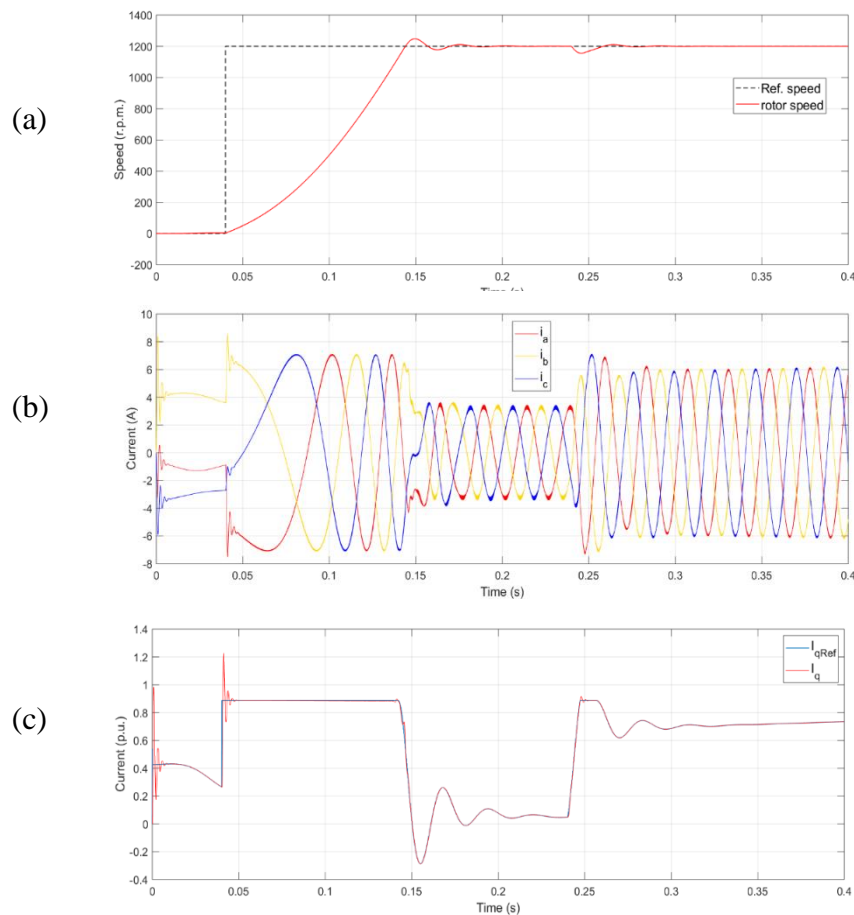


Figure 48 Simulation results for closed loop system. (a) Speed, (b) Stator Currents, (c) Q-axis currents (torque component)

The Figure 48 is the simulation result for sensed closed-loop speed control. The simulation result showed a successful tracking of reference speed with permissible

limit of rise time, overshoot and settling time. When full load is applied to motor shaft at 0.24 second, the controller can compensate the speed drift within few milliseconds and bringing back motor to steady state.

When the load torque is applied, the motor has to generate shaft torque to counter-balance the load torque to keep motor in steady state. This is evident from Figure 49 (a).

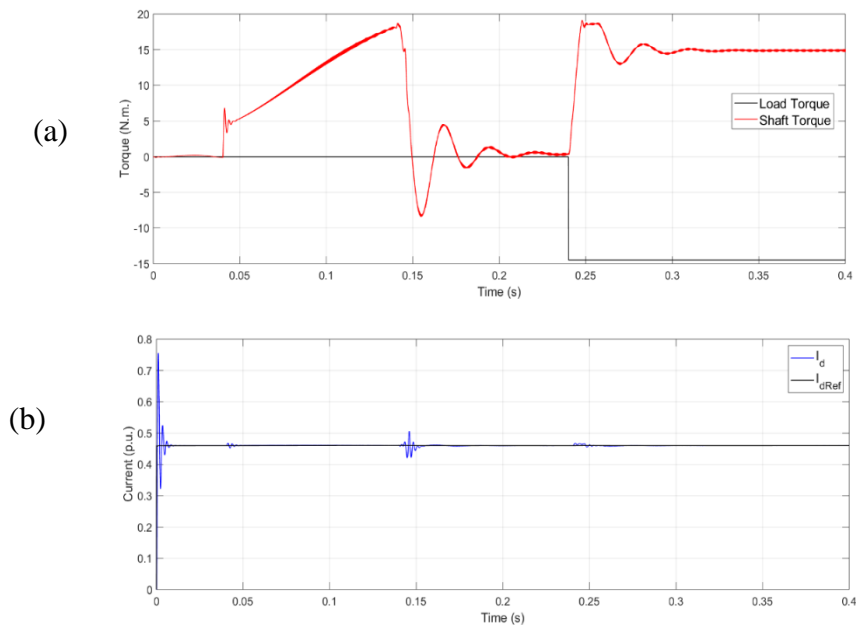


Figure 49 Torque and flux components. (a) Load and Shaft torque, and (b) d-axis current

The closed loop control is also implemented with fuzzy logic controller to have basis setup to prove that fuzzy logic controller has better controlling capability compared to conventional PI controller. The results are compared and is presented in Figure 50. The speed graph shows that the motor exhibits harsh behavior with conventional PI controller. However, it showed that the motor dynamics are greatly been improved with fuzzy logic controller. When having closer look on the current waveform in Figure 50 (b), the waveform is distorted and also have higher magnitude leading to higher ohmic losses when using PI controller but these problem is solved with the use of FLC. Moreover, the torque response in (c) exhibits continuous oscillation which would cause motor to vibrate and thus causing heating in motor. But with the implementation of FLC, the vibration is removed making smooth operation.

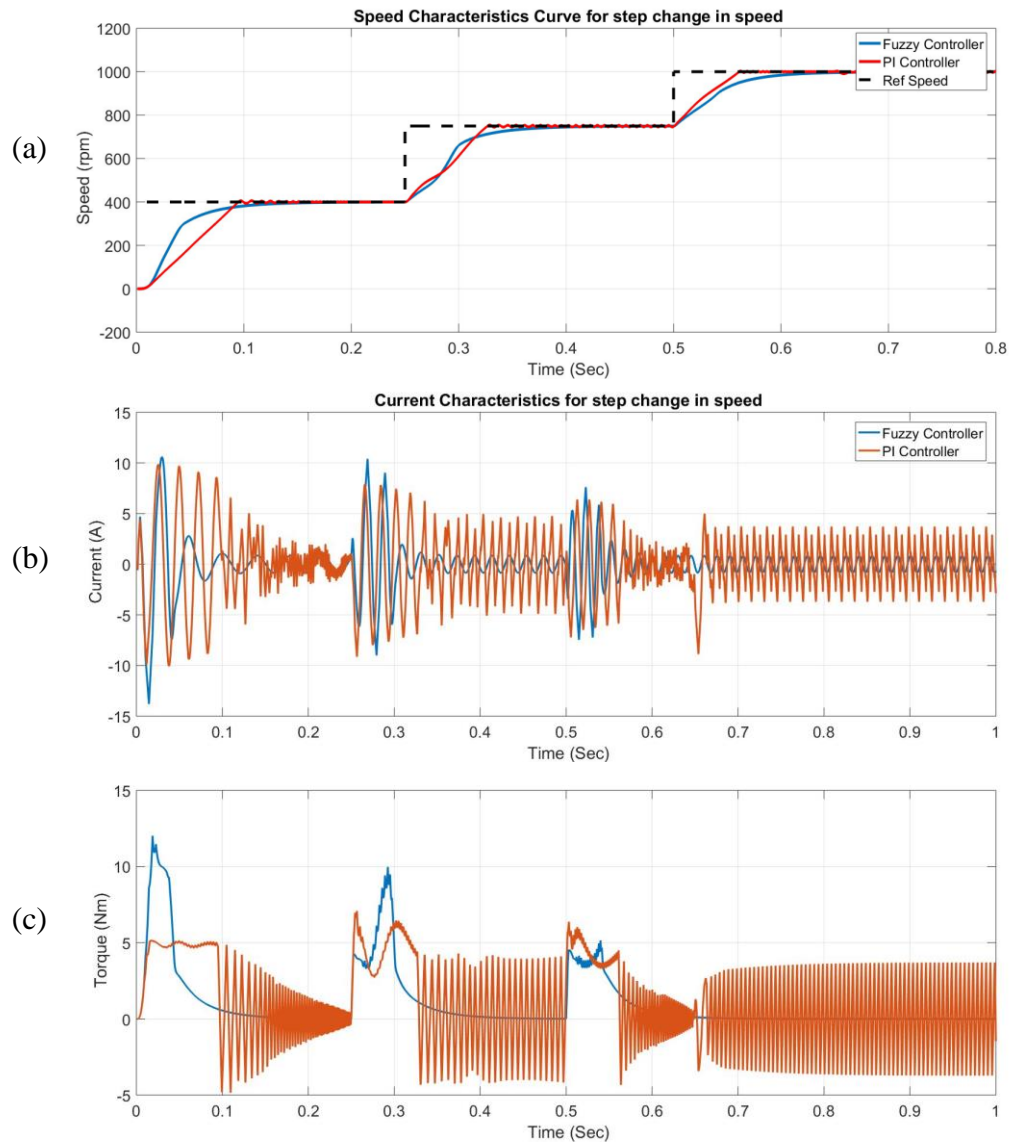


Figure 50 Comparative results for PI and Fuzzy PI controller. (a) Speed, (b) current, and (c) torque

In Figure 51 and Figure 52, the simulation results for the forward-reverse phenomenon for the sensorless control using Fuzzy Logic Controller is presented. The motor speed following the set speed satisfactorily with best performance even at low and negative speed settings is shown. A full load is applied at 0.68 sec. The fuzzy logic controller-based speed estimator as evident from Figure 51 (a), showed an equivalent behavior with the sensed one. The main problem with the sensorless control nowadays is the dynamics when it is desired to operate at lower or zero speeds. This was also been simulated and showed much improved dynamic behavior with replacing Fuzzy PI controller on the classical PI controller. However, the tuning of controller requires maximum time since there is no automatic tuning developed in the literatures like we have for classical PID controllers.

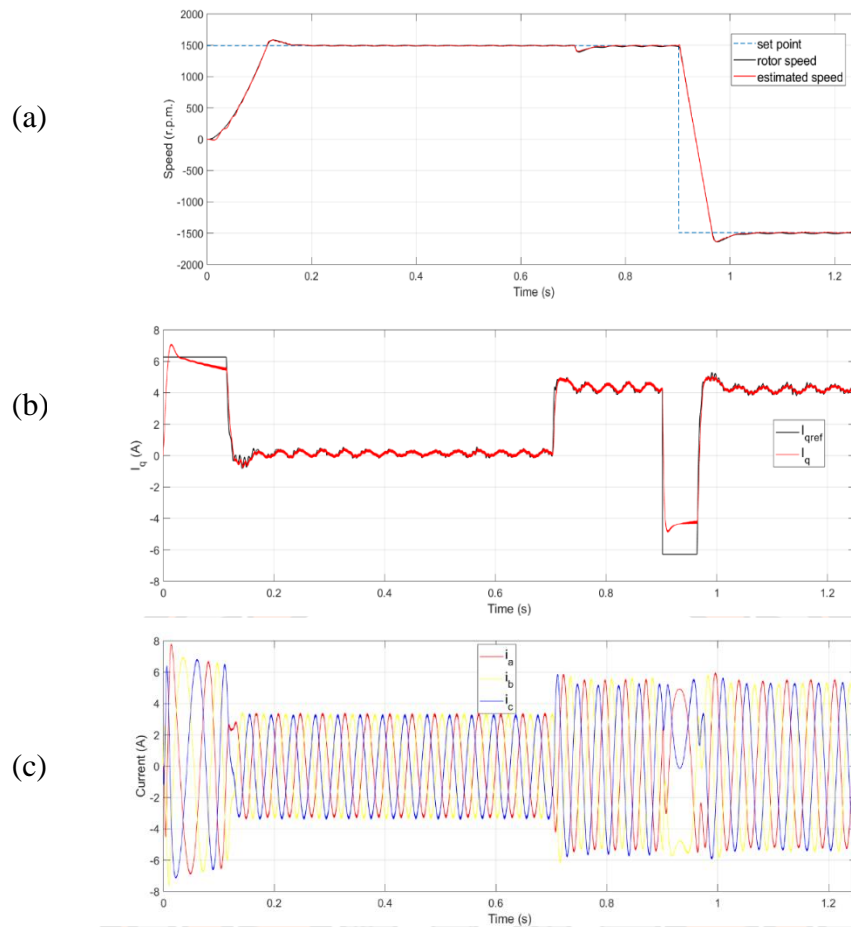


Figure 51 sensorless behavior using Fuzzy Logic Controller. (a) Motor speed, (b) Torque producing current (I_q), (c) stator currents

The speed behavior alone cannot determine the level of success it can produce on the control drive system. The current and torque are equally important variables to be observed. The stator currents, torque producing current (I_q), and flux-producing current (I_d) are also presented to be able to make a comparative analysis. For the proposed method, the motor variables are always being controlled within the permissible limit. The rotor angle (position) estimated through rotor model and the sine and cosine of angle which is required for Park and Inverse Park Transformation are also presented. It also makes evident that the currents in stationary reference frame are constant (DC equivalent), while in the stationary reference frame are sine wave with fundamental frequency.

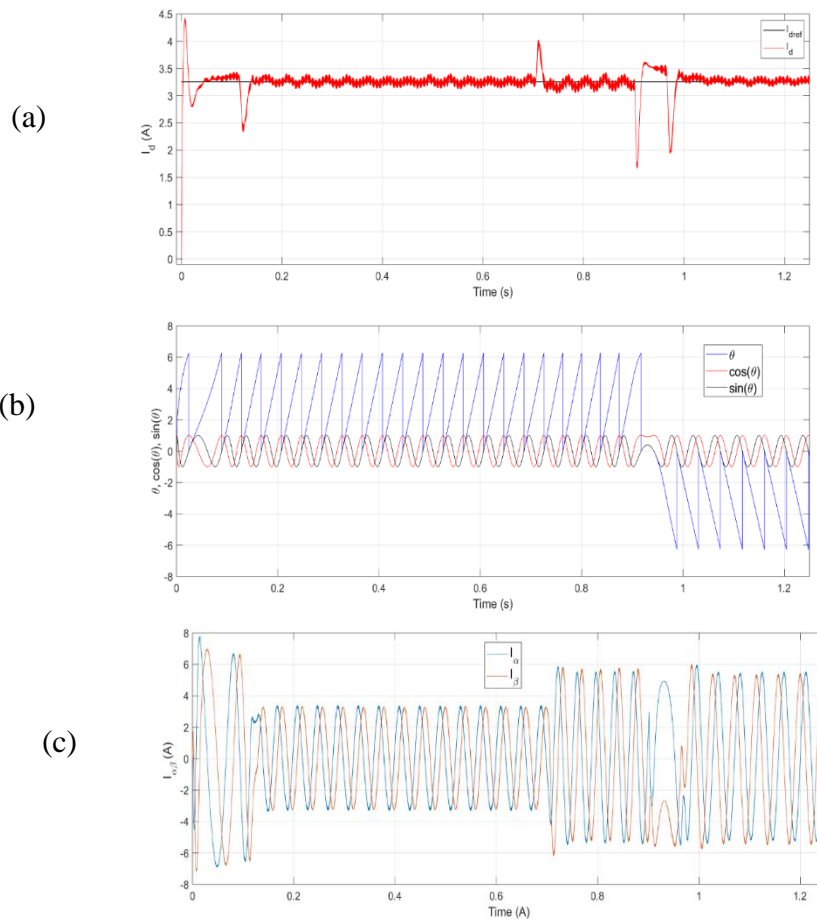


Figure 52 currents and angle for the sensorless control. (a) d-axis current, (b) rotor position and sine and cosine of rotor position, and (c) Stationary reference frame currents.

3-hp, 4-pole Motor Results

The experimental result for the 3-hp, 4-pole, 3-phase induction motor with induction generator as load is presented in this section. Similar to the one explained in the simulation, the forward and reversing phenomenon was observed in experiment also. The experimental results show a fairly satisfactory outcome with close reference tracking behavior of the rotor speed as shown in Figure 53 (a). The current waveform presented in Figure 53 (b) also showed a good trait with the steady-state value representing closely to pure sine wave. However, it is to be noted that the controller parameter used in simulation cannot obtain same smooth operation in real motor due to the fact that the simulation motor is developed with lots of assumptions. However, these parameter values serve as initial values to start tuning little bit until we obtain good operation.

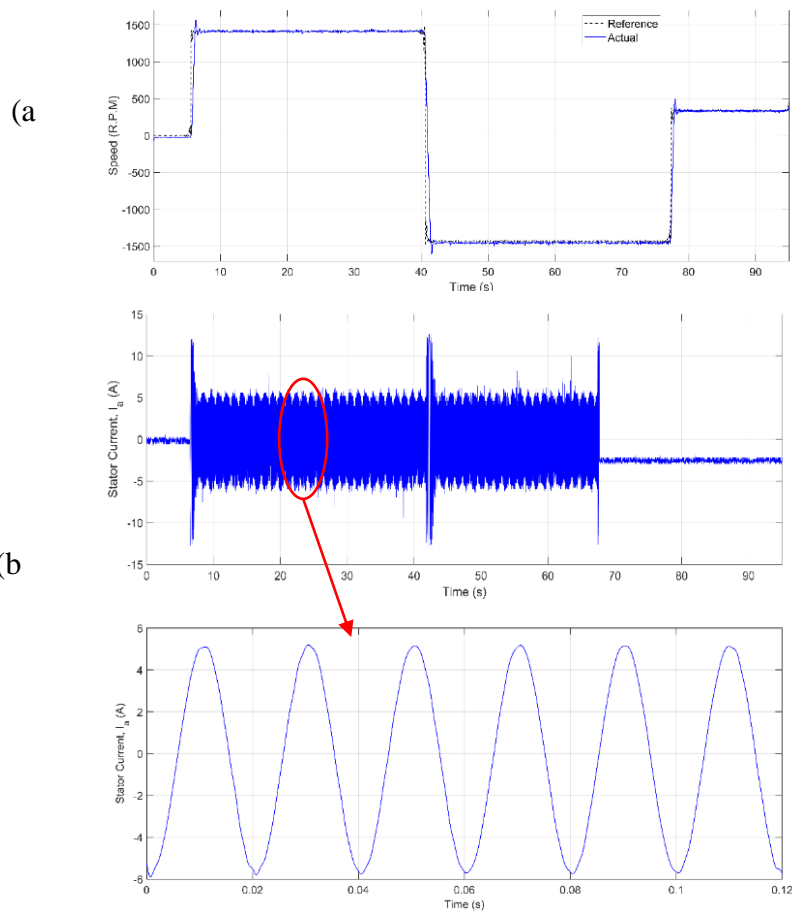


Figure 53 Forward-reversing phenomenon for induction motor

Harmonics are caused by nonlinear loads attached to the power system. Nonlinear loads draw non-sinusoidal current. Resistors, inductors, and capacitors are linear devices. When a resistive load is applied to an AC power system, it draws sinusoidal current. Even when an inductive or capacitive load is applied, it too draws sinusoidal current although it is phase shifted compared to the resistive load. There are many types of nonlinear loads which cause harmonics. According to literatures, the largest sources of harmonics are converters. Thus, it is also important to mitigate the THD in line with achieving good control algorithm for motor drives with VFD technology. Thus, to mitigate the THD, the space vector modulation (SVM) algorithm was implemented which helped in reducing the THD.

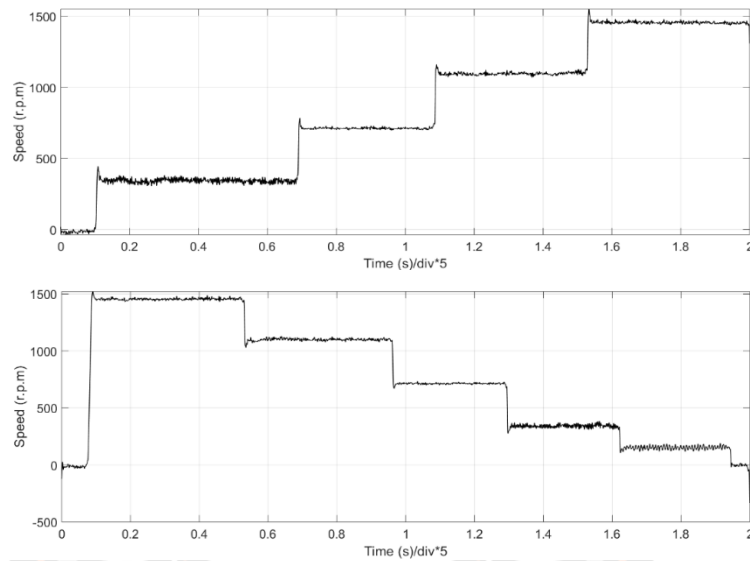


Figure 54 Step reference tracking behavior for motor

The THD in this experiment was achieved at 14.03%. Moreover, the tracking of step change in reference speed was experimented. The results for both forward and backward step change are observed in Figure 54. The reference tracking demonstrates good behavior with minimal overshoot which proves a smooth operation even for the rapid transitions.

Similarly, the step response is observed to mainly observe the starting characteristics of motor. It includes observing current, torque and speed responses at the same time. As shown in Figure 55, all the parameters are behaving the way it is supposed to be. The starting current is almost twice the load current but the current value settles at its rated current after attaining the steady-state. Moreover, the torque producing current (q –axis) provides good idea of the motor behavior. At the starting, to compensate the high torque demand to reach to demanded speed, the torque producing current ramps but settles at some value to provide continuous torque for the load.

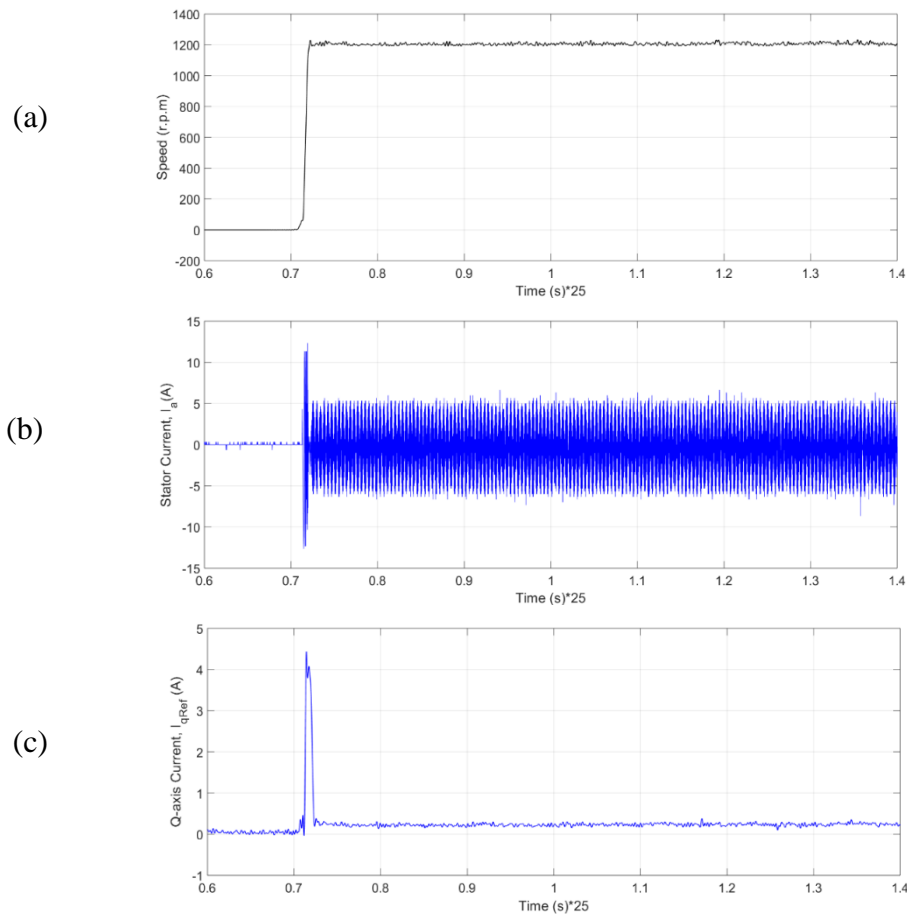


Figure 55 Hardware results for closed loop system. (a) Speed, (b) Stator current (I_a), (c) Q-axis current

Results for Compressor Motor

The main aim is to evaluate the energy saving obtainable when the fuzzy algorithm, which continuously regulates the compressor speed by an inverter, is employed to control the compressor refrigeration capacity instead of the classical thermostatic control, which imposes on/off cycles on the compressor that works at the nominal frequency of 50 Hz.

The experimental setup was arranged in electrical engineering laboratory on one of the two 78900 BTU/hr air conditioners installed. The measurement was taken for 6 hours (9.15 am till 3.15 pm) in two consecutive days. In the first day, the measurement with normal power supply from utility grid was taken. On the second day, the measurement was taken with the motor supply from inverter instead of from direct line. Since the room is quite big for one air conditioner unit to cool, so the second unit was also turned ON for first one hour and the measurement continued with just one unit (under test). The power measurement is taken using Fluke 1738 Power Logger and the data is analyzed using Fluke Energy Analyze Plus 2.3 software.

The real time room temperature is measured using testo 805i infrared-thermometer and coolant pressure was measured using testo 549i high-pressure measuring instrument for analysis purposes. The device has capability to send real time data to smartphone at every 2 seconds.



Figure 56 Active Power requirement for each method

The results show that the average power consumption is greater in normal frequency operation compared to inverter-fed operation at the starting due to reduced speed operation with latter. Moreover, the initial peak power in the starting is 6.748 kW and 6.532 kW respectively for normal and with inverter-fed operation. This is evident from Figure 56 (a). However, the power consumption is almost same and constant with the normal operation as depicted in Figure 56 (b) because the temperature lost in the room is greater than the temperature gain. This means the compressor motor is running at full and constant speed throughout to provide the temperature requirement. The temperature and pressure of the room measured for whole range of measurement is presented in Figure 59.

It is interesting note that the significant power factor improvement was achieved with inverter-fed operation at 0.91 compared to 0.84 for normal operation. The power and power factor measurement screenshot are presented in Figure 57.

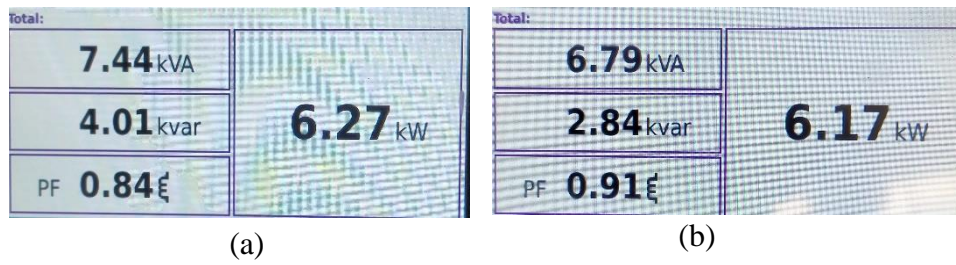


Figure 57 Power and power factor measurement. (a) Normal operation, (b) inverter-fed operation

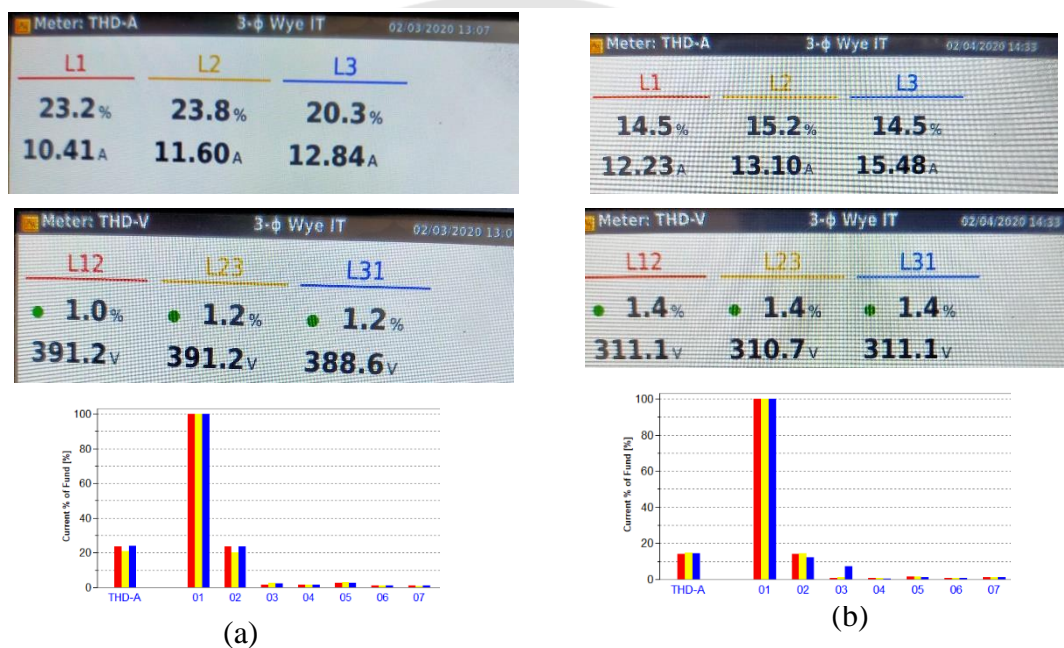


Figure 58 Total Harmonic Distortion (THD) for voltage and current. (a) Normal operation, (b) inverter-fed operation.

The total harmonic distortion (THD) for voltages and currents are also been compared and found that the current harmonic has reduced considerably in inverter-fed operation as evident from Figure 58. However, the current drawn by load has increased due to the operation at reduced voltage. The figure also shows the bar graph of the current harmonics.

The energy consumption of each method for the whole range of time noted at 30-minute interval is tabulated in Table V.

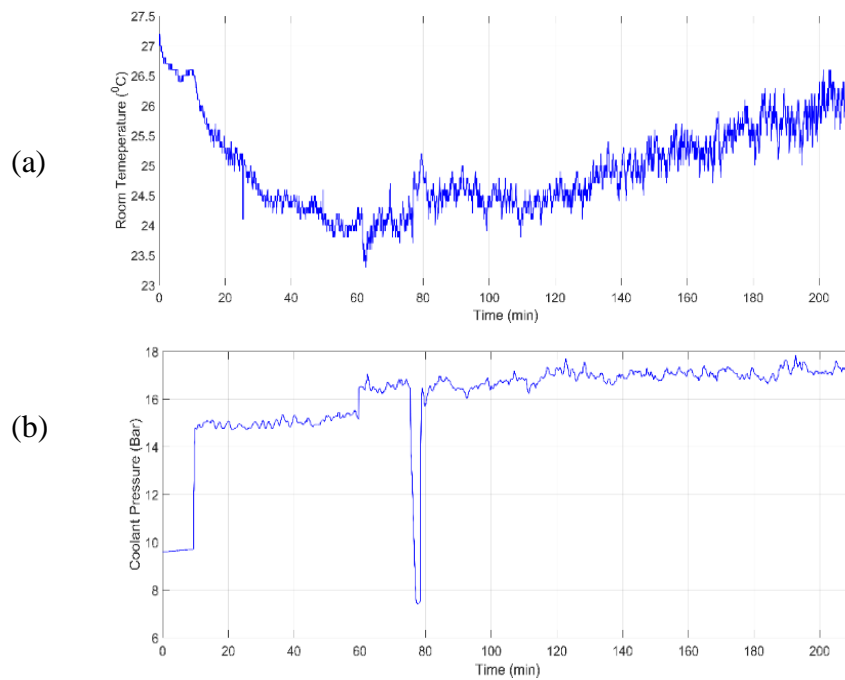


Figure 59 Coolant pressure and room temperature. (a) room temperature, (b) coolant pressure

Table V Energy consumption for 6 hours

| Recording Time (mins) | Energy (kWh) | |
|-----------------------|------------------|------------------------|
| | Normal Operation | Inverter-fed Operation |
| 30 | 2.673 | 2.328 |
| 60 | 6.08 | 4.76 |
| 90 | 8.58 | 6.283 |
| 120 | 11.17 | 8.92 |
| 150 | 15.00 | 12.28 |
| 180 | 18.15 | 16.30 |
| 210 | 19.98 | 19.69 |
| 240 | 23.80 | 23.5 |
| 270 | 26.96 | 26.5 |
| 300 | 30.83 | 27.74 |
| 330 | 33.79 | 33.12 |
| 360 | 37.45 | 36.03 |

CHAPTER V

DISCUSSION, FUTURE WORKS AND CONCLUSION

Discussion and Future Works

The performance and robustness of the proposed method have been evaluated under variety of operating conditions of induction motor in simulation. The equivalent drive is developed in laboratory and the performance for closed loop control loop as well as open-loop control are also evaluated. Some of the observations from this research are:

- i. The indirect method provides reasonably good performance and is simple to implement. However, the estimation of the rotor parameters with adequate accuracy is indeed challenging. It is further complicated by parameter variation with temperature and frequency.
- ii. The steady-state speed accuracy depends on the accurate adjustments of the rotor time constant in the estimated model. For example, rotor resistance may greatly be affected by variation of temperature and adversely affect the performance of the drive
- iii. For sensorless operation, the rotor speed is estimated by synthesizing the rotor-flux which is the function of both stator and rotor parameters. The stator parameters in addition to rotor parameter both varying with temperature and frequency can deteriorate the performance. This creates difficulty in obtaining satisfactory result.
- iv. Improved low speed performance can be achieved by exploiting the anisotropic properties of induction motor (Holtz, 2002). The spatial orientation of such anisotropies is related to the field angle, and to the mechanical rotor position. They can be identified by either by injecting high-frequency carrier signal into the stator windings and the process the response of the machine, or by making use of the transients that a PWM inverter generates.
- v. Open-loop control system are particularly robust at very low and very high speeds, but satisfy only low and moderate dynamic requirements.
- vi. Not a substantial amount of energy saving could be achieved for the open-loop control because it is implemented for big laboratory which has temperature lost greater than the cooling effect provided by the system. This resulted in almost same performance for both normal and inverter-fed operations.

Some of the future works and recommendations to future researcher:

- i. Variable frequency drive technology is recent but are finding wider applications including smart grid, motor control and many more.

- ii. Having good knowledge on vector/Field-oriented control is a plus point for electrical and industrial engineers because the technology is advancing faster and now it is finding its application also in DC brushless motors.
- iii. Sensorless algorithm has advantage of obtaining improved reliability and reduction in cost due to absence of speed encoder. However, an appropriate and most successful method is not discovered yet. The critical issue still lies with estimation algorithm which are highly influenced by motor parameters.
- iv. In this thesis, sensorless algorithm with speed estimator couldn't be established due to unavailable motor parameters. The algorithm could be possible if the motor parameters are available and if there is possibility to measure it.
- v. The energy saving could improve if the control algorithm is implemented for smaller room.

Conclusion

In this thesis, the performance of fuzzy logic-based rotor-flux model reference adaptive system technique applied to squirrel induction motor are designed and simulated in MATLAB/SIMULINK software. The simulated result confirmed the efficiency and the precision of the proposed method during sudden load torque application, forward and reversal, high and low speed and even for low and zero speed. The proposed method can provide equivalent performance with robustness against load variation.

The VFD technology is implemented in laboratory with developed universal voltage source inverter with TMS320F28069M Texas Instrument's launchpad. The drive is tested with 3 hp, 4 pole cage motor. The closed loop vector control algorithm is developed in CCS using basic C programming knowledge. The test results showed a good performance of the drive and also good performance characteristics are also achieved for the aforementioned motor.

The drive is finally implemented in the commercial air conditioner to control the compressor motor. The Fuzzy logic controller-based temperature controller implementation showed a remarkable improvement in the overall system. The power factor improvement and reduced total harmonic distortion are two important improvements shown in addition to energy saving and improved thermal comfort.

REFERENCES

- A. S. Muktar, T., R. Umale, A., & K. Kirpane, R. (2017). Vector Control Methods For Variable Speed of AC Motors. *International Research Journal of Engineering and Technology (IRJET)*, 4(2), 340–343. Retrieved from <https://www.irjet.net/archives/V4/i2/IRJET-V4I267.pdf>
- Admin. (2017, January 9). Various Induction Motor Speed Control Methods| Advantages | Limitations. Retrieved January 19, 2020, from DIY Electrical Electronics Projects website: <http://www.electricalbasicprojects.com/induction-motor-speed-control-methods/>
- Alizadeh, M., Masoumi, M., & Ebrahim, E. (n.d.). *Closed Loop Speed Control of Induction Motor using Constant V/F Applying SPWM and SVM Based Inverter*. 6(5), 8.
- Alsofyani, I. M., & Idris, N. R. N. (2016). Simple Flux Regulation for Improving State Estimation at Very Low and Zero Speed of a Speed Sensorless Direct Torque Control of an Induction Motor. *IEEE Transactions on Power Electronics*, 31(4), 3027–3035. <https://doi.org/10.1109/TPEL.2015.2447731>
- Ammar, A., Bourek, A., Benakcha, A., & Ameid, T. (2017). Sensorless stator field oriented-direct torque control with SVM for induction motor based on MRAS and fuzzy logic regulation. *2017 6th International Conference on Systems and Control (ICSC)*, 156–161. <https://doi.org/10.1109/ICoSC.2017.7958692>
- Asgharpour-Alamdari, H., Alinejad-Beromi, Y., & Yaghoobi, H. (2016). A Fuzzy-based Speed Controller for Improvement of Induction Motor's Drive Performance. *Iranian Journal of Fuzzy Systems*, 13(2), 61–70.

<https://doi.org/10.22111/IJFS.2016.2359>

- Blaschke, F. (1972). The Principle of Field Orientation as Applied to the NEW Transvector Closed-Loop System for Rotating-Field Machines. *Siemens Review*, 34(3), 217–220.
- Borgnakke, C., & Sonntag, R. E. (2012). *Fundamentals of Thermodynamics* (8th ed.). Retrieved from <https://umairbfrend.files.wordpress.com/2015/01/borgnakke-fundamentals-of-thermodynamics-8th-c2013-txtbk.pdf>
- Bose, Bimal. K. (2002). *Modern Power Electronics and AC Drives*. Prentice-Hall.
- Bose, Bimal. K. (2006). *Control and Estimation of Induction Motor Drives*. New Delhi, India: Prentice-Hall.
- Brenman, L. (1995). *Setting up TMS320 DSP Interrupts in “C”* (p. 45) [Application Report]. Retrieved from Texas Instrument website: <http://www.ti.com/lit/an/spra036/spra036.pdf>
- Casadei, D., Profumo, F., Serra, G., & Tani, A. (2002). FOC and DTC: Two viable schemes for induction motors torque control. *IEEE Transactions on Power Electronics*, 17(5), 779–787. <https://doi.org/10.1109/TPEL.2002.802183>
- Chengand, C.-C., & Lee, D. (2014). Smart Sensors Enable Smart Air Conditioning Control. *Sensors*, 14, 11179–11203. <https://doi.org/11179-11203>; doi:10.3390/s140611179
- Chiou, C. B., Chiou, C. H., Chu, C. M., & Lin, S. L. (2009). The application of fuzzy control on energy saving for multi-unit room air-conditioners. *Applied Thermal Engineering*, 29(2), 310–316. <https://doi.org/10.1016/j.applthermaleng.2008.02.031>

- Comanescu, M., & Xu, L. (2006). Sliding-mode MRAS speed estimators for sensorless vector control of induction Machine. *IEEE Transactions on Industrial Electronics*, 53(1), 146–153. <https://doi.org/10.1109/TIE.2005.862303>
- Das, B. (2016). *Vector Control of 3-Phase Induction Motor by Space Vector Modulation*. 5.
- Divyasree, P., & Binojkumar, A. C. (2017). Vector control of voltage source inverter fed induction motor drive using space vector PWM technique. *2017 International Conference on Energy, Communication, Data Analytics and Soft Computing (ICECDS)*, 2946–2951. <https://doi.org/10.1109/ICECDS.2017.8389996>
- Filizadeh, S. (2013). *Electric Machines and Drives: Principles, Control, Modeling, and Simulation* (1st ed.). Boca Raton: CRC Press.
- Hannan, M. A., Ali, J. A., Ker, P. J., Mohamed, A., Lipu, M. S. H., & Hussain, A. (2018). Switching Techniques and Intelligent Controllers for Induction Motor Drive: Issues and Recommendations. *IEEE Access*, 6, 47489–47510. <https://doi.org/10.1109/ACCESS.2018.2867214>
- Hee Nam, K. (2018). *AC Motor Control and Electrical Vehicle Applications* (2nd ed.). Retrieved from <https://www.crcpress.com/AC-Motor-Control-and-Electrical-Vehicle-Applications/Nam/p/book/9781138712492>
- Holmes, D. G., Lipo, T. A., McGrath, B. P., & Kong, W. Y. (2009). Optimized Design of Stationary Frame Three Phase AC Current Regulators. *IEEE Transactions on Power Electronics*, 24(11), 2417–2426. <https://doi.org/10.1109/TPEL.2009.2029548>

- Holtz, J. (2002). Sensorless control of induction motor drives. *Proceedings of the IEEE*, 90(8), 1359–1394. <https://doi.org/10.1109/JPROC.2002.800726>
- Hughes, A., & Drury, W. (2013). *Electric Motors and Drives: Fundamentals, Types and Applications, 4th Edition* (4th ed). Amsterdam: Newnes.
- Hule, S. V., Bindu R., & Vincent, D. (2014). Sensorless vector control of three phase induction motor. *2014 International Conference on Advances in Communication and Computing Technologies (ICACACT 2014)*, 1–6. <https://doi.org/10.1109/EIC.2015.7230749>
- Iancu, I. (2012). A Mamdani Type Fuzzy Logic Controller. In E. Dadios (Ed.), *Fuzzy Logic—Controls, Concepts, Theories and Applications*. <https://doi.org/10.5772/36321>
- Isa, S. N. M., Azri, M., Ibrahim, Z., Talib, M. H. N., Sulaiman, M., Meng, Q. L., ... Rahim, N. A. (2017). Experimental investigation on scaling factor of fuzzy logic speed control for induction motor drives. *2017 6th International Conference on Electrical Engineering and Informatics (ICEEI)*, 1–6. <https://doi.org/10.1109/ICEEI.2017.8312439>
- Jih-Sheng Lai, & Fang Zheng Peng. (1996). Multilevel converters-a new breed of power converters. *IEEE Transactions on Industry Applications*, 32(3), 509–517. <https://doi.org/10.1109/28.502161>
- Kansagara, R. (2018, December 18). Different Types of Inverters and Their Applications. Retrieved January 7, 2020, from CircuitDigest website: <https://circuitdigest.com/tutorial/different-types-of-inverters>
- Kayacan, E. (2011). *Interval Type-2 Fuzzy Logic System: Theory and Design* (PhD

- Thesis). Bogazici university, Istanbul, Turkey.
- Kim, S.-H. (2017). *Electric Motor Control: DC, AC, and BLDC Motors* (1 edition). Cambridge, Massachusetts: Elsevier Science.
- Kimiaghalam, B., Rahmani, M., & Halleh, H. (2008, October 14). *Speed & torque vector control of induction motors with Fuzzy Logic Controller*. 360–365. <https://doi.org/10.1109/ICCAS.2008.4694671>
- Kojima, M., & Watanabe, M. (2016). Effectiveness of Promoting Energy Efficiency in Thailand: The Case of Air Conditioners. *Institute of Developing Economics, Jetro*, 577, 1–13.
- Krause, P. C., Wasynczuk, O., & Sudhoff, S. D. (2002). *Analysis of Electric Machinery and Drive Systems* (second). New York, NY: Wiley-Interscience.
- Kumar, A., & Batra, V. (2016). A Novel Simulation and Analysis of SPWM Inverter. *International Journal of Advanced Research in Electrical, Electronics and Instrumentation Engineering*, 5(11), 5.
- Leekwijck, W. V., & Kerre, E. E. (1999). Defuzziycation: Criteria and classiycation. *Fuzzy Sets and Systems*, 20.
- Leonhard, W. (1996). *Control of Electrical Drives* (2nd ed.). Berlin, Heidelberg: Springer-Verlag.
- Lftisi, F., George, G. H., & Rahman, M. A. (2017, October 3). *Implementing fuzzy logic controller techniques for indirect vector control induction motor drives*. 6–11. <https://doi.org/10.1109/IEMCON.2017.8117129>
- Lin, J.-L., & Yeh, T.-J. (2007). Modeling, identification and control of air-conditioning systems. *International Journal of Refrigeration*, 30(2), 209–220.

<https://doi.org/10.1016/j.ijrefrig.2006.08.009>

- Ma, Z., & Wang, S. (2009). Energy efficient control of variable speed pumps in complex building central air-conditioning systems. *Energy and Buildings*, *41*(2), 197–205. <https://doi.org/10.1016/j.enbuild.2008.09.002>
- Maamoun, A., Alsayed, Y. M., & Shaltout, A. (2013). Fuzzy logic based speed controller for permanent-magnet synchronous motor drive. *2013 IEEE International Conference on Mechatronics and Automation*, 1518–1522. <https://doi.org/10.1109/ICMA.2013.6618139>
- Maiti, S., Chakraborty, C., Hori, Y., & Ta, M. C. (2008). Model Reference Adaptive Controller-Based Rotor Resistance and Speed Estimation Techniques for Vector Controlled Induction Motor Drive Utilizing Reactive Power. *IEEE Transactions on Industrial Electronics*, *55*(2), 594–601. <https://doi.org/10.1109/TIE.2007.911952>
- Mamdani, E. H., & Assilian, S. (1975). An Experiment in Linguistic Synthesis with a Fuzzy Logic Controller. *Int. J. Man-Machine Studies*, *7*, 13.
- Nasution, H., Jamaluddin, H., & Mohd. Syeriff, J. (2011). Energy Analysis for Air Conditioning System Using Fuzzy Logic Controller. *TELKOMNIKA (Telecommunication Computing Electronics and Control)*, *9*(1), 139. <https://doi.org/10.12928/telkomnika.v9i1.680>
- Ong, C.-M. (1998). *Dynamic Simulation of Electric Machinery: Using Matlab/Simulink*. Retrieved from <http://lib.ugent.be/catalog/rug01:002022353>
- Orlowska-Kowalska, T., & Dybkowski, M. (2010). Stator-Current-Based MRAS Estimator for a Wide Range Speed-Sensorless Induction-Motor Drive. *IEEE*

- Transactions on Industrial Electronics*, 57(4), 1296–1308.
<https://doi.org/10.1109/TIE.2009.2031134>
- P. Kazmierkowski, M., Blaabjerg, F., & Krishna, R. (2002). *Control in Power Electronics_ Selected Problems*. USA: Academic Press Series in Engineering.
- Rashid, M. H. (2001). *Power Electronics Handbook*. Retrieved from https://www.academia.edu/9565229/RASHID_M._H._2001_Power_Electronics_Handbook
- Reney, D. (2011). Modeling and Simulation of Space Vector PWM Inverter. *2011 International Conference on Devices and Communications (ICDeCom)*, 1–4.
<https://doi.org/10.1109/ICDECOM.2011.5738466>
- Ross, T. J. (2010). *Fuzzy logic with engineering applications* (3rd ed). Chichester, U.K: John Wiley.
- Schauder, C. (n.d.). Adaptive speed identification for vector control of induction motor without rotational transducers. *In Con\$ Rec. 1989 IEEE IAS Annu. Mtg*, 493–499.
- Sivanandam, S. N., Sumathi, S., & Deepa, S. N. (2007). *Introduction to Fuzzy Logic using MATLAB*. <https://doi.org/10.1007/978-3-540-35781-0>
- Sugeno, M., & Kang, G. T. (1988). Structure identification of fuzzy model. *Fuzzy Sets and Systems*, 28(1), 15–33. [https://doi.org/10.1016/0165-0114\(88\)90113-3](https://doi.org/10.1016/0165-0114(88)90113-3)
- Sulaiman, M., Salleh, Z., & Omar, R. (2015). Effects of Parameters Variation in Fuzzy Based Induction Motor Drives. *TELKOMNIKA Indonesian Journal of Electrical Engineering*, 16(2), 272 ~ 280. <https://doi.org/10.11591/telkomnika.v15i3.8776>
- Tamai, S., Sugimoto, H., & Masao, Y. (1987). *Speed sensorless vector control of IM*

- with model reference adaptive system.* 189–195. Retrieved from https://www.researchgate.net/publication/283173718_Speed_sensor-less_vector_control_of_induction_motor_using_model_reference_adaptive_system
- Tsuji, M., Shuo Chen, Izumi, K., & Yamada, E. (2001). A sensorless vector control system for induction motors using q-axis flux with stator resistance identification. *IEEE Transactions on Industrial Electronics*, 48(1), 185–194. <https://doi.org/10.1109/41.904579>
- Varma, P. S., & Narayanan, G. (2006). Space Vector PWM as a Modified Form of Sine-Triangle PWM for Simple Analog or Digital Implementation. *IETE Journal of Research*, 52(6), 435–449. <https://doi.org/10.1080/03772063.2006.11416484>
- Vas, P. (1999). *Artificial-Intelligence-based Electrical Machines and Drives: Application of Fuzzy, Neural, Fuzzy-neural, and Genetic-algorithm-based Techniques*. Retrieved from <https://books.google.co.th/books?id=16Ai4r7qjuIC>
- Vas, Peter. (1998). *Sensorless Vector and Direct Torque Control*. Oxford, New York: Oxford University Press.
- Yuntao, Y., & Yan, L. (2011). A novel sensor-less induction motor based on fuzzy sliding-mode control. *2011 6th IEEE Conference on Industrial Electronics and Applications*, 2747–2751. <https://doi.org/10.1109/ICIEA.2011.5976063>
- Zadeh, L. A. (1965). Fuzzy Sets. *Information and Control*, 8, 338–353. Retrieved from https://www-liphy.ujf-grenoble.fr/pagesperso/bahram/biblio/Zadeh_FuzzySetTheory_1965.pdf
- Zadeh, L. A. (1973). Outline of a New Approach to the Analysis of Complex Systems

and Decision Processes. *IEEE Transactions on Systems, Man, and Cybernetics, SMC-3*(1), 28–44. <https://doi.org/10.1109/TSMC.1973.5408575>

Zaky, M. S., Khater, M., Yasin, H., & Shokralla, S. S. (n.d.). *Review of Different Speed Estimation schemes for Sensorless Induction Motor Drives*. 40.

Zhao, K., Liu, X.-H., Zhang, T., & Jiang, Y. (2011). Performance of temperature and humidity independent control air-conditioning system in an office building. *Energy and Buildings*, 43(8), 1895–1903. <https://doi.org/10.1016/j.enbuild.2011.03.041>

Zipan Nie, Preindl, M., & Schofield, N. (2016). SVM strategies for multiphase voltage source inverters. *8th IET International Conference on Power Electronics, Machines and Drives (PEMD 2016)*, 6 .-6 . <https://doi.org/10.1049/cp.2016.0214>

